The Pennsylvania State University

The Graduate School

John and Willie Leone Family Department of Energy and Mineral Engineering

MATHEMATICAL DEVELOPMENT FOR FLOWBACK RATE TRANSIENT ANALYSIS

A Thesis in

Energy and Mineral Engineering

by

Yun Yang

Submitted in Partial Fulfillment
of the Requirements
for the Degree of

Master of Science

December 2017

The thesis of Yun Yang was reviewed and approved* by the following:

Luis F. Ayala H.

Professor of Petroleum and Natural Gas Engineering

Associate Department Head for Graduate Education

Thesis Co-advisor

Hamid Emami-Meybodi

Assistant Professor of Petroleum and Natural Gas Engineering

Thesis Co-advisor

Turgay Ertekin

Professor of Petroleum and Natural Gas Engineering

George E. Trimble Chair in Earth and Mineral Sciences

*Signatures are on file in the Graduate School

ABSTRACT

Unconventional gas reservoirs, such as tight gas and shale gas, appear to have great potential to supply future demand for hydrocarbon. Economics of these reservoirs are tied closely to the performance of multi-fractured horizontal wells (MFHWs), which is the most direct indicator of stimulation effectiveness. Thus, greater understanding and analysis of the factors affecting performance of MFHWs are critical for the efficient exploitation of such reservoirs. Hydrocarbon production data analysis (PDA) techniques have been commonly used to characterize hydraulic fracture (HF) and, ultimately, to evaluate hydraulic-fracturing jobs. Recent studies have shown that rate transient analysis of flowback data can also provide early insight into HF attributes. While PDA methods seek long-time production data, flowback analysis can be conducted using early water and gas production data obtained immediately after the completion of stimulation jobs. However, in comparison with the long-term hydrocarbon production period, the physics of the process is more difficult to capture during flowback production because of its short duration, at which one or more flow regimes may occur. In addition, the flowback flow system could be single- or two-phase, depending on reservoir type. According to reported field data, single-phase flowback can be observed in tight sands, but two-phase flow is expected in the case of shale gas. Although various mathematical models have been proposed to analyze single-phase (water) and two-phase (gas and water) flowback data, analytical models for interpretation of data are still at an early stage of development.

The objectives of this study are first to reproduce the relevant analytical models available in literature and understand their advantages and limitations; then, to develop single-phase

and two-phase analytical models capable of predicting HF attributes such as fracture half-length and fracture permeability using early water and gas production data.

In this study, a set of numerical simulations was conducted using CMG (IMEX) to examine the capacity of available mathematical models. It was found that most of the single-phase flowback models in the literature are accurate only under pseudo steady-state conditions, where a boundary-dominated flow regime with a constant production rate has been established. Another limitation of current models is that they can only estimate one fracture attributes: k_f or x_f. Knowing the shortcomings of current models, I developed a set of analytical models for both single- and two-phase systems, which were validated against numerical simulations. The single-phase model can closely estimate HF attributes, such as permeability and half-length under constant pressure as well as constant flowrate condition, for both transient and boundary dominated flow periods. Furthermore, I extended the developed single-phase model to variable bottomhole conditions by employing superposition principle.

In the case of two-phase flow system, I developed an analytical model under fracture depletion mechanism for both early gas production (EGP) and late gas production (LGP) periods. In the case of EGP, gas flux from matrix to HF is assumed to be negligible. Comparisons of numerical results with those obtained from the analytical model show that the developed two-phase model for EGP can accurately predict fracture attributes. In the case of LGP, a coupled model is developed to include the effect of gas influx from matrix to HF on flowback data, where a uniform pressure decline rate is assumed in fracture-matrix system. The two-phase model has the advantage of linear behavior of water

properties and avoids the computational complexity. With typical Barnett shale properties input in the numerical simulation, the analytical model can accurately estimate fracture attributes within a 10% error margin. Sensitivity analyses of fracture conductivity and initial water saturation in fracture have been conducted to illustrate the validity of two-phase flowback model applied in LGP. The results reveal that, within the physical range of fracture conductivity and initial water saturation, the two-phase flowback model can accurately evaluate fracture attributes. However, the model is more accurate for cases with smaller fracture conductivity and higher initial water saturation in fracture.

TABLE OF CONTENTS

LIST OF FIGURES

LIST OF TABLES

ACKNOWLEDGEMENTS

First, I would like to thank my advisers, Dr. Luis F. Ayala H. and Dr. Hamid Emami-Meybodi, for being the greatest supervisors and friends to me. I am honored to have worked with them. I really appreciate that Dr. Luis F. Ayala H. gave me the opportunity to attend graduate school and work under his supervision. He equipped me with technical knowledge on how to conduct successful research. I would like to express my deepest gratitude to Dr. Hamid Emami-Meybodi for his patience and help during all the tough moments.

I would like to thank my committee member, Dr. Turgay Ertekin, for being on my committee, and for all of his advice, suggestions and contributions.

I want to acknowledge the endless support of my parents. They always listen to me and gave helpful suggestions when I was depressed.

I would like to thank my best friends, Yuzhe Cai and Peiwen Yang, for their encouragement and friendship during my Master's.

Finally, I would like to thank Penn State's Department of Energy and Mineral Engineering faculty and staff for keeping me on track and making my time at the university a unique experience.

NOMENCLATURE

b : intercept of the fitted linear line
B_g : gas compressibility
B_s : water formation factor at surface condition
B_w: water formation factor
BDF: boundary dominated flow
BHP: bottomhole pressure
c_{eff}: effective compressibility
c_g: gas compressibility
c_{gi}: initial gas compressibility
c_p: proppant compressibility
c_t : total compressibility of rock and fluid in fracture
c_{ti}: total compressibility at initial condition
C_{st} : storage coefficient
c_r: fracture compressibility
c_w: water compressibility
c_{wi}: initial water compressibility
c_{wb} : compressibility of fluid in wellbore
CBM: coalbed methane
DPM: dual porosity model
DRP: dynamic-relative-permeability
EGP: early gas production
G_i: initial free gas storage in fracture and stimulated matrix
G_{fi}: initial gas storage in fracture at surface condition
G_p: cumulative gas production at surface condition
G_r: remaining gas volume in fracture at surface conditon
GWR: gas to water ratio
h : fracture height
HF: hydraulic fracture
J_w: water productivity index
k_f: fracture permeability
k_{rw}: relative permeability of water
L_f: fracture spacing
LGP: late gas production
m: slope of the fitted linear line
MB: material-balance
MBT: material balance time
MFHWs: multi-fractured horizontal wells
P: fracture pressure
$\bar{P}$: average pressure of the fracture-matrix system
P_D: dimensionless pressure
P_f: average fracture pressure

P_i: initial pressure at HF
P_p: water pseudo pressure
P_{pD}: dimensionless pseudo pressure
P_{pi} : pseudo pressure at initial condition
P_{pwf} : pseudo pressure at wellbore
P_{wf}: well flowing pressure
P_{wfn}: wellbore pressure at the end of period t_n
PDA: production data analysis
PSS: pseudo steady-state
q: production rate at wellbore
q_w : specified flowback rate of water at surface condition
q_{Dw}: dimensionless water flow rate
RNP: rate normalized pressure
RTA: rate transient analysis
s_{gi}: initial gas saturation in fracture
s_{gim}: initial gas saturation in matrix
s_w: water saturation
s_{wi}: initial water saturation in fracture
s_{wim}: initial water saturation in matrix
$\bar{s}_w$: average water saturation in fracture
TCF: trillion cubic feet
t: flowback time
t_a: water pseudo time
t_D: dimensionless time
t_e: equivalent time
t_n: flowback period *n*
t_{spt}: superposition time of transient period
t_{sppss}: superposition time of BDF
UGR: unconventional gas reservoirs
V_f: pore volume in fracture
V_{fi} : initial pore volume of fracture at the start of flowback operation
V_{pi}: initial pore volume in fracture and stimulated matrix
V_w: initial water volume in fracture at reservoir condition
V_{wr}: remaining water volume in fracture at reservoir condition
V_{wb}: fluid volume in wellbore
w_f: the fracture width
W_i: initial water storage in fracture and stimulated matrix
W_{fi}: initial water volume in fracture at surface condition
W_p: cumulative water production at surface condition
x: distance from wellbore along the fracture
x_D: dimensionless space
x_f: fracture half-length
μ_w: water viscosity

ϕ_f: fracture porosity
ϕ_m: matrix porosity
η : pressure diffusivity constant
$\eta_{2-phase}$: pressure diffusivity constant of two-phase flow
Δq_j: change in flow rate
1D: one-dimensional
2D: two-dimensional

CHAPTER 1 : INTRODUCTION

1.1 Background

The development of multi-fractured horizontal wells (MFHWs) enables operators to recover unconventional resources within a profitable range, especially for shale plays. Over the past decade, shale gas has become a great source of energy. Energy Information of Administration (EIA) reported that shale gas production in the United States increased from 1.0 trillion cubic feet (TCF) in 2006, to 4.8 TCF in 2010, accounting for 23% of total U.S. natural gas production in volume base.

As Figure 1.1 shows, in 2015, 67% of U.S. natural gas production came from MFHWs. Hydraulic fracturing has become the most significant technique in developing unconventional resources. After stimulation, most MFHWs undergo a short shut-in period to clean up the fracturing job before production, followed by a flowback period (see Figure 1.2).

The flowback rate and shut-in time are important in liquid recovery. High fracking liquid recovery indicates less leak-off from the fracture, which yields better ultimate well performance. Andrews (2010) indicated that more than 500,000 gallons of water are used for a single fracture treatment where less than 10 % to more than 70 % of the original fracturing fluid can be recovered during flowback (API, 2010). In field operation, the recovery factor is most likely less than 10%. Large amounts of fracking fluid are produced during flowback. In principle, analyzing production data of fracking fluid and hydrocarbon

would provide the earliest possible estimates of fracture attributes, which is important in field planning, such as re-stimulation.

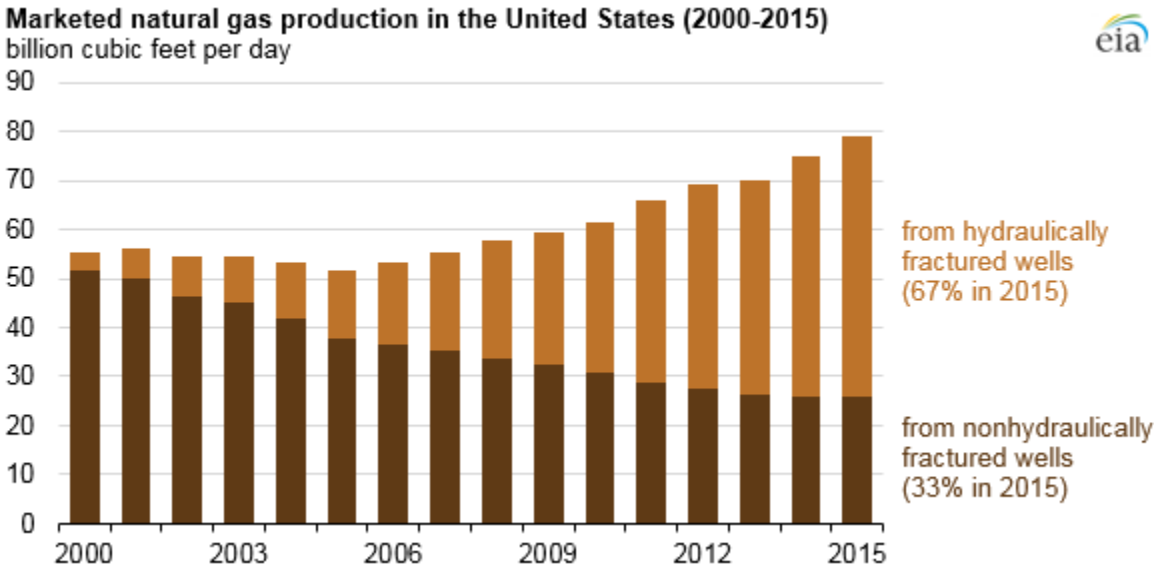

Figure 1.1: Overview of hydraulically fractured wells in united states reported by the U.S. department of energy (EIA, 2016).

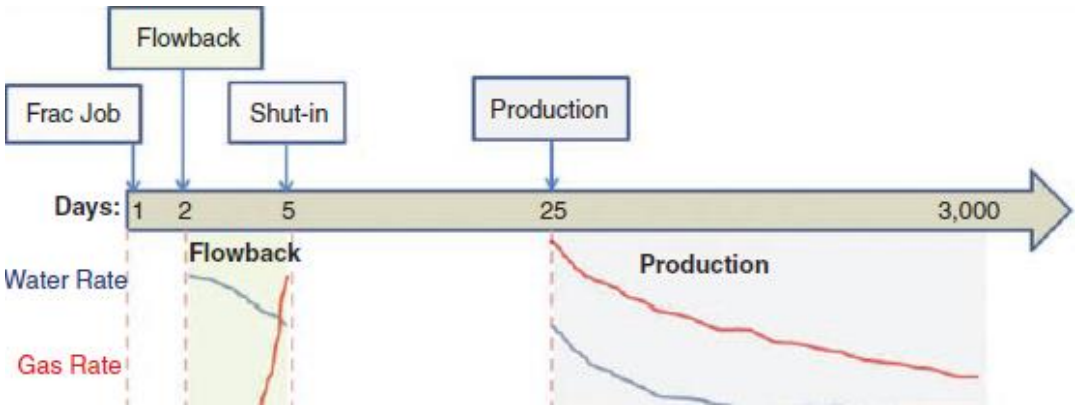

Figure 1.2: Flowback routine operation (Alkouh et al., 2013)

Flowback period is usually in the first 1- to 10-day flow of single-phase fracturing fluid. or two-phase of fracturing fluid and hydrocarbon. Adefidipe et al. (2014a) noted that single-phase flowback could only be expected in tight sand reservoirs and is absent in shale gas due to immediate gas breakthrough. As Figure 1.3 depicts, flowback can be categorized into two periods: early gas production (EGP) and late gas production (LGP). The EGP is characterized by a negative GWR slope, while the LGP is characterized by a positive gas-to-water ratio (GWR) slope. Water imbibition and gravity segregation during the shut-in period before flowback operation are two important mechanisms responsible for initial gas saturation in fracture. The negative GWR slope during EGP represents the gas production from free gas storage in fracture, where gas matrix influx is negligible. The positive GWR slope during LGP highlights the impact of matrix gas influx into hydraulic fracture (HF) on flowback data.

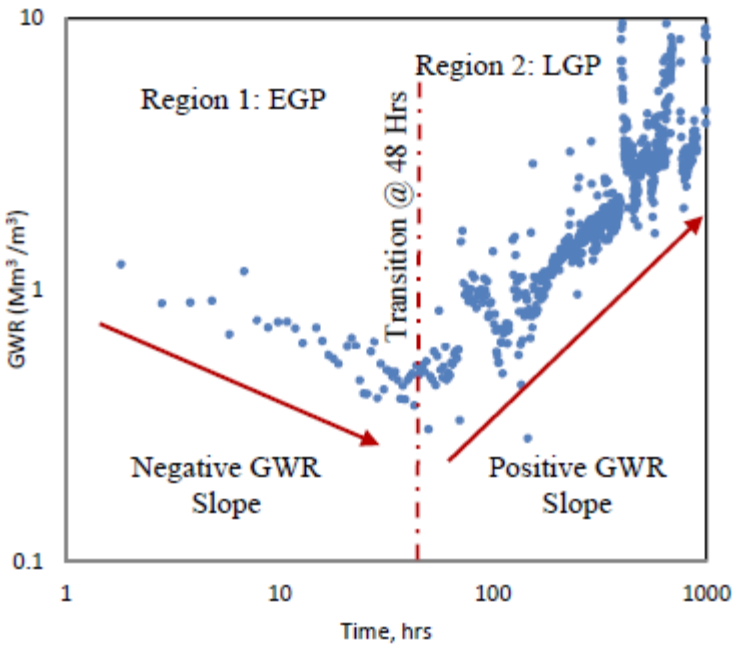

Figure 1.3: GWR vs. time for a Muskea shale gas well (Adefidipe et al., 2014a)

1.2 Statement of Problem

After stimulation of MFHWs, it is important to evaluate the fracturing jobs for obtaining the HF properties, such as fracture half-length and fracture permeability. These parameters are critical to hydrocarbon production from tight sand and shale reservoirs. Due to the low permeability of such reservoirs, common methods in conventional production data analysis (PDA), such as Arp's decline curve analysis, cannot be applied because of the long transient period in hydrocarbon production. Instead, rate transient analysis (RTA) techniques have been used to obtain HF properties (Clarkson, 2013), where hydrocarbon production data are key inputs. The HF properties can be also obtained from flowback production data, such as water rate, gas rate, and bottomhole pressure. In comparison with the relatively late-time hydrocarbon RTA, the flowback analysis is desirable because, at the early times, hydrocarbon production data is usually unavailable or of low quality and fracture is initially filled with fracking fluid instead of hydrocarbon. Therefore, mathematical models on flowback data can serve to complete the hydrocarbon RTA. In addition, the flowback analysis can potentially provide early estimation of HF properties, which is crucial in managing field operation, i.e., field development and re-stimulation.

Several single- and two-phase analytical models have been previously developed for flowback analysis, which contain assumption(s) causing some limitations. Therefore, the main objectives of this study are:

1) to explore the limitations caused by the assumptions that were made in development of available analytical models in the literature by reproducing and testing them against numerical simulations and

2) to develop single- and two-phase analytical models capable of predicting HF properties, such as fracture half-length and permeability, from flowback data by relaxing some assumptions made in previous studies.

This report consists of five chapters. **Chapter 1** provides a brief introduction on the subject matter, statement of problem, and the main objectives of this study. **Chapter 2** reviews the available literature on flowback along with various mathematical models developed for flowback analysis. **In Chapter 3,** the available single- and two-phase analytical models are reproduced and then their limitations are discussed. In addition, the chapter discusses our analytical models. For single-phase systems, I proposed a set of one-dimensional (1D) models developed under different boundary conditions. In contrast with previous single-phase models valid under pseudo steady-state (PSS) conditions, our simple 1D models are valid for transient and boundary-dominated flow regimes under both constant bottomhole pressure (BHP) and constant flowrate boundary conditions. For two-phase systems, I propose a one-dimensional (1D) model to analyze water flow in fracture before gas flows into fracture; and a two-dimensional (2D) model to analyze water flow in fracture after gas flows into fracture. In **Chapter 4**, the developed analytical models are validated against numerical simulations (CMG-IMEX) and compared with previously developed analytical models. It was shown that the developed models can closely predict the fracture properties for various flow conditions where other models fail to offer good estimations of HF half-length and permeability. Finally, **Chapter 5** summarizes the findings of this study and provides recommendations for future research.

CHAPTER 2 : LITERATURE REVIEW

This chapter discusses the flowback analysis and its importance for future hydrocarbon production and ultimate well performance by reviewing the body of literature. In addition, a brief introduction is provided on the flowback analytical models that were published in the literature.

Crafton (1998) studied the effect of excessive pressure drawdown, shut-in time, and the duration of flowback on well clean-up, which is crucial in hydrocarbon production from fractured well. He successfully used the reciprocal productivity index method to estimate hydraulic-fracture (HF) half-length, effective wellbore radius, and the product of effective fracture permeability and thickness. However, while his approach is valid for single-phase flow of water in HF vertical wells, it is not the case for multi-fractured horizontal wells (MFHWs) in unconventional gas reservoirs (UGR). Subsequently, Crafton and Gunderson (2006) illustrated the importance of recording high frequency of flowback data; namely, pressure and production rate. The production data during flowback conveys valuable information to characterize fracture and to evaluate HF stimulation jobs. In a follow-up study, Crafton and Gunderson (2007) developed an analytical model to calculate fracture conductivity using early flowback data. Their numerical simulations results indicated that the timing of flowback and shut-ins affect ultimate performance of the HF well. In addition, high flowback rates result in excessive production of proppant due to higher fluid velocity,

which cause serious problems in production facility. Therefore, careful management of flowback is required for long-term well performance. Crafton (2008) continued his discussion on the effect of flowback management on long-term well performance by ignoring capillary pressure and gravity segregation. He complemented the simulation results by conducting field experiments to examine the effects of flowback rate, shut-in times, fracture complexity, and lateral orientation on the water production data. In an extended study, Crafton (2010) numerically examined the effects of shut-in times on the production and well performance in a multi-fractured system.

Ilk et al. (2010b) developed diagnostic plots to construct workflow to qualitatively analyze early flowback data. The diagnostic can be used to analyze water unloading effect, fracture depletion, and early dominance of the water production.

Abbasi et al. (2012) investigated the relationship between flowback rate and average pressure drop of fracture by proposing a mathematical model that predicts the lump of HF half-length and permeability. In their conceptual model, the production time is divided into three regions: water dominated, transition, and gas dominated. Their mathematical model can only be applied to the first region for single-phase water flow before gas flows into fracture.

Wattenbarger and Alkouh (2013) numerically simulated HF water production from a MFHW in shale gas reservoir with natural fractures. They compared their flowback results against the field data obtained from Fayetteville and Barnett formations. Alkouh et al. (2013) and Alkouh et al. (2014) extended their studies by combining flowback data with long-term gas production data to estimate effective fracture volume for single-phase water

flow in transient period as well as two-phase water and gas flows in boundary dominated flow (BDF).

As mentioned earlier, in shale gas reservoirs, single-phase region does not occur. Instead, an instant two-phase production (i.e., gas and water) is expected once the wells are opened. The immediate two-phase behavior was observed in Barnett (Zhang & Ehlig-Economides, 2014) and Marcellus (Clarkson & Williams-Kovacs, 2013b) flowback data.

Besides analysis on single-phase water flowback, Alkouh et al. (2014) combined two-phase flowback data with long term gas production data to analyze shale gas reservoirs. Based on numerical simulation results, they concluded that gas is the dominant phase in the system and that water production is driven mainly by gas expansion. Gas compressibility at initial reservoir pressure is used as the total compressibility of the system. Alkouh (2014) further validated this assumption by observing how gas volumetric compressibility varies with production time and the distance from wellbore. He demonstrated that fracture pressure and water saturation would affect volumetric gas compressibility (i.e. a multiplication of gas saturation in fracture and gas compressibility) at different times. In their method, total compressibility is calculated as gas volumetric compressibility at initial pressure and gas saturation = 1. The determined gas volumetric compressibility always shows an average value since it is high near the perforation, and low near the fracture tip. However, in their analysis, they ignored the contribution of fracture closure and water expansion as a drive mechanism. Also, in their analytical solution, they did not account for gas production in the material balance. Therefore, their purposed two-phase model can only

be properly applied when gas production is negligible compared with water production, which is a rare condition in field practice.

Clarkson and McGovern (2001) proposed a material-balance (MB) equation for the coal bed methane (CBM) matrix to account for both adsorbed and free gas storage. Applying the MB, average reservoir pressure can be estimated using an iterative scheme. In their paper, they also explained other practical applications of the MB to estimate reservoir properties. Four years later, Clarkson and McGovern (2005) reproduced their previous model with slightly different coefficients. Their main assumption is that average water saturation in the coal matrix is constant with time, which is a valid assumption if initial water saturation is smaller than immobile water saturation. However, in CBM production, this assumption is not considered in many other purposed models (King, 1990; Seidle, 1999). Clarkson et al. (2012) further developed a flowing MB equation for two-phase (i.e., gas and water) CBM by adding radial well inflow equation for vertical and horizontal wells to predict production over time. The development of these inflow equations can be attributed to Dake (1983) and Economides et al. (2012). They modified the CBM model by separating initial water saturation from average water saturation during production. Following the purposed workflow and applying the material balance equation, they were able to history match the gas and water rates and cumulative production by adjusting one or multiple reservoir parameters, such as matrix permeability or perforation thickness.

Clarkson et al. (2012) proposed a two-phase tank model to characterize fracture using two-phase flowback data for multistage fractures completed in shale. They adopted the MB developed in their previous work on CBM to analyze two-phase flowback behavior in shale,

where cylindrical shape of fracture is assumed and shape factor can be added later to consider rectangular shape of fracture. Based on their analysis, the flow regimes in flowback period could be categorized into transient flow in fracture, fracture depletion and transient linear flow. Fracture depletion usually is the first flow regime that can be identified in conventional flowback data. With the MB and well inflow equations, flowback rate and cumulative production of gas and water can be history-match with model output to obtain fracture properties.

Clarkson and Williams-Kovacs (2013b) modified the conceptual model with cylindrical shape fracture to rectangular shape fracture and included a shape factor in the well inflow equation to account for linear flow in fracture. However, they neglected the difference between fracture and matrix length in the development of analytical model on shale gas flowback, which contributes to potential errors in the history-match process. As Appendix D illustrates, this thesis briefly modified their solution. The authors also extended the analytical model on shale gas flowback to be applicable in tight oil formation (Clarkson & Williams-Kovacs, 2013a) and liquid rich tight formation (Clarkson et al., 2016).

Williams-Kovacs and Clarkson (2013a; 2013b) realized that the non-unique results may be obtained in the history-match process for flowback on shale gas and tight oil formations. Therefore, they used Monte Carlo simulation to test the impact of individual parameters. Several case studies have been conducted with field observations (Williams-Kovacs & Clarkson, 2014a, 2014b, 2015).

Ilk et al. (2010b) proposed a series of diagnostic plot to analyze production data in tight gas formation. They used gas to water ratio (GWR) versus time plots to identify flow

regimes and drive mechanisms in shale gas production. In an extended study, Ilk et al., (2010a) provided guidelines on how to use diagnostic plots to explain the associated pitfalls and challenges.

While GWR monotonically increases in tight sand formations (Abbasi et al., 2012; Abbasi et al. (2014)), the GWR exhibits a V-shaped behavior in shale reservoirs (Clarkson & Williams-Kovacs, 2013a; Ghanbari et al., 2013; Zhang & Ehlig-Economides, 2014). The early decline during the early gas production (EGP) period in GWR of shale reservoirs is due to initial gas saturation in HF. A late gas production (LGP) period with increasing GWR occurs after gas breakthrough from matrix to fracture. Therefore, during EGP, fluid influx from matrix is negligible and fracture can be treated as a closed system.

Adefidipe et al. (2014a) proposed a two-phase flowback model to determine fracture attributes based on the diffusivity equation for the gas phase. They considered gas expansion, water expansion, and fracture closure as main production mechanisms. They used GWR plots to separate the flowback region into EGP and LGP periods. Their analytical solution is applicable for flowback under BDF and constant BHP. One issue with their model is that their material balance includes both water and gas productions but they employed gas diffusivity equation in which gas compressibility is replaced with total compressibility. The other potential error in their derivation is that they assumed that the equivalent gas rate, a function of relative permeability of gas, is independent of space, which cannot accurately capture the changes in gas properties along the fracture length during depletion.

Adefidipe et al. (2014b) used conventional gas MB equation to evaluate fracture attributes for flowback period. They included gas, water and fracture compressibility in their MB equation, where fracture closure is dependent on fracture stiffness as defined in Craig and Blasingame (2006). Also, in this work, they indicated that the transition time from EGP to LGP can be found at the global minimum in GWR plot. After realizing that a polynomial correlation can be assumed in the plot of cumulative gas and water production, they obtained the mathematical expression of transition time. However, the polynomial correlation needs to be further validated so as to have general application in the field.

Xu et al. (2015b) and Xu et al. (2015c) improved upon Adefidipe et al.'s (2014b) work and conducted numerical simulations using Cheng's (2012) model to validate their results. But the problem in their MB approach is that boundary conditions are neglected in the flow problem and variation of fluid properties cannot be found with space. Later, Xu et al. (2016) extended the discussion on the development of mathematical models for EGP by investigating the mechanisms corresponding to the V-shaped GWR diagnostic plot. They showed that water imbibition and gravity segregation during the shut-in period before flowback operation are the two main mechanisms responsible for early gas flowback in shale formation. Their model assumes that the gas compressibility at any time is equal to gas compressibility at initial pressure of HF, which is not reasonable, considering the highly dependent nature of gas properties to pressure.

Ezulike and Dehghanpour (2014) developed an analytical solution for LGP period based on dual porosity model (DPM) to evaluate fracture properties. In their two-dimensional (2D) system, they considered flow of gas from matrix to fracture. They then proposed a

time-dependent dynamic-relative-permeability (DRP) function, which directly relates relative permeability to time and simplified their solution on two-phase flowback. However, their study found that the DRP varied for different formations, and a general formula could not be obtained. Ezulike and Dehghanpour (2015) also analyzed the uncertainty in the flowback data since not all the required input parameters may be available or accurate. They suggested that post-flowback data analysis should be combined with flowback data, so as to improve the accuracy of the history-match process.

In summary, current mathematical models for flowback data analysis have revealed varying degrees of inaccuracy, which need to be improved upon. In this work, I carefully examined the proposed models in literature and developed new mathematical models for both single phase and two phase flowback systems.

CHAPTER 3 : MATHEMATICAL DEVELOPMENTS

In this chapter, first, I carefully review some of the available mathematical models for flowback data analysis. Then I present a new set of analytical models for both single- and two- phase flowback systems. For single phase flowback of water, new models are developed for BDF and transient flow regimes. For the two phase flowback of water and gas, new models are developed by including and excluding gas influx from matrix to HF.

The development of mathematical models for flowback data analysis can be treated as a single- or multiphase flow in porous media problems, where fracture is the porous medium and fracturing (i.e., water) and formation fluids (i.e., water and gas) are the fluids. Figure 3.1(a) shows a schematic of the conceptual model for flowback. Figure 3.1(b) depicts 1D flow in HF. Figure 3.1(c) illustrates 2D flow in both matrix and HF. In this present work, the 1D conceptual model is considered for both single- (i.e., only water) and two-phase (i.e., both water and gas) scenarios, whereas the 2D conceptual model is only used for two-phase flow of gas (from matrix to HF and then to wellbore) and water (from HF to wellbore). As mentioned earlier, while single-phase flowback of water is only observed in tight sand formations (Adefidipe et al., 2014a), and the two-phase flowback is common in shale gas reservoirs. Therefore, both 1D and 2D models need to be developed to obtain comprehensive solution of fracture attributes.

(a)

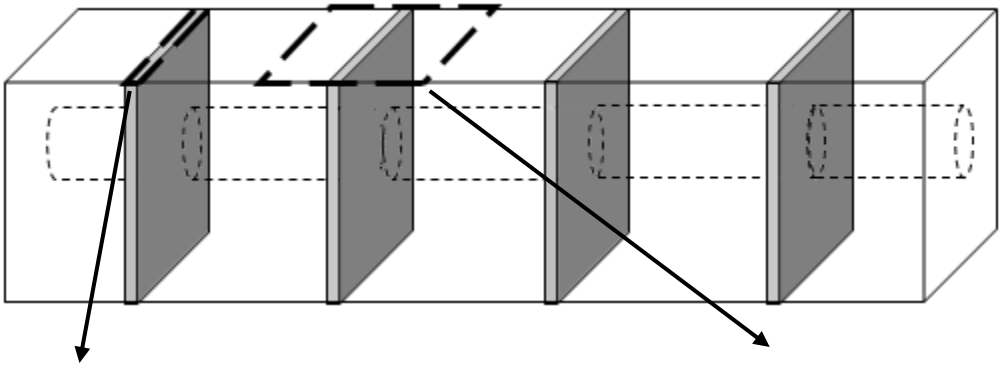

(b) 1D Model (Top view)

(c) 2D Model (Top view)

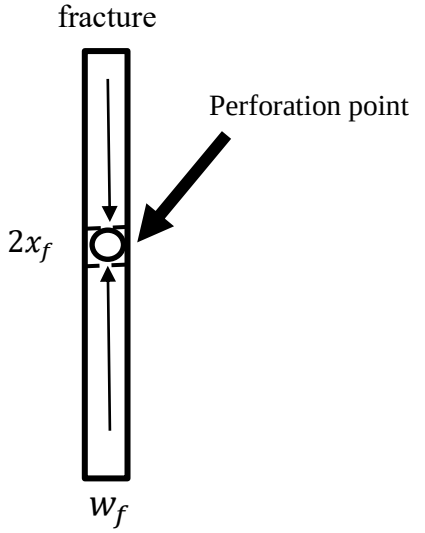

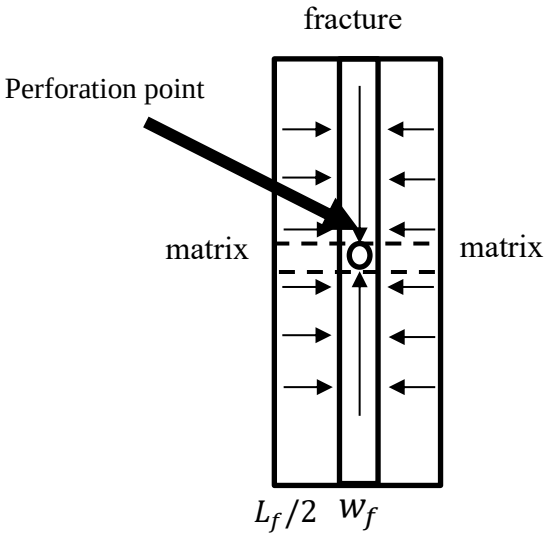

Figure 3.1: Conceptual model of analytical development

For 1D single-phase flowback,

- gravity segregation is neglected,
- there is no flow of water and gas from matrix, and
- water is assumed to be incompressible.

The mathematical developments for the single-phase flowback can be categorized into BDF and transient models. The BDF models are applied to flowback data with constant production rate, as well as constant bottomhole pressure (BHP) inner boundary condition. The outer boundary condition (tip of HF) would be:

$$\frac{\partial P}{\partial x}|_{x=x_f} = 0, \tag{3.1}$$

where x is the distance from wellbore along the fracture; x_f is the fracture half-length; and P is the fracture pressure.

In this study, transient models are also developed under constant flow rate and constant BHP condition by considering the following condition for the outer boundary:

$$P(\infty, t) = P_i, \tag{3.2}$$

where P_i is the initial pressure at HF.

After developing mathematical solutions, it is common to plot rate normalized pressure (RNP) against time (or pseudo time) to obtain fracture attributes,

$$RNP = \frac{P_i - P_{wf}}{q_w}, \tag{3.3}$$

where P_{wf} is the well flowing pressure and q_w is the flowback rate of water.

A general workflow for analyzing single-phase flowback data follows:

1. Carefully collect flowback data: flowback rate and well flowing pressure,
2. Determine defined parameters: RNP and a time related parameter,
3. Plot and curve fit RNP vs. the time related parameter, and
4. Extract slope from the fitted line and evaluate fracture attributes.

For 1D and 2D two-phase flowback,

- gravity segregation is neglected,
- water production only sources from HF networks,
- BDF flow is assumed for gas and water flow through primary fracture network, and
- Desorbed gas is neglected during flowback period.

The two-phase models are classified as early gas production (EGP) and late gas production (LGP) models, based on the presence of gas matrix influx. The similar workflow as the single-phase flowback is used for two-phase flowback but RNP and time-related parameter are defined differently to account for two-phase flow. Table 3.1 summarizes the analytical models developed in this study, which are discussed in detail in the following subsections.

Table 3.1: Summary of mathematical models developed for flowback data analysis.

Fluids	Flow Regime in HF	Wellbore BC	Gas Influx from Matrix	Gas Flow in HF	Section
Water	BDF	Constant q (PSS)	No	No	3.1.1-3.1.3
		Constant BHP	No	No	3.1.4
		Variable q	No	No	3.1.8
	Transient	Constant q	No	No	3.1.5
		Constant BHP	No	No	3.1.6
		Variable q	No	No	3.1.7
Water + Gas	BDF	Constant BHP	No	Yes	3.2.1
	BDF	Constant BHP	Yes	Yes	3.2.2

3.1 Single-Phase Flowback Model

Analytical model for single-phase flowback is mainly for very early data (one day) and can be only observed in flowback data from tight sand gas reservoirs.

3.1.1 BDF Constant q (PSS): Abbasi et al.'s Model

Abbasi et al. (2012) developed an analytical solution capable of modeling single-phase flowback of water under PSS condition by including wellbore and HF volume. They treated the fracture as a closed chamber, assuming that whatever flowed into the fracture would be produced at surface level. In the form of *RNP*, their analytical model can be expressed by:

$$RNP = \frac{B_s}{C_{st}} MBT + \frac{\phi_f c_t \mu_w B_s}{3 k_f C_{st}} x_f^2, \tag{3.4}$$

where MBT is the material balance time and equivalents to the ratio of cumulative water production to flowback rate; B_s is the water formation factor at surface condition; c_t is the total compressibility of rock and fluid in fracture; μ_w is the water viscosity; ϕ_f is the fracture porosity; k_f is the fracture permeability; C_{st} is the storage coefficient and is defined as the summation of $\frac{dV_f}{dP}, V_f c_f,$ and $V_{wb} c_{wb}$; V_f is the fracture volume, V_{wb} is the fluid volume in wellbore, and c_{wb} is the compressibility of fluid in wellbore.

Alternatively, C_{st} can be defined as:

$$C_{st} = (c_w + c_r) V_w + c_w V_{wb}, \tag{3.5}$$

where c_r is fracture compressibility the and V_w is the initial water volume in fracture at reservoir condition.

Equation (3.4) can be written in the field unit as:

$$RNP = \frac{B_w}{C_{st}} MBT + 52.7 \frac{\phi_f c_t \mu_w B_w}{k_f C_{st}} x_f^2. \quad (3.6)$$

Detailed derivation of Equation (3.6) is given in Appendix A. According to Equation (3.6), one can estimate C_{st} and x_f^2/k_f from the slope and intercept of RNP vs. MBT plot, respectively.

3.1.2 BDF Constant q (PSS): Alkouh et al.'s Model

Alkouh et al. (2013) and Alkouh et al. (2014) developed a mathematical model for single-phase flowback under BDF, with constant flowback rate at wellbore. In their developments, they only included fracture volume, ignored wellbore storage, and assumed no water contribution from matrix (i.e., cumulative water production equals to effective fracture volume). The *RNP* form of their solution reads

$$RNP = \frac{B_w}{V_w c_t} MBT \quad (3.7)$$

where V_w is the initial water volume in fracture at reservoir condition (effective fracture volume).

In the derivation of Equation (3.7), the authors neglected water productivity index (J_w), which can be an important term at early times. The full solution in the field unit system can be expressed as:

$$RNP = 5.615 \frac{B_w}{c_t w_f h x_f \phi_f} MBT + 296.41 \frac{x_f \mu_w B_w}{w_f h k_f}, \quad (3.8)$$

$$P_f - P_{wf} = \frac{x_f \mu_w}{3 w_f h k_f} q_w, \tag{3.9}$$

$$J_w = \frac{x_f \mu_w}{3 w_f h k_f}, \tag{3.10}$$

where w_f is the fracture width; h is the fracture height or formation height if fracture is fully penetrated; and P_f is the average fracture pressure. Detailed derivation of Equation (3.8) can be found in Appendix B.

According to Equation (3.8), fracture volume (or fracture half-length if cross sectional area of fracture is known) and fracture permeability can be estimated from slope and intercept of *RNP* vs. *MBT* plot.

3.1.3 BDF Constant q (PSS): 1D Analytical Model (Case 1)

Using single-phase diffusivity equation for water, I developed simple 1D analytical solutions under different boundary conditions based on the conceptual model depicted in Fig. 3.1(b) to examine the above-mentioned models (Abbasi et al.'s Model and Alkouh et al.'s Model) as well as the numerical simulation results. The diffusivity equation for the linear flow of water in the fracture can be written as:

$$\frac{\partial^2 P}{\partial x^2} = \frac{1}{\eta} \frac{\partial P}{\partial t}, \tag{3.11a}$$

$$\eta = \frac{k_f}{\phi_f c_t \mu_w}, \tag{3.11b}$$

where η is the pressure diffusivity constant.

To solve the diffusivity equation, the following dimensionless parameters are defined:

$$x_D = \frac{x}{x_f}, \tag{3.12}$$

$$t_D = \frac{t\eta}{x_f^2}, \tag{3.13}$$

$$q_{Dw} = \frac{q_w x_f \mu_w B_w}{k_f w_f h P_i}, \tag{3.14}$$

$$P_D = 1 - \frac{P}{P_i}, \tag{3.15}$$

where q_w is the constant flowback rate of water at surface condition.

For a 1D BDF flowback system with constant flowback rate at wellbore (Case 1), diffusivity equation and boundary conditions can be expressed in dimensionless form as:

$$\frac{\partial^2 P_D}{\partial x_D^2} = \frac{\partial P_D}{\partial t_D}, \tag{3.16}$$

$$\frac{\partial P_D(0,t_D)}{\partial x_D} = q_{Dw}, \tag{3.17}$$

$$\frac{\partial P_D(1,t_D)}{\partial x_D} = 0, \tag{3.18}$$

$$P_D(0, x_D) = 0. \tag{3.19}$$

Using separation of variables technique, the solution to Equation (3.16) in the field unit would be:

$$P_{wf} = P_i - 887.31 \frac{q_w x_f \mu_w B_w}{k_f w_f h} \left(\frac{1}{3} + t_D - 2 \sum_{n=1}^{\infty} \frac{exp(-(n\pi)^2 t_D)}{(n\pi)^2} \right), \tag{3.20}$$

or in the form of *RNP* would be:

$$RNP = 887.31 \frac{x_f \mu_w B_w}{k_f w_f h} \left(\frac{1}{3} + t_D - 2 \sum_{n=1}^{\infty} \frac{exp(-(n\pi)^2 t_D)}{(n\pi)^2} \right). \tag{3.21}$$

At large production time, the summation term on the right side of Equation (3.21) becomes negligible. Therefore, in the case of BDF, Equation (3.21) can be simplified to:

$$RNP = \frac{5.615B_w}{w_f h x_f c_t \phi_f} t + 296 \frac{x_f \mu_w B_w}{k_f w_f h}, \quad (3.22)$$

which is same the solution proposed by Alkouh et al. (2014). However, the 1D flowback model given in Equation (3.21) can be used to match flowback data during transient period.

The general expression of three analytical models discussed in Sec 3.1.1, 3.1.2, and 3.1.3 (for single-phase flowback under PSS regime) can be given by

$$RNP = mt + b, \quad (3.23)$$

where m is the slope, b is the intercept of the fitted linear line, and t is the flowback time. The m and b values for each of these models are given in Table 3.2.

Table 3.2: Summary of Single-Phase Flowback Models under PSS condition.

Model	***m***	***b***
Abbasi et al.'s Model	$\frac{B_w}{C_{st}}$	$52.7 \frac{\phi_f c_t \mu_w B_w}{k_f C_{st}} x_f^2$
Alkouh et al.'s Model	$\frac{5.615 B_w}{w_f \mathrm{h} x_f c_t \phi_f}$	$296 \frac{\mu_w B_w}{w_f \mathrm{h} k_f} x_f$
1D flowback model (Case 1)	$\frac{5.615 B_w}{w_f \mathrm{h} x_f c_t \phi_f}$	$296 \frac{\mu_w B_w}{w_f \mathrm{h} k_f} x_f$

3.1.4 BDF Constant BHP: 1D Analytical Model (Case 2)

Production under constant bottom hole pressure is a common practice adopted in the field. The 1D flowback model can be developed based on constant BHP and no flow boundary

conditions and, thus, successfully model flowback for BDF under constant BHP. To develop a 1D constant BHP flowback model (Case 2), the following dimensionless parameters are defined

$$P_D = \frac{P - P_{wf}}{P_i - P_{wf}}, \tag{3.24}$$

$$x_D = \frac{x}{x_f}, \tag{3.25}$$

$$t_D = t\frac{\eta}{x_f^2}. \tag{3.26}$$

Dimensionless initial and boundary conditions can be expressed as:

$$P_D(0, t_D) = 0, \tag{3.27}$$

$$\frac{\partial P_D(1, t_D)}{\partial x_D} = 0, \tag{3.28}$$

$$P_D(x_D, 0) = 1. \tag{3.29}$$

Using the separation of variables techniques, the solution of diffusivity equation subject to the conditions given by Equations (3.27) – (3.29) reads:

$$P(x,t) = \left(P_i - P_{wf}\right) \sum_{n=1}^{\infty} \frac{4}{(2n-1)\pi} \sin\left(\frac{(2n-1)\pi x}{2x_f}\right) \exp\left(-\frac{0.001582(2n-1)^2\pi^2 t k_f}{\phi_f c_t \mu_w x_f^2}\right) + P_{wf}. \tag{3.30}$$

Using Darcy's flowrate equation, Equation (3.30) can be written in the form of *RNP* as:

$$RNP = \frac{887.31\, B_w \mu_w}{k_f w_f h \sum_{n=1}^{\infty} \frac{2}{x_f} \exp\left(-\frac{0.001582(2n-1)^2\pi^2 t k_f}{\phi_f c_t \mu_w x_f^2}\right)}. \tag{3.31}$$

Equation (3.31) can be used to predict flowback behavior under constant BHP flowback. Detailed derivation of Equation (3.31) can be found in Appendix C.

3.1.5 Transient Constant q: 1D Analytical Model (Case 3)

Single-phase flowback period starts with a transient flow regime that usually lasts less than a day. However, for HFs with low permeability, the transient regime would be longer and it would be worth analyzing the flowback data. Earlier in this chapter, I discussed the analytical solutions for transient flowback under constant rate (Section 3.1.3) and BHP (Section 3.1.4) condition. Another transient analytical solution under constant rate can be obtained using the following dimensionless parameters, which are given by

$$\mathrm{x_D} = \frac{x}{x_f}, \tag{3.32}$$

$$\mathrm{t_D} = \frac{t\eta}{x_f^2}, \tag{3.33}$$

$$\mathrm{P_D} = 1 - \frac{P}{P_i}, \tag{3.34}$$

$$\mathrm{q_{Dw}} = \frac{q_w x_f \mu_w B_w}{0.001127 k_f w_f h P_i}, \tag{3.35}$$

The corresponding boundary conditions are expressed by

$$\mathrm{P_D}(x_D, 0) = 0, \tag{3.36}$$

$$\frac{\partial \mathrm{P_D}(0, t_\mathrm{D})}{\partial \mathrm{x_D}} = \mathrm{q_{Dw}}, \tag{3.37}$$

$$\mathrm{P_D}(\infty, t_D) = 0. \tag{3.38}$$

Using Laplace transformation technique, the non-dimensional form of solution to the diffusivity equation subject to the initial and boundary conditions given by Equations (3.36) – (3.38) reads

$$P_D(x_D, t_D) = q_{Dw}\left(2\sqrt{\frac{t_D}{\pi}}\exp\left(-\frac{x_D^2}{4t_D}\right) - x_D erfc\left(\frac{x_D}{2\sqrt{t_D}}\right)\right). \quad (3.39)$$

At wellbore, i.e. $x = 0$, bottomhole pressure in dimensional form reads

$$P_{wf} = P_i - 79.65\frac{q_w B_w}{w_f h}\sqrt{\frac{\mu_w t}{k_f \phi_f c_t}}, \quad (3.40)$$

and in RNP form reads

$$RNP = 79.65\frac{B_w}{w_f h}\sqrt{\frac{\mu_w t}{k_f \phi_f c_t}}. \quad (3.41)$$

According to Equation (3.41) the HF permeability can be obtained from the slope of *RNP* vs. $\sqrt{t}$ plot. Detailed derivation of Equation (3.41) can be found in Appendix C.

3.1.6 Transient Constant BHP: 1D Analytical Model (Case 4)

Under constant BHP condition, a transient analytical solution can be obtained using the following dimensionless parameters and

$$P_D = \frac{P - P_{wf}}{P_i - P_{wf}}, \quad (3.42)$$

$$x_D = \frac{x}{x_f}, \quad (3.43)$$

$$t_D = t\frac{\eta}{x_f^2}. \quad (3.44)$$

and following dimensionless initial and boundary conditions

$$P_D(x_D, 0) = 1, \tag{3.45}$$

$$P_D(\infty, t_D) = 1, \tag{3.46}$$

$$P_D(0, t_D) = 0. \tag{3.47}$$

Using the Laplace transformation technique, the solution to diffusivity equation subject to conditions given by Equations (3.45) – (3.47) reads

$$P(x,t) = \left(P_i - P_{wf}\right) \operatorname{erf}\left(\frac{x}{2\sqrt{t\eta}}\right) + P_{wf}. \tag{3.48}$$

The flowback rate in field unit reads

$$q = 0.008\left(P_i - P_{wf}\right) w_f h \sqrt{\frac{k_f \phi_f c_t}{\mu_w t}}, \tag{3.49}$$

and in *RNP* form it would be

$$RNP = 125 \frac{B_w}{w_f h} \sqrt{\frac{\mu_w t}{k_f \phi_f c_t}}. \tag{3.50}$$

According to Equation (3.41) the HF permeability can be obtained from the slope of *RNP* vs. $\sqrt{t}$ plot. The model can also predict flowback rate in transient period, whereas the previous BHP flowback model can predict flowback rate for entire flowback period. Detailed derivation of Equation (3.50) can be found in Appendix C.

A summary of the 1D flowback models and corresponding dimensionless boundary conditions/parameters are given in Tables 3.4 and 3.3, respectively.

Table 3.3: A Summary of Dimensionless Boundary Conditions/Parameters for Case 1-4.

Boundary Conditions	Case 1	$\frac{\partial P_D(0,t_D)}{\partial x_D} = q_{Dw}$	$\frac{\partial P_D(1,t_D)}{\partial x_D} = 0$
	Case 2	$P_D(0,t_D) = 0$	$\frac{\partial P_D(1,t_D)}{\partial x_D} = 0$
	Case 3	$\frac{\partial \mathrm{P_D}(0,t_\mathrm{D})}{\partial \mathrm{x_D}} = -\mathrm{q_{Dw}}$	$\mathrm{P_D}(\infty,t_D) = 0$
	Case 4	$P_D(0,t_D) = 0$	$P_D(\infty,t_D) = 1$
P_D and q_{Dw}	Case 1	$P_D = 1 - \frac{P}{P_i}$	$\mathrm{q_{Dw}} = \frac{q_w x_f \mu_w B_w}{0.001127 k_f w_f \mathrm{h} P_i}$
	Case 2	$P_D = \frac{P - P_{wf}}{P_i - P_{wf}}$	
	Case 3	$\mathrm{P_D} = 1 - \frac{P}{P_\mathrm{i}}$	$\mathrm{q_{Dw}} = \frac{q_w x_f \mu_w B_w}{0.001127 k_f w_f \mathrm{h} P_i}$
	Case 4	$P_D = \frac{P - P_{wf}}{P_i - P_{wf}}$	

Table 3.4: A Summary of 1D Analytical Solutions Case 1-4.

Analytical Solution in P_D form	Case 1	$P_D(x_D, t_D) = q_{Dw}\left(\frac{1}{3} + \frac{x_D^2}{2} - x_D + t_D - 2\sum_{n=1}^{\infty}\frac{1}{n\pi^2}\exp(-(n\pi)^2 t_D)\cos(n\pi x_D)\right)$
	Case 2	$P_D(x_D, t_D) = \sum_{n=1}^{\infty}\frac{4}{(2n-1)\pi}\sin\frac{(2n-1)\pi x_D}{2}\exp\left(-\frac{(2n-1)^2\pi^2 t_D}{4}\right)$
	Case 3	$P_D(x_D, t_D) = q_{Dw}\left(2\sqrt{\frac{t_D}{\pi}}\exp\left(-\frac{x_D^2}{4t_D}\right) - x_D erfc\left(\frac{x_D}{2\sqrt{t_D}}\right)\right)$
	Case 4	$P_D(x_D, t_D) = \mathrm{erf}\left(\frac{x_D}{2\sqrt{t_D}}\right)$
Analytical Solution in RNP form	Case 1	$RNP = 887.31\frac{x_f \mu_w B_w}{k_f w_f h}\left(\frac{1}{3} + \frac{0.006328 k_f}{\phi_f c_t \mu_w x_f^2}t - 2\sum_{n=1}^{\infty}\frac{\exp\left(-(n\pi)^2\frac{0.006328 k_f}{\phi_f c_t \mu_w x_f^2}t\right)}{(n\pi)^2}\right)$
	Case 2	$RNP = \frac{887.31\, B_w \mu_w}{k_f w_f h \sum_{n=1}^{\infty}\frac{2}{x_f}\cos\left(\frac{(2n-1)\pi}{2}\right)\exp\left(-\frac{0.001582(2n-1)^2\pi^2 t k_f}{\phi_f c_t \mu_w x_f^2}\right)}$
	Case 3	$RNP = 141.17\frac{B_w}{w_f h}\sqrt{\frac{\mu_w t}{\phi_f c_t k_f \pi}}$
	Case 4	$RNP = 70.587\frac{B_w}{w_f h}\sqrt{\frac{\mu_w \pi t}{\phi_f c_t k_f}}$

3.1.7 Transient Variable q

In field practice, flowback rate is always controlled by production conditions such as excess sand production. Therefore, it is common to have variable flowback rate over time. However, the previous mathematical models were developed for constant BHP or constant q. To overcome this shortcoming, I adopted the superposition principle (Dake, 1983) to be able to analyze the flow back data obtained from variable rate (e.g., Figure 3.3) cases for both transient (section 3.1.7) and BDF (section 3.1.8) flow regime.

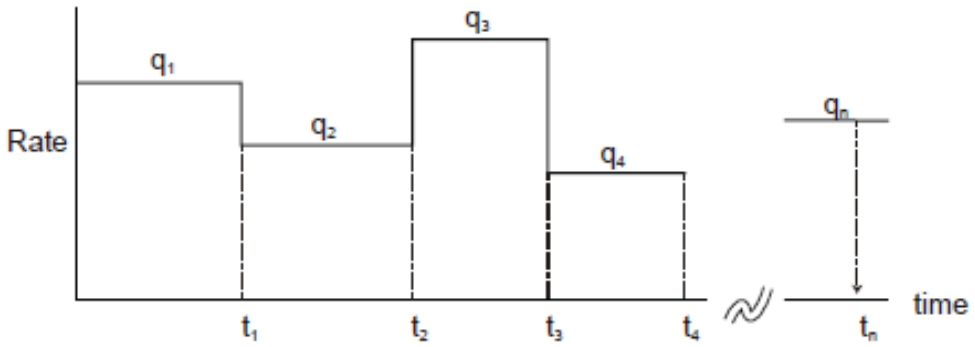

Figure 3.2: Variable Flowrate Profile (Dake, 1983).

The general formula of superposition principle are given by

$$\frac{2\pi kh}{q\mu}(P_i - P_{wfn}) = \sum_{j=1}^{n} \Delta q_j P(t_n - t_{j-1}), \qquad (3.51)$$

where P_{wfn} is wellbore pressure at the end of period t_n, Δq_j is the change in flow rate, P can be substituted with any general expression of pressure.

For transient flowback period, I superimpose the 1D model (i.e., Case 3), which is the transient flowback model with constant flowback rate. Then, the relationship between pressure drawdown and flowback rate can be obtained by

$$P_i - P_{wfn} = 79.65 \frac{B_w}{w_f h} \sqrt{\frac{\mu_w}{k_f} \phi_f c_t} \sum_{j=1}^{n} \Delta q_j \sqrt{(t_n - t_{j-1})}. \quad (3.52)$$

To linearize Equation (3.52), superposition time of transient period (t_{spt}) is defined by

$$t_{spt} = \sum_{j=1}^{n} \Delta q_j \sqrt{(t_n - t_{j-1})}. \quad (3.53)$$

The linearized equation for pressure would be:

$$P_i - P_{wfn} = m t_{spt}, \quad (3.54a)$$

$$m = 79.65 \frac{B_w}{w_f h} \sqrt{\frac{\mu_w}{k_f} \phi_f c_t}. \quad (3.54b)$$

According to Equation (3.54), the HF permeability can be obtained from the slope of $(P_i - P_{wfn})$ vs. t_{spt} plot. Detailed derivation of Equation (3.54) can be found in Appendix C. Linear relationship can be established between pressure drawdown and superposition time.

3.1.8 BDF Variable q

For BDF period, the relation between pressure drawdown and flowback rate can be found by

$$P_i - P_{wfn} = \frac{5.615 B_w}{\phi_f c_t w_f h x_f} \sum_{j=1}^{n} (q_j - q_{j-1})(t_n - t_{j-1}) + \frac{x_f \mu_w B_w}{0.003381 k_f w_f h} (q_n). \quad (3.55)$$

In order to linearize Equation (3.55), superposition time of BDF (t_{sppss}) is defined by

$$t_{sppss} = \sum_{j=1}^{n} (q_j - q_{j-1})(t_n - t_{j-1}). \quad (3.56)$$

To estimate fracture properties from flowback data, the production time should first be converted to t_{sppss} and pressure drawdown should be plotted against t_{sppss} in a log-log

plot. Then those flowback data that follow a unit slope should be extracted to create a plot of $(P_i - P_{wfn})$ vs. t_{sppss} in normal scale. The x_f and k_f can be estimated from the slope and intercept of the plot. It worth noting that water flow would experience a transient period every time flowback rate is changed. For fracture with low permeability, longer transient time is expected after flowback rate is changed. Errors may arise, since our mathematical model is developed based on no-flow boundary, and is not valid for the period right after flowback rate is changed. As k_f increases, the errors are diminished for less pressure transient time. For that reason, usually accurate estimate of k_f cannot be obtained with Equation (3.56), especially for HF having low permeability. Therefore, two plots should be constructed to obtain fracture properties. First plot is $(P_i - P_{wfn})$ vs. t_{spt}, and k_f can be estimated from the slope of the linear portion of the line. Second plot is pressure drawdown vs. t_{sppss} and x_f can be estimated from the slope of straight line using the late time flowback data. This variable flowback rate model for single-phase flowback can give accurate estimate of fracture properties and predict flowback behavior under variable flowback rate operation.

In summary, Abbasi et al. (2012) and Alkouh et al. (2014) proposed two analytical models that I discussed here. I modified the existing models to make them more practical. For example, from Alkouh et al.'s (2014) solution, I re-derived to estimate x_f and k_f simultaneously. In addition, I developed 1D flowback models under different boundary conditions to predict flowback behavior and estimate fracture properties for various flowback operation (constant q and constant BHP). To allow for a more general application

in a realistic case, I adopted superposition principle to apply the constant rate analytical solution to variable flow rate conditions.

3.2 Two Phase Flowback Model

As many researchers (Clarkson, 2012; Adefidipe et al., 2014a; Zhang & Ehlig-Economides (2014)) have shown, immediate gas breakthrough is a common behavior found in shale gas flowback, and the discussed single-phase models cannot be applied to shale formation. (Clarkson, 2012; Clarkson et al., 2012) proposed a semi-analytical model where two fracture parameters need to be adjusted simultaneously, for two-phase flowback analysis, which exhibits a degree of uncertainty, due to the non-uniqueness of the history-matching parameters. In this chapter, I propose a new two-phase flowback model, based on material balance equation and two-phase diffusivity equation of water phase. Applying the proposed two-phase flowback model, fracture properties can be evaluated.

As discussed earlier, flowback period can be subdivided into two distinct regions of EGP (with negative GWR slope) and LGP (with positive GWR slope). During EGP, gas production only sources from initial free gas stored in HF, and gas influx from matrix is negligible. During LGP, however, gas production sources from both HF and matrix. I first develop an analytical model to analyze two-phase flowback of EGP. Then the model is extended for LGP by incorporating matrix flow. Our methodology is similar to Adefidipe et al. (2014a); and Xu et al. (2016), where MB and diffusivity equation are applied to estimate fracture properties with flowback data. In literature, the previously proposed model (Adefidipe et al., 2014a; Xu et al., 2016) was based on gas diffusivity equation, which exhibits a high degree of non-linearity and brings about errors in estimating fracture properties. Our approach is based on water-phase diffusivity equation, where relative

permeability (k_{rw}) and saturation (s_w) of water are added to the single-phase flowback model (see section 3.1.4) to account for two-phase flow.

3.2.1 HF Flow without Matrix Influx (EGP)

To develop the EGP model, HF is treated as a closed system with negligible gas and water matrix influx, where fracture depletion is the driving mechanism (see Figure 3.1(b)). The material balance under fracture depletion is given by

$$\text{Produced Gas } (G_p) = \text{Initial Gas in Fracture } (G_{fi}) - \text{Remaining Gas in Fracture } (G_r), \tag{3.57}$$

where G_p, G_{fi} and G_r are all expressed at surface condition.

The following assumptions were made to develop the MB equation:

- only expansion of proppant is considered assuming aperture of fracture (w_f) is constant, and
- proppant compressibility (c_p) is pressure-independent.

Then pore volume in fracture (V_f) at any time can be expressed as a function of pressure drawdown and c_p by

$$V_f = V_{fi}\left(1 - c_p\left(P_i - P_f\right)\right), \tag{3.58a}$$

$$V_{fi} = whx_f\phi_f, \tag{3.58b}$$

where V_{fi} is the initial pore volume of fracture at the start of flowback operation.

Remaining water volume in fracture (V_{wr}) can be found by (Adefidipe et al., 2014b)

$$V_{wr} = \left(W_{fi} - W_p\right)B_w, \tag{3.59}$$

where W_{fi} is the initial water volume in fracture, and W_p is cumulative water production, all expressed at surface condition.

Then remaining gas in fracture (G_r) can be determined by

$$G_r = \frac{V_f - V_{wr}}{B_g}. \tag{3.60}$$

Substituting Equations (3.58b) – (3.60) into (3.58a), average fracture pressure (P_f) can be determined by

$$P_f = P_i - \frac{V_{fi} - \left((G_{fi} - G_p)B_g + (W_{fi} - W_p)B_w\right)}{V_{fi}c_p}, \tag{3.61}$$

where G_{fi} is the initial free gas volume in fracture, G_p is the cumulative gas production, B_g is the gas compressibility, and G_{fi} and G_p are expressed at surface condition.

Since B_g is pressure-dependent, appropriate iteration scheme needs to be adopted to determine P_f for each time point in flowback history. The average pressure profile is further used in water diffusivity equation to obtain fracture attributes.

For single-phase flowback, the diffusivity equation is given by

$$\frac{\partial^2 P}{\partial x^2} = \frac{1}{\eta}\frac{\partial P}{\partial t}. \tag{3.62}$$

For two-phase flow of water and gas in fracture, water saturation (s_w) and relative permeability of water (k_{rw}) should be included and two-phase diffusivity equation of water phase is:

$$\frac{\partial}{\partial x}\left(\frac{k_{rw}k_f}{\mu_w}\frac{\partial P}{\partial x}\right) = \phi_f\left(s_w c_w + s_w c_r + \frac{\partial s_w}{\partial P}\right)\frac{\partial P}{\partial t}. \tag{3.63}$$

To linearize the equation, water pseudo pressure (P_p) is defined by

$$P_p = \int_{P_b}^{P} \frac{k_{rw}}{\mu_w} dP. \tag{3.64}$$

Then, two-phase diffusivity equation can be expressed by

$$\frac{\partial^2 P_p}{\partial x^2} = \frac{\phi_f}{k_f}\mu_w \frac{s_w}{k_{rw}}\left(c_w + c_r + \frac{1}{s_w}\frac{\partial s_w}{\partial P}\right)\frac{\partial P_p}{\partial t}. \tag{3.65}$$

The diffusivity equation can be further linearized with water pseudo time (t_a) defined by

$$t_a = \frac{k_{rw}}{s_w} t. \tag{3.66}$$

The effective compressibility (c_{eff}) responsible for water production is defined by

$$c_{eff} = c_w + c_r + \frac{1}{s_w}\frac{\partial s_w}{\partial P}. \tag{3.67}$$

Applying definition of P_p and t_a, the linearized diffusivity equation is given by

$$\frac{\partial^2 P_p}{\partial x^2} = \frac{1}{\eta_{2-phase}}\frac{\partial P_p}{\partial t_a}, \tag{3.68a}$$

$$\eta_{2-phase} = \frac{k_f}{\phi_f c_{eff}\mu_w}. \tag{3.68b}$$

For two-phase flowback under BDF and constant BHP, the initial and boundary conditions are given by

$$P_p(x, 0) = P_{pi}, \tag{3.69}$$

$$P_p(0, t) = P_{pwf}, \tag{3.70}$$

$$\frac{\partial P_p(x_f,t_a)}{\partial x} = 0, \tag{3.71}$$

where P_{pi} is the pseudo pressure at initial fracture pressure and P_{pwf} is the pseudo pressure at P_{wf}.

Similar to the previous development for single-phase flowback model, the dimensionless group is applied to homogenize boundary conditions and solve the diffusivity equation. The dimensionless parameters are given by

$$P_{pD} = \frac{P_p - P_{pwf}}{P_{pi} - P_{pwf}}, \tag{3.72}$$

$$x_D = \frac{x}{x_f}, \tag{3.73}$$

$$t_D = t_a \frac{k_f}{\phi_f \mu_w x_f^2}, \tag{3.74}$$

where P_{pD} is the dimensionless pseudo pressure; x_D is the dimensionless distance; and t_D is the dimensionless pseudo time.

Applying dimensionless group, the two-phase diffusivity equation of water phase can be expressed by

$$\frac{\partial^2 P_{pD}}{\partial x_D^2} = \left(c_w + c_r + \frac{1}{s_w}\frac{\partial s_w}{\partial P}\right)\frac{\partial P_{pD}}{\partial t_D}. \tag{3.75}$$

The homogenized boundary conditions are given by

$$P_{pD}(x_D, 0) = 1, \tag{3.76}$$

$$P_{pD}(0, t_D) = 0, \tag{3.77}$$

$$\frac{\partial P_{pD}(1,t_D)}{\partial x} = 0. \tag{3.78}$$

To solve Equation (3.75) for fracture pressure, the partial differential equation should be linearized. The term $\frac{1}{s_w}\frac{\partial s_w}{\partial P}$ in the coefficient varies with time and space; thus, analytical expression cannot be obtained explicitly. Numerical differentiation is applied to evaluate this term at average pressure (P_f) and average water saturation ($\bar{s}_w$). To evaluate $\bar{s}_w$ of fracture, pore volume shrinkage is considered. The average water saturation in fracture can be obtained by

$$\bar{s}_w = 1 - \frac{W_p}{W_{fi}}, \tag{3.79a}$$

or

$$\bar{s}_w = \frac{(W_{fi} - W_p)B_w}{V_{fi}\left(1 - c_p\left(P_i - P_f\right)\right)}, \tag{3.79b}$$

where Equation (3.79a) is proposed by Clarkson (2012) and Equation (3.79b) is proposed by us, by considering the effect of proppant expansion on pore volume.

Using the separation of variables technique, pseudo pressure (P_p) can be expressed as a function of time and space by

$$\frac{P_p - P_{pwf}}{P_{pi} - P_{pwf}} = \sum_{n=1}^{\infty} \frac{4}{(2n-1)\pi} \sin\left(\frac{(2n-1)\pi}{2}\frac{x}{x_f}\right) \exp\left(-\frac{(2n-1)^2\pi^2}{4}\frac{k_f}{\phi_f \mu_w x_f^2}\int_0^{t_a} \frac{1}{s_w c_w + s_w c_r + \frac{\partial s_w}{\partial P}}\partial\tau_a\right) \tag{3.80}$$

To further simplify Equation (3.80), equivalent time (t_e) is defined by

$$t_e = c_{ti}\int_0^{t_a} \frac{1}{c_w + c_r + \frac{1}{s_w}\frac{\partial s_w}{\partial P}}\partial\tau_a, \tag{3.81a}$$

$$c_{ti} = c_r + s_{gi}c_{gi} + s_{wi}c_{wi}, \tag{3.81b}$$

where c_{ti} is the total compressibility determined based on initial water saturation in fracture (s_{wi}), initial gas saturation in fracture (s_{gi}), water compressibility at P_i (c_{wi}), and gas compressibility at P_i (c_{gi}).

The rate normalized pseudo pressure (*RNP*) is averaged across the fracture and determined as only a function of t_e by

$$RNP = \frac{x_f}{2} \frac{1}{\sum_{n=1}^{\infty} \exp\left(-\frac{(2n-1)^2\pi^2}{4} \frac{k_f}{\phi_f \mu_w x_f^2 c_{ti}} t_e\right)}, \tag{3.82a}$$

$$RNP = \frac{P_{pi} - P_{pwf}}{q_w}. \tag{3.82b}$$

If the long-time approximation introduced by Wattenbarger et al. (1998) is applied, the infinite summation term can be truncated to only the first term, and Equation (3.82a) can be simplified to:

$$RNP = \frac{1}{2} \frac{x_f}{whk_f} \exp\left(\frac{k_f}{\phi_f \mu_w x_f^2} \frac{t_e}{c_{ti}}\right), \tag{3.83a}$$

which in field unit would be

$$RNP = 79.01 \frac{x_f B_w}{whk_f} \exp\left(0.0156 \frac{k_f}{\phi_f \mu_w x_f^2} \frac{t_e}{c_{ti}}\right). \tag{3.83b}$$

In the semi-log plot of *RNP* vs. t_e, linear relation can be established. The linear relation can be expressed by

$$ln(RNP) = m\, t_e + b, \tag{3.84a}$$

$$m = \frac{0.0156\, k_f}{\phi_f \mu_w x_f^2 c_{ti}}, \tag{3.84b}$$

$$b = ln\left(\frac{79.01\, x_f B_w}{whk_f}\right), \tag{3.84c}$$

where m is the slope, and b is the intercept of the fitted linear line of Equation (3.83).

The $\frac{k_f}{x_f^2}$ can be evaluated from the slope. If either x_f or k_f is known, the other property can be determined.

The workflow to determine fracture properties can be summarized as:

1. Obtain flowback history from field data, which typically includes W_p, G_p and q_w vs. time,
2. Use appropriate iteration scheme to determine average fracture pressure profile using Equation (3.61),
3. Update $\bar{s}_w$ using Equation (3.79) and evaluate corresponding $\frac{1}{s_w}\frac{\partial s_w}{\partial P}$ at average fracture pressure with appropriate numerical differentiation method, and
4. Determine RNP and t_e as defined in Equations (3.82b) and (3.81a). From the semi-log plot, fracture properties (x_f and k_f) can be evaluated.

The water diffusivity equation 2-phase flowback model for EGP can be summarized by

$$\ln(RNP) = \frac{0.0156\, k_f}{\phi_f \mu_w x_f^2} t_e + \ln\left(\frac{79.01\, x_f B_w}{whk_f}\right), \tag{3.85a}$$

$$t_e = c_{ti} \int_0^{t_a} \frac{1}{c_w + c_r + \frac{1}{s_w}\frac{\partial s_w}{\partial P_f}} \partial \tau_a, \tag{3.85b}$$

$$c_{ti} = c_r + s_{gi} c_{gi} + s_{wi} c_{wi}, \tag{3.85c}$$

$$t_a = \frac{k_{rw}}{s_w} t, \tag{3.85d}$$

$$RNP = \frac{P_{pi} - P_{pwf}}{q_w}, \tag{3.85e}$$

$$P_p = \int_{P_b}^{P} \frac{k_{rw}}{\mu_w B_w} dP. \tag{3.85f}$$

3.2.2 HF Flow with Matrix Influx (LGP)

Although previous field observations (Clarkson, 2012; Ghanbari et al., 2013; Zhang & Ehlig-Economides, 2014) established the presence of EGP or V-shape in GWR diagnostic plot in flowback on shale gas formation, EGP cannot always be recognized in flowback data, as seen in the field data of Marcellus shale released by Clarkson and Williams-Kovacs (2013b), where GWR increases monotonically with cumulative gas production or production time. Due to the inadequate quality of early flowback data collection, or perhaps the presence of immediate gas breakthrough from matrix to fracture, the EGP model without matrix influx cannot generally be applied to analyze the flowback on shale gas formation. Therefore, mathematical model of LGP should be developed to analyze two-phase flowback on shale gas formation practically.

The conceptual model of two-phase flowback is described in Figure 3.1(c). The most important is the fact that water flow in fracture can be treated as a one-dimensional, two-phase diffusivity problem. Therefore, the same water diffusivity equation model of EGP can be applied for LGP period. The model is given by

$$\ln(RNP) = \frac{0.0156\, k_f}{\phi_f \mu_w x_f^2} t_e + \ln\left(\frac{79.01\, x_f B_w}{whk_f}\right). \tag{3.58a}$$

Linear relationship can be found between $\ln(RNP)$ and t_e and fracture properties (x_f or k_f) can be estimated from the slope. However, $\frac{1}{s_w}\frac{\partial s_w}{\partial P_f}$ needs to be evaluated in a way that accounts for gas matrix influx.

If gas flow from matrix to fracture presents, depletion of pressure becomes smoother, since total compressibility becomes larger. MB should be to consider the effect of gas flow in matrix and P_f can be obtained as a function of time. To avoid the complexity brought in by coupling flow of gas, a common assumption that primary fracture network and stimulated matrix volume are under a homogeneous pressure is applied (Clarkson, 2012; Clarkson & Williams-Kovacs, 2013b). Although the proposed MB is not accurate in estimation of P_f, it can still be applied to evaluate the change in $\bar{s}_w$ with respect to P_f since only rate of change in P_f matters when applying the two-phase flowback model and it greatly reduces the computational complexity by avoiding the calculation of amount of gas matrix influx into fracture at each time point. In **Chapter 4**, sensitivity analysis has been conducted to test the accuracy of the proposed material balance.

The main assumptions behind this model can be summarized as:

- Water production only sources from primary fracture network,
- Fracture and stimulated matrix volume are under homogeneous pressure decline rate,
- BDF of gas and water in fracture, and
- BDF of gas in stimulated matrix and no flow boundary are established between two nearby clusters.

For EGP, average fracture pressure (P_f) can be found from material balance by

$$P_f = P_i - \frac{V_{fi} - \left((G_{fi} - G_p)B_g + (W_{fi} - W_p)B_w\right)}{V_{fi}c_p}. \quad (3.61)$$

For LGP case, matrix volume needs to be added to determine depletion of pressure in matrix-fracture system and, thus, initial pore volume in fracture and stimulated matrix (V_{pi}) can be determined by

$$V_{pi} = x_f w_f h \phi_f + x_f L_f h \phi_m, \quad (3.86)$$

where L_f is fracture spacing, and ϕ_m is matrix porosity.

Initial free gas storage (G_i) in fracture and stimulated matrix can be determined by

$$G_i = \frac{x_f h}{B_{gi}}(w_f \phi_f s_{gi} + L_f \phi_m s_{gim}), \quad (3.87)$$

where s_{gi} is initial gas saturation in fracture, and s_{gim} is initial gas saturation in matrix.

Initial water storage (W_i) in fracture and stimulated matrix is given by

$$W_i = \frac{x_f h}{B_w}(w_f \phi_f s_{wi} + L_f \phi_m s_{gim}), \quad (3.88)$$

where s_{wi} is initial water saturation in fracture. s_{wim} is initial water saturation in matrix.

Applying MB, the average pressure ($\bar{P}$) for the fracture-matrix system can be obtained by

$$\bar{P} = P_i - \frac{V_{pi} - \left((G_i - G_p)B_g + (W_{fi} - W_p)B_w\right)}{V_{pi}c_r}. \quad (3.89)$$

Appropriate convergence method is required to find $\bar{P}$ since gas properties (B_g) is a function of pressure. Once $\bar{P}$ is determined, t_e and RNP can be evaluated with Equations (3.81a) – (3.82a).

According to Equation (3.85a), a linear correlation can be established between $ln(RNP)$ and t_e for the production period when the assumption that fracture and stimulated matrix volume are under homogeneous pressure decline rate is valid. When a flowback interval with a unit slope presents in the log-log plot of $ln(RNP)$ vs. t_e, it should correspond a straight-line relationship when plotting $ln(RNP)$ against t_e ,in normal scale. Then the analytical model is valid to be applied.

The corresponding slope in the linear fitting line is same as EGP model and is given by

$$m = \frac{0.0156\, k_f}{\phi_f \mu_w x_f^2}. \tag{3.84b}$$

If k_f or x_f is available, then the other fracture properties can be estimated. The workflow to apply water diffusivity equation in LGP period is same as in EGP period except a modified material balance equation (Equation (3.94)) should be changed to determine average fracture pressure (P_f).

In summary, the developed mathematical model for two-phase flowback is applicable to flowback with, and without, gas influx from matrix. For EGP, the proposed MB can predict average fracture pressure (P_f) accurately; for LGP, the proposed MB cannot give exact estimate of P_f but instead can evaluate fracture pressure decline rate accurately for some flowback time interval when unit-slope can be found in log-log plot of $\ln(RNP)$ vs. t_e. Compared with previously developed two-phase flowback model (Clarkson, 2012; Clarkson & Williams-Kovacs, 2013b; Adefidipe et al., 2014b; Ezulike & Dehghanpour, 2014; Xu et al., 2015a; Xu et al., 2016), the proposed model based on two-phase diffusivity

equation of water phase exhibits high degree of linearity and estimates fracture properties analytically and explicitly.

CHAPTER 4 : RESULTS AND DISCUSSIONS

4.1 Single-Phase Flowback Model

The single-phase flow case has water flowing in the fracture only, and no gas flows from matrix and in fracture. CMG (IMEX) simulator is used to model the 1D fracture and to validate the analytical models. For single-phase flowback, only fracture grids are considered in the numerical model. Since all HF are assumed to be symmetrical, only one fracture is simulated here. Figure 4.1 shows the simulated segment with HF width of w_f (i-direction) and fracture half-length of x_f (j-direction).

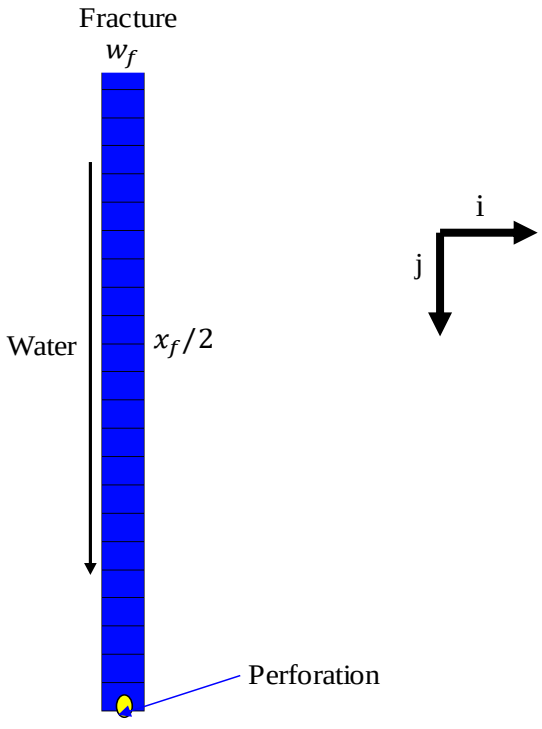

Figure 4.1: Numerical model for single-phase flowback without matrix influx.

The number of grids along j direction has a major effect on the linear flow of water in the system. Number of grids depends on many parameters such as grid size, and fracture permeability. As fracture permeability increases, finer grid number is assigned to avoid truncation error in numerical simulation. The input reservoir parameters in the simulator are tabulated in Table 4.1.

Table 4.1: Input of flowback properties for single-phase numerical model.

Initial pressure, P_i(psi)		2650
Reservoir temperature, T (°F)		160
Specific gravity, SG_g		0.65
Water compressibility, c_w(psi^{-1})		3.33×10^{-6}
Fracture porosity, ϕ_f (fraction)		0.8
Rock compressibility, c_r (psi^{-1})		1×10^{-6}
Reservoir thickness, h (ft)		300
Well constraint		q_w or P_{wf}
Flowback rate, q_w(stb/day)		2
Flowing BH pressure, P_{wf}(psi)		500
Fracture width, w_f (ft)		0.1
Water formation volume factor, B_w(bbl/STB)		1.029
Water viscosity @P_i, μ_w(cp)		0.331
Water density @P_i, ρ_w(lb/ft^3)		61.9615
Fracture half length, x_f(ft)		500
Fracture permeability, k_f(mD)	Example A	15
Fracture permeability, k_f(mD)	Example B	150
Fracture permeability, k_f(mD)	Example C	1500

In the 1D fracture model, only one grid is assigned in i and k direction to exclude the water flow toward perforation and in vertical direction. Refinement of grid distribution is applied in j direction to accurately capture linear flow of water along the fracture (j-direction). Grid distribution is shown in Table 4.2.

Table 4.2: Grid distribution for different simulation cases.

Orientation	Number of grids	
Fracture width (i)	1	
Fracture half-length (j)	Example A	100
	Example B	1000
	Example C	10000
Fracture height (k)	1	

The assumptions of the numerical model can be summarized as:

- No matrix influx of water,
- Gravity effect is negligible,
- Open-hole production is assumed, and
- Single phase linear flow inside fracture.

4.1.1 Constant q Models

In conventional well testing, reservoir properties can be estimated from pressure drawdown or pressure build up test. The same methodology is applied to estimate fracture properties during flowback. Constant terminal rate is set in the simulator. This section is to validate analytical models developed for constant q with numerical simulation. The analytical models are applied to predict pressure drawdown in fracture with time (i.e., forward prediction of pressure) and compared against numerical simulation. Then the analytical models are used to estimate fracture properties (i.e., inverse estimation of HF half-length and permeability) with the flowback data obtained from the numerical model.

The validation of constant q models (Sec. 4.1.1) can be subdivided into two parts. The first part is to test the accuracy of BDF Constant q (PSS) Models (Sec. 3.1.1, 3.1.2, and 3.1.3). The second part is to test the accuracy of Transient Constant q Model (Sec 3.1.5), which is

1D Analytical Model (Case 3) and compared against the BDF Constant q Model (Sec 3.1.3), the 1D Analytical Model (Case 1) to illustrate the proper range of application of the different analytical models.

The validation starts with BDF Constant q (PSS) Models (Sec. 3.1.1, 3.1.2 and 3.1.3). After short period of transient flow, BDF can be established. Since constant rate is assumed in the production, PSS flow regime can be expected (i.e., constant pressure depletion rate along HF). Therefore, constant flowback rate model in numerical simulation can be used to validate the PSS mathematical model for single-phase flowback.

As discussed in **Chapter 3**, Abbasi et al.'s model, Alkouh et al.'s models and 1D model (Case1) (Sec. 3.1.1-3.1.3) are categorized as PSS model. In this work, I first predict P_{wf} with time during flowback, with one set of rock and fluid properties using PSS model, and compare the results against numerical simulation. The rock and fluid properties are described in Table 4.1. In addition, fracture attributes can be estimated from the flowback data output from the numerical model when fracture properties are unavailable. Accuracy of mathematical models can be illustrated by determining the discrepancy between estimated value from the mathematical models and input value in the simulator.

As discussed, the general formula PSS mathematical model for single-phase flowback is given by $RNP = mt + b$. To model the flowback behavior during transient period, infinite summation term in the 1D analytical model (i.e., Case1, Equation 3.21) should be included. I employed 10,000 terms for the summation term.

Three cases with k_f values of 15, 150, and 1500 mD (Example A, B, and C) are considered to mimic low, medium, and high fracture conductivity. The results of prediction for all

cases are shown in Figures 4.2-4.4. These comparisons show that Abbasi et al.'s and Alkouh et al.'s models cannot predict flowing pressure during transient period, which is expected. By including the summation term, the 1D analytical model (Case 1) can be used for entire flowback period.

From these figures, it can be observed that the stabilization time (the time at which BDF begins) reduces from 0.1 days to 0.001 days as k_f increases, resulting in faster establishment of BDF. In addition, Abbasi et al.'s and Alkouh et al.'s models can only be applied to BDF, where a match with numerical simulation can be found at late times. Unlike the developed 1D model (Case 1), Abbasi et al.'s and Alkouh et al.'s models can only be used when the transient period is short (e.g., high fracture permeability).

Now I examine the capability of the models in estimation of the fracture properties. In the Abbasi et al.'s model, x_f can be determined by

$$x_f = \sqrt{\frac{bk_f}{52.7\phi_f c_t \mu_w m}}, \tag{4.1}$$

where m and b are slope and intercept of the RNP vs. time plot, respectively.

In the Alkouh et al.'s and 1D (Case 1) model, x_f and k_f can be estimated using

$$x_f = \frac{5.615 B_w}{whmc_t\phi_f}, \tag{4.2}$$

$$k_f = 295.77 \frac{x_f \mu_w B_w}{bwh}. \tag{4.3}$$

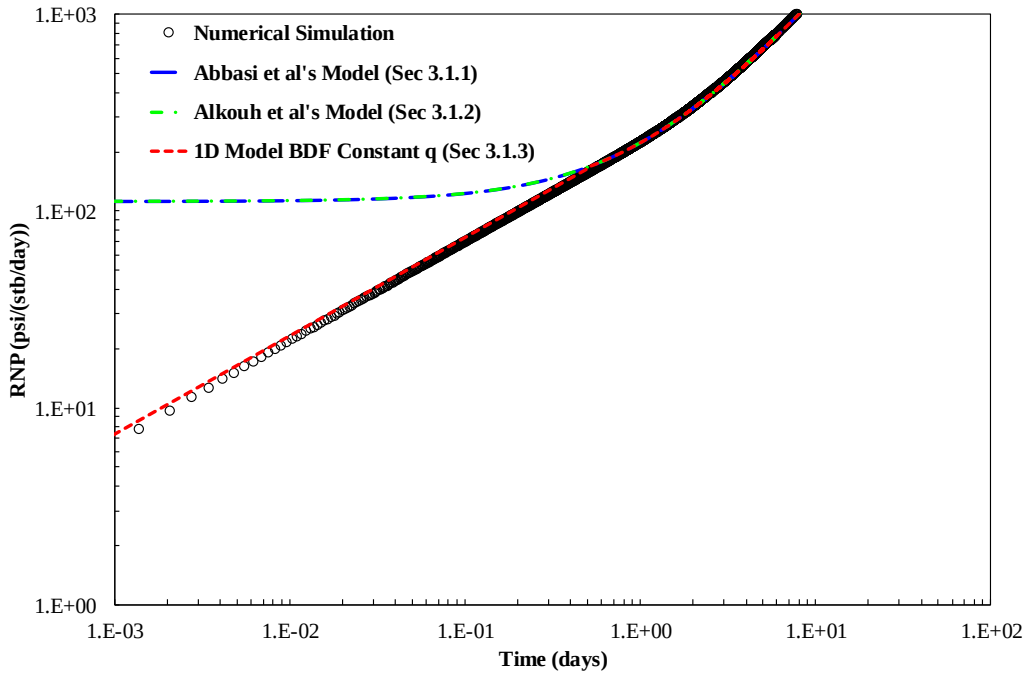

Figure 4.2: Prediction of *RNP* using Abbasi et al.'s Model, Alkouh et al.'s Model, and 1D Model BDF Constant *q* during flowback period compared against numerical results at k_f =15 mD (Example A).

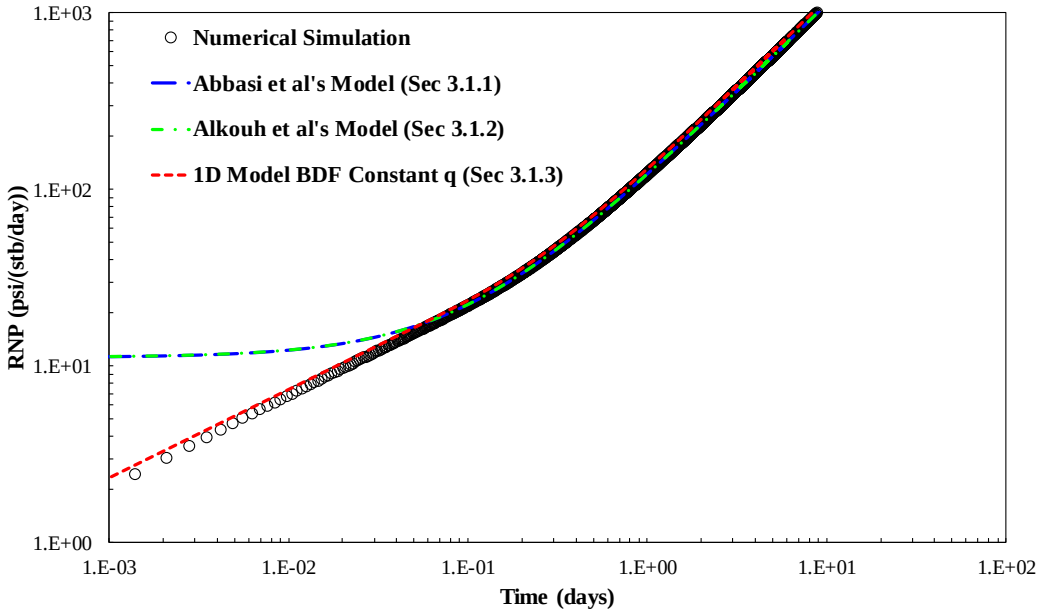

Figure 4.3: Prediction of *RNP* using Abbasi et al.'s Model, Alkouh et al.'s Model, and 1D Model BDF Constant *q* compared against numerical results at k_f =150 mD (Example B).

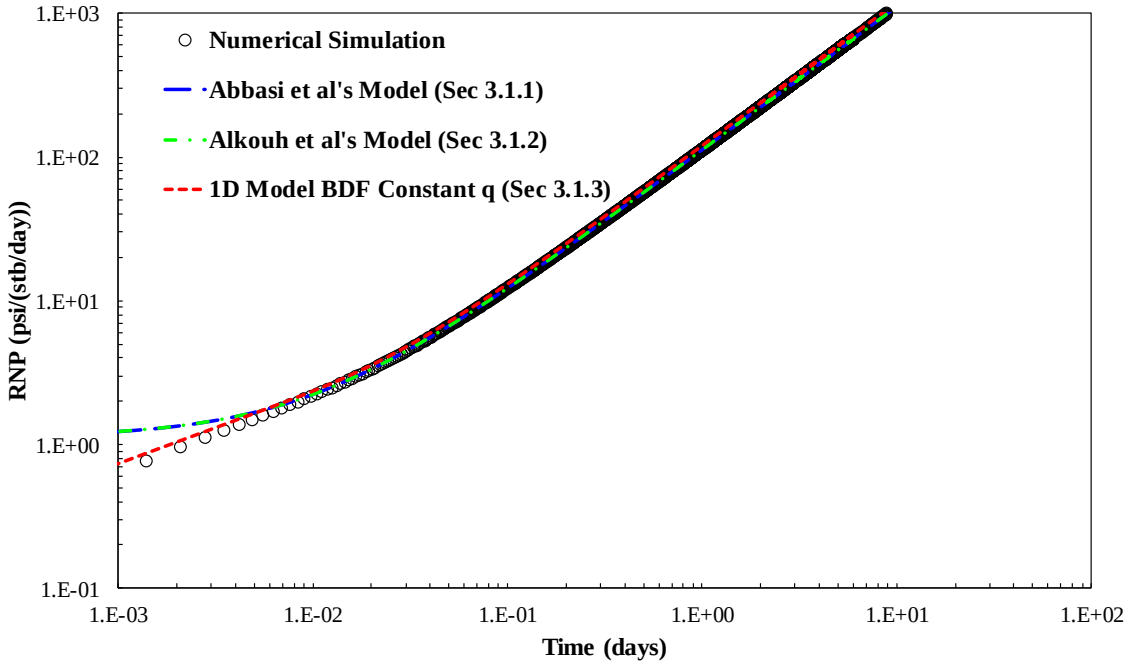

Figure 4.4: Prediction of *RNP* using Abbasi et al.'s Model, Alkouh et al.'s Model, and 1D Model BDF Constant q compared against numerical results at k_f =1500 mD (Example C).

Figure 4.5 provides the water production and pressure data for Case A having k_f=15 mD. These data are obtained from numerical simulations by using data given in Tables 4.1 and 4.2. Figure 4.6 shows the *RNP* changes with time of the production data in a log-log plot (diagnostic plot), where the data corresponding to BDF can be identified by unit-slope.

From the diagnostic plot, the estimated stabilization time is about one day, which is very close to the time that can be obtained using (Behmanesh et al. (2014)),

$$y_{inv} = c\sqrt{\left(\frac{k}{\phi\mu c_t}\right)_i t}, \tag{4.4}$$

where c is the constant rate production constant and is equal to 0.113.

Using Equation (4.4) the stabilization time for Example A would be 1.5 days, which agrees with the BDF window determined from the log-log plot. Knowing the stabilization time, I use BDF data from Example A to plot *RNP* vs. time as shown in Figure 4.7. Then I extract slope and intercept by fitting data with a straight line. The straight-line equation is

$$RNP = 112.06\, t + 110.58, \tag{4.5}$$

where slope is 112.06 psi/stb, and intercept is 110.58 $psi/(stb/day)$. Having slope and intercept, I use Equations (4.1) – (4.3) to estimate x_f and k_f, which are given in Table 4.3 for all three examples.

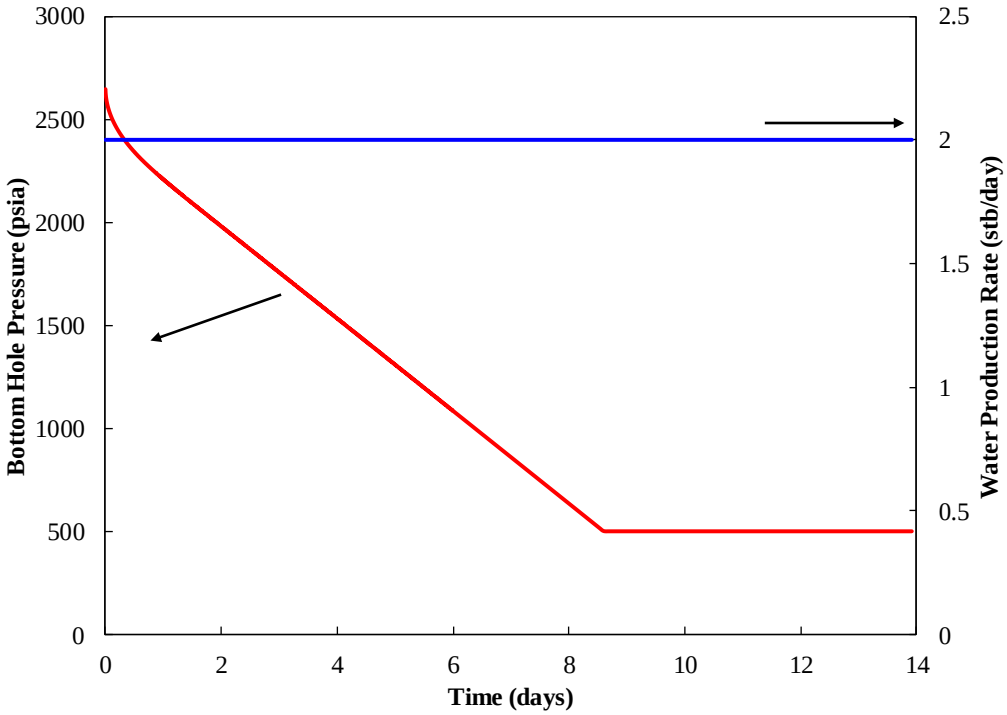

Figure 4.5: Flowback history from numerical simulation for k_f =15 mD (Example A) based on the simulation input and grid discretization data listed in Table 4.1 and Table 4.2, respectively.

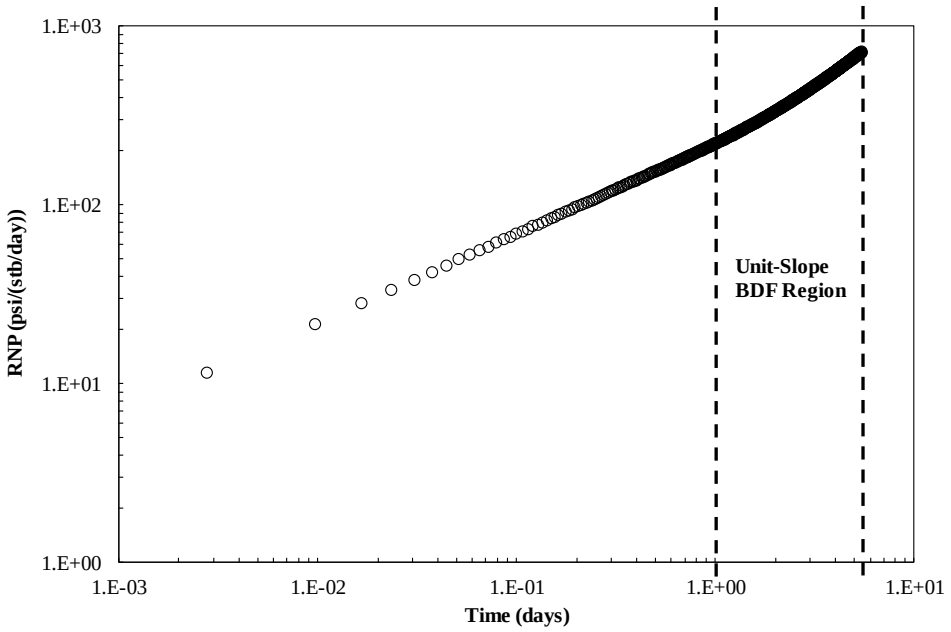

Figure 4.6: Diagnostic plot of flowback data for k_f =15 mD, where t_{BDF} = 1 day.

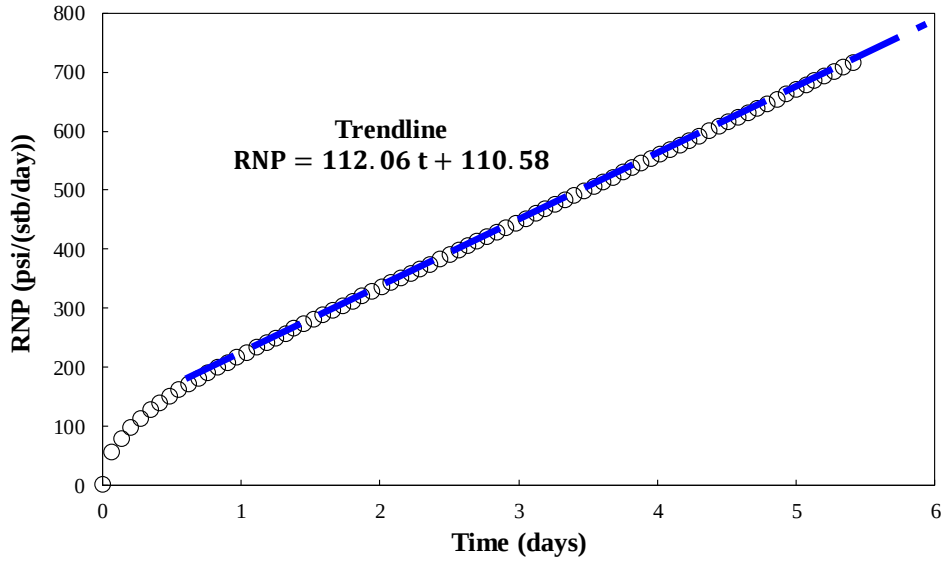

Figure 4.7: *RNP* vs. time plot for BDF data of the flowback period.

The estimated fracture properties from the three PSS models are within a 1% error margin with numerical input value, which proves the accuracy of the three PSS models. Abbasi et al.'s model can only estimate fracture half-length, not fracture permeability, but wellbore storage is considered. When wellbore storage is comparable to fracture storage, then Abbasi et al.'s model is more accurate than the other two models, where only fracture is considered.

Table 4.3: Summary of results for fracture properties obtained from three PSS models.

Example	**Model**	**x_f (ft)**	**k_f (mD)**	**x_f error**	**k_f error**
Example A	Numerical Simulation Input	500.00	15.00		
	Abbasi et al. (Sec 3.1.1)	495.07	-	0.99%	-
	Alkouh et al. (Sec 3.1.2)	496.1	15.1	0.77%	0.66%
	1D BDF Constant *q* (Sec 3.1.3)	496.1	15.1	0.77%	0.66%
Example B	Numerical Simulation Input	500.0	150.0		
	Abbasi et al. (Sec 3.1.1)	496.2	-	0.76%	-
	Alkouh et al. (Sec 3.1.2)	497.4	151.08	0.51%	0.69%
	1D BDF Constant *q* (Sec 3.1.3)	497.4	151.08	0.51%	0.69%
Example C	Numerical Simulation Input	500.0	1500.0		
	Abbasi et al. (Sec 3.1.1)	497.5	-	0.50%	-
	Alkouh et al. (Sec 3.1.2)	497.2	1488.6	0.56%	0.76%
	1D BDF Constant *q* (Sec 3.1.3)	497.2	1488.6	0.56%	0.76%

Validation of transient constant q model, which is 1D Analytical Model (Case 3) is conducted with the same numerical model (see Figure 4.1). As seen in the results shown in Figure 4.3 and 4.4, transient period is very short and not observable in conventional flowback data for fracture with medium to high conductivity. However, if available, analysis of transient flowback data provides the earliest opportunity to evaluate stimulation job for poor-treatment fractures.

According to Equation (3.41), during transient period, there is a linear relation between *RNP* and $\sqrt{t}$. The slope of fitted line can be employed to estimate fracture permeability using

$$k_f = 6344 \frac{B_w^2 \mu_w}{w_f^2 h^2 \phi_f c_t m^2}. \tag{4.6}$$

Using information from the same three examples discussed earlier, the predictability of the transient model is examined. The transient model is first applied to predict change in *RNP* with time for transient flowback period. Then with the transient flowback data obtained from numerical simulation, the analytical model is used to estimate fracture permeability (Equation (4.6)). The prediction of *RNP* with time for all three cases (Example A, Example B, and Example C) are shown in Figures 4.8-4.10 and compared against 1D analytical model (Case 1), which is a PSS model, and the numerical simulation to illustrate accuracy and the proper interval of application of 1D model (Case 3), which is a transient model. The comparisons made in these figures show that the transient model can accurately predict the transient data obtained from numerical simulation.

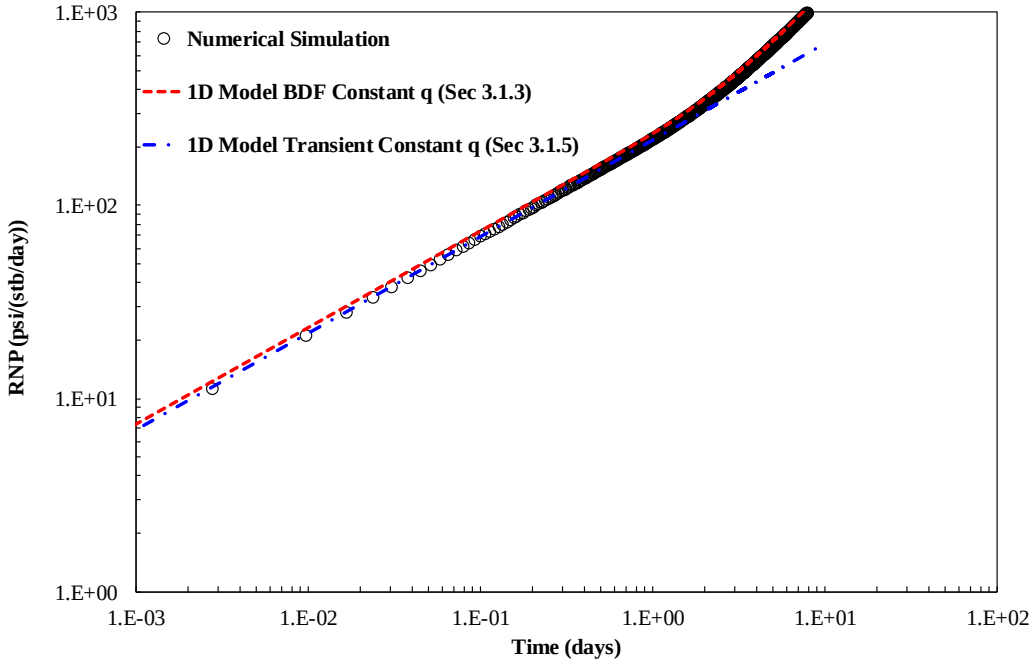

Figure 4.8: Prediction of *RNP* using 1D model BDF Constant *q* and 1D Model Transient Constant *q* against numerical results at k_f =15 mD (Example A).

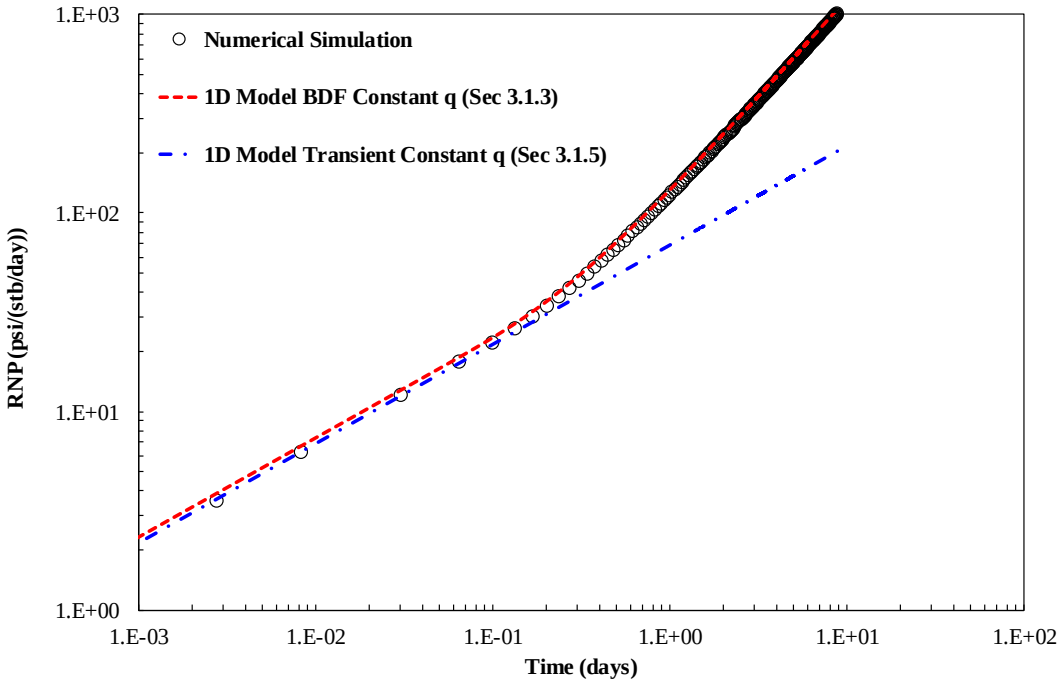

Figure 4.9: Prediction of *RNP* using 1D model BDF Constant *q* and 1D Model Transient Constant *q* compared against numerical results at k_f =150 mD (Example B).

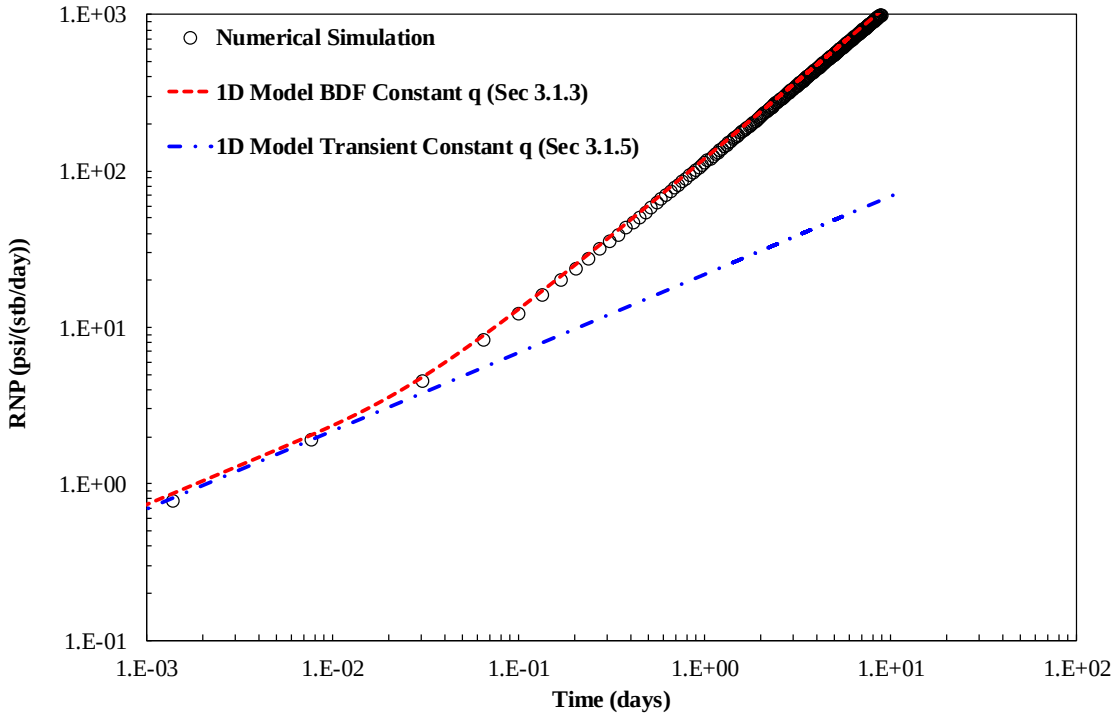

Figure 4.10: Prediction of *RNP* using 1D model BDF Constant q and 1D Model Transient Constant q compared against numerical results at k_f =1500 mD (Example C).

To estimate fracture permeability using transient data, I use the corresponding numerical data to plot *RNP* vs. $\sqrt{t}$ and to obtain slope. For example, in Example A, transient period lasted 12 hrs. Using these data, the straight-line that fits the data would be

$$RNP = 219.53\,\sqrt{t}, \tag{4.7}$$

from which the slope would be 219.53 $psi\sqrt{day}/stb$, and therefore k_f = 15.08 mD is obtained using Equation (4.6). A summary of estimated k_f values for all three examples are given in Table 4.4. These results reveal that the 1D analytical model (Case 3) can be used to accurately estimate fracture permeability.

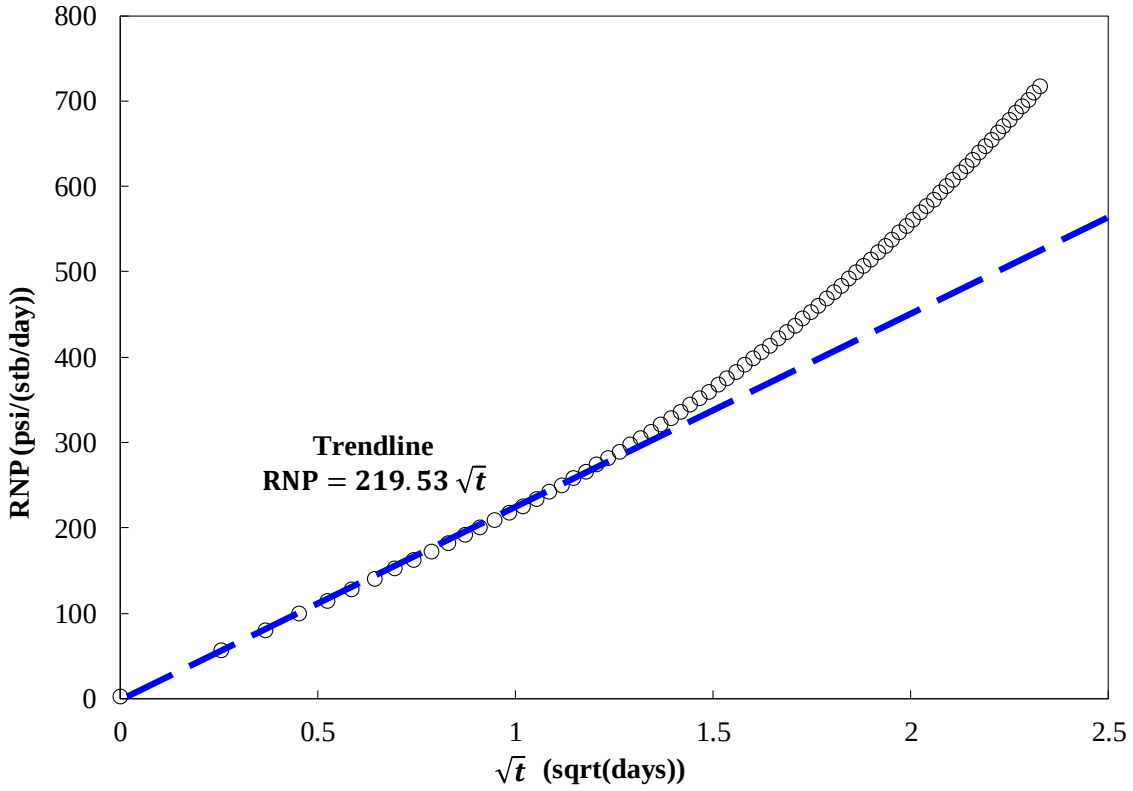

Figure 4.11: *RNP* is plotted against square root of *t* using transient flowback data, where linear fitted line is drawn as described in Equation (4.7).

Table 4.4: Summary of estimated fracture permeability (k_f) from 1D model (Case 3).

Example	k_f input (mD)	k_f estimate (mD)	k_f error
Example A	15.00	15.08	0.50%
Example B	150.00	150.88	0.59%
Example C	1500.00	1486.9	0.87%

4.1.2 Constant BHP Models

This section validates the analytical models developed for flowback under constant BHP (Sec. 3.1.4 and 3.1.6), following the same workflow of validation. The analytical models are first applied to predict flowback rate with time, and compared against numerical simulation. Then the analytical models are applied to estimate fracture properties with flowback data output from the numerical model (see Figure 4.1). The only modification in the numerical simulation is that well constraint is changed from constant q to constant BHP, where the numerical value is 500 psi. The rest of inputs in simulator are set as listed in Table 4.1.

As discussed, 1D Analytical model (Case 2) and (Case 4) are applicable in BDF period and transient period, respectively. 1D Analytical Model (Case 2) is compared with 1D Analytical Model (Case 4) to illustrate the proper range of application of the models under different boundary conditions.

The models are given by

$$RNP = \frac{887.31\, B_w \mu_w}{k_f w_f h \sum_{n=1}^{\infty} \frac{2}{x_f} e^{-\frac{0.001582(2n-1)^2 \pi^2 t k_f}{\phi_f c_t \mu_w x_f^2}}}, \tag{3.30}$$

$$RNP = 125 \frac{B_w}{w_f h} \sqrt{\frac{\mu_w t}{k_f \phi_f c_t}}, \tag{3.50}$$

Where Equation (3.30) is valid for flowback in BDF, and Equation (3.50) is valid for flowback in transient period.

Three numerical examples (Example A, B and C) are applied to validate the analytical models. The prediction of *RNP* with the analytical models are compared against the numerical simulation and the results are shown in Figures 4.12, 4.13 and 4.14.

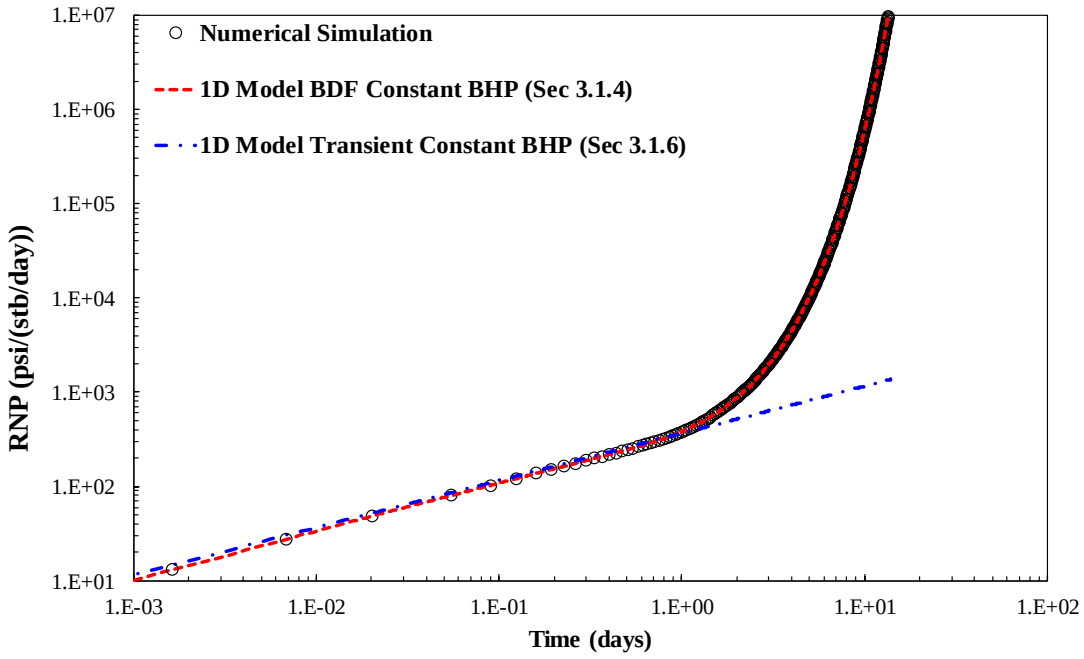

Figure 4.12: Prediction of *RNP* using 1D model BDF Constant BHP and 1D Model Transient Constant BHP against numerical results at k_f =15 mD (Example A).

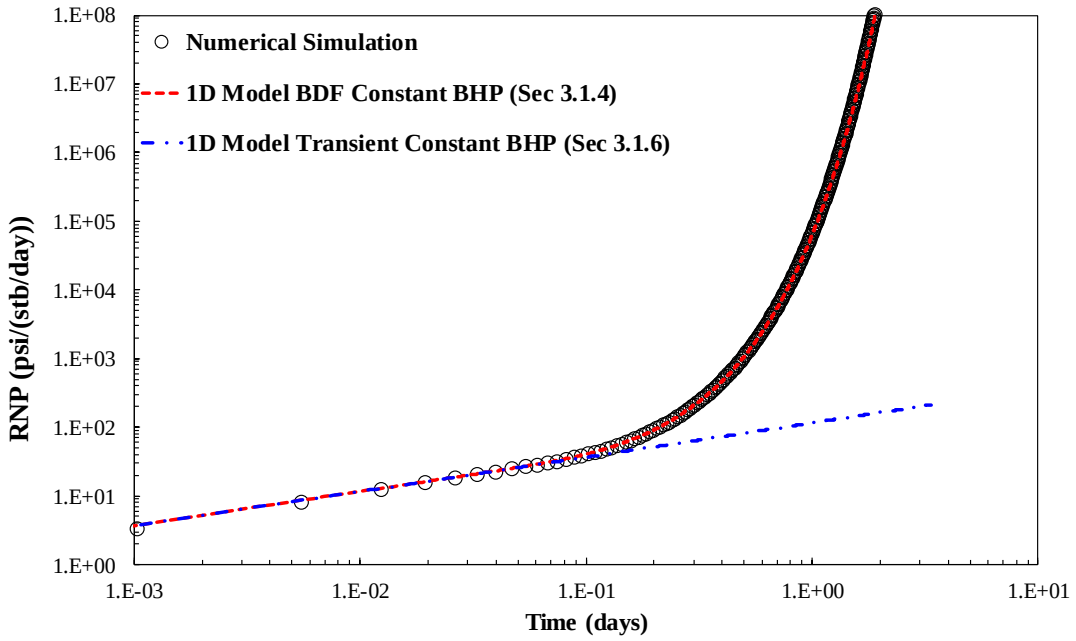

Figure 4.13: Prediction of *RNP* using 1D model BDF Constant BHP and 1D Model Transient Constant BHP against numerical results at k_f =150 mD (Example B).

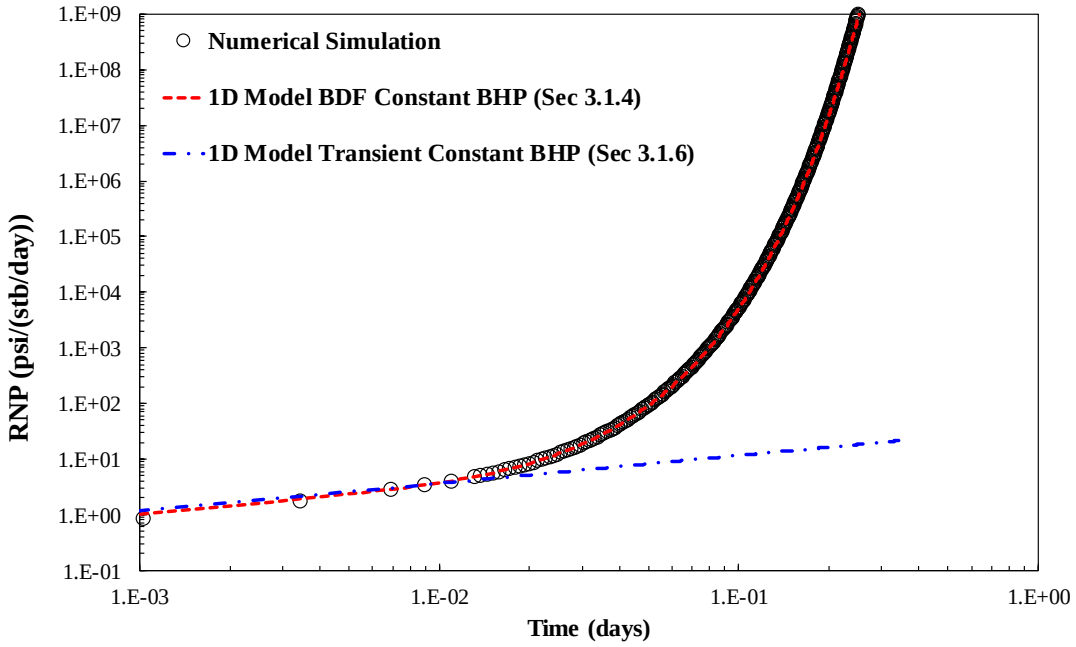

Figure 4.14: Prediction of *RNP* using 1D model BDF Constant BHP and 1D Model Transient Constant BHP against numerical results at k_f =1500 mD (Example C).

As fracture permeability increases from 15 mD to 1500 mD, transient period decreases from 1- to 0.01-day. Observable discrepancy between 1D analytical model (Case 4) and the numerical simulation can be found in late flowback period, which agrees with the boundary condition applied in the development of the transient model. The 1D analytical model (Case 2) can successfully history-match numerical simulation for the entire flowback period, where the first 1000 terms are included in the infinite summation term in Equation (3.30).

To estimate fracture properties, explicit expression to estimate fracture properties is required. However, 1D analytical model (Case 2) cannot solve for the fracture properties explicitly; 1D analytical model (Case 2) is applied instead, to estimate fracture properties with flowback data from transient period.

As discussed in **Chapter 3**, linear correlation can be found between *RNP* and $\sqrt{t}$ in transient period and fracture permeability can be estimated from slope of the fitted linear line by

$$k_f = 15625 \frac{B_w^2 \mu_w}{m^2 w^2 h^2 \phi_f c_t}, \tag{4.8a}$$

$$c_t = c_r + c_w. \tag{4.8b}$$

It needs to be pointed out that c_r should not be neglected to determine c_t since the numerical value of c_r is comparable to c_w.

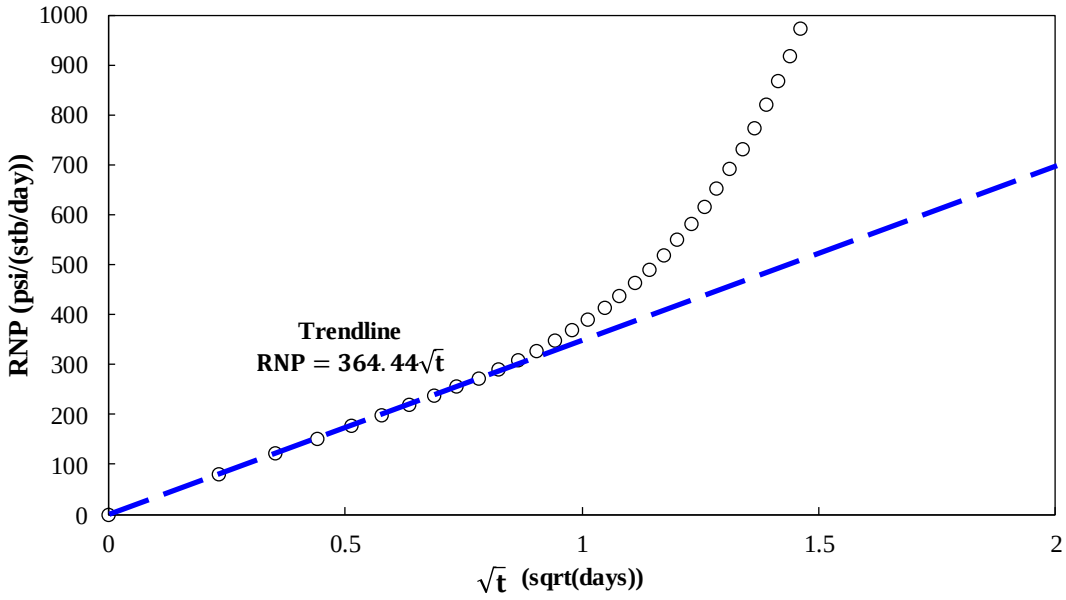

Figure 4.15: *RNP* vs. time plot with flowback data from transient period.

Linear relationship between *RNP* and $\sqrt{t}$ can be expressed by

$$RNP = 364.44\,\sqrt{t}, \tag{4.9}$$

where slope of the fitted linear line is $364.44\ psi\sqrt{day}/stb$.

Substituting into Equation (4.8a), k_f can be determined. In this work, we worked on three examples from very low fracture permeability 15 mD to high fracture permeability 1500 mD to test the generality of the 1D Analytical (Case 4). The results of estimation of k_f for all three cases are listed in Table 4.5.

Table 4.5: Summary of estimated fracture permeability (k_f) from 1D model (Case 3).

Example	k_f input (mD)	k_f estimate (mD)	k_f error
Example A	15.00	15.66	4.4%
Example B	150.00	156.92	4.6%
Example C	1500.00	1570.09	4.7%

The estimated fracture permeability from 1D Analytical Model (Case 4) are within 5% error with the numerical inputs, which validates the constant BHP mathematical model in application. For 1D analytical model (Case 2), explicit expression is required to estimate fracture attributes, where the infinite summation term can be truncated to only include the first term, as Wattenbarger et al. (1998) suggested. Then fracture half-length can be determined with 1D analytical model (Case 2). It is just a further one-step simplification, but I do not further develop it here, since the purpose is to validate the accuracy of the constant BHP models.

4.1.3 Variable q Models

This section is the application of analytical models proposed for flowback with variable rate (Sec 3.1.7 and 3.1.8). As discussed in **Chapter 3**, analytical solutions developed under constant q flowback for BDF and transient period are superimposed to solve flowback problem under variable q. With variable flowback rate schedule (see Figure 4.16) set in the numerical simulation, P_{wf} can be predicted with time analytically and compared against numerical simulation. Then applying the analytical models with flowback data output from the numerical model (see Figure 4.1), fracture properties can be estimated from the linear

relationship between pressure drawdown and defined superposition time for BDF and transient period.

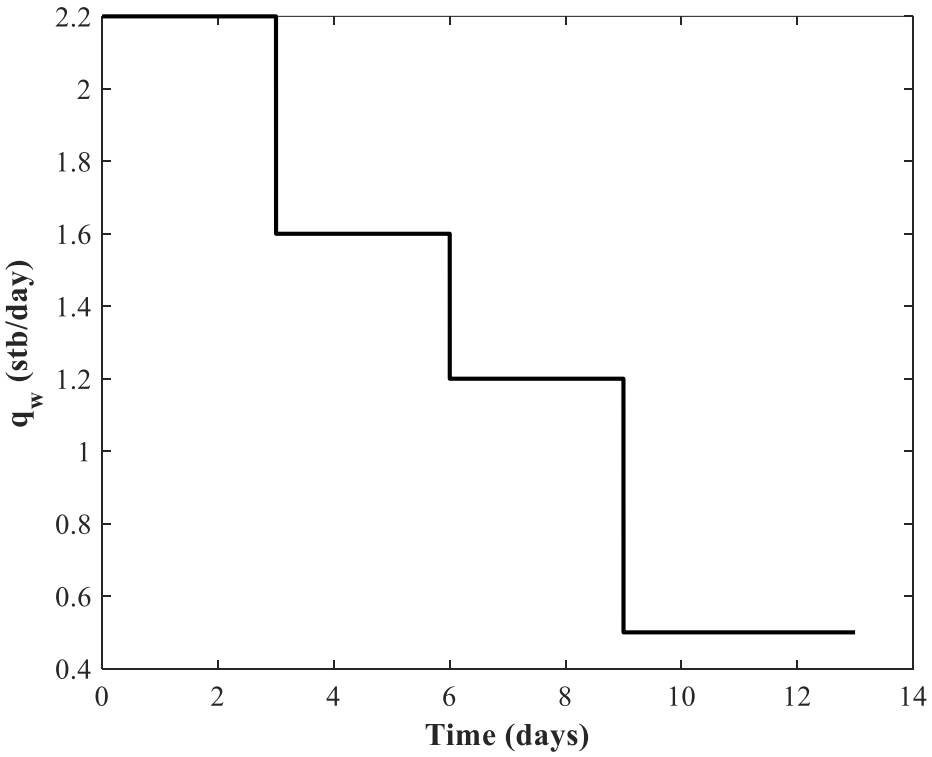

Figure 4.16: Variable flowback rate schedule with time input in numerical simulator. To mimic the real field operation, flowback rate drops from 2.2 stb/day to 0.5 stb/day.

Using Equations (3.52) – (3.56) and the flowrate schedule shown in Figure 4.16, the flowing pressure are calculated and compared against numerical results for all three cases, as shown in Figures 4.17-4.19. These comparisons show that 1D transient model can recover the numerical data at early times. whereas the 1D BDF model valid for late times, which is expected.

Transient period is longer at lower k_f since it requires less time for pressure transient to reach fracture boundary. As seen in Figure 4.17, for $k_f = 15$ mD or fracture with low conductivity, the 1D Model under transient and variable q can history-match early flowback data accurately. As seen in Figures 4.18 and 4.19, for fracture with medium to high conductivity, the transient model only has a narrow range of application and usually transient period is too short to be seen in conventional flowback data. Compared with the transient model, 1D Model of BDF and variable q has a much wider range of application. At lower k_f (Example A), there are some discrepancies or sharp fronts in prediction of P_{wf} with the BDF model immediately after flowback rate changes. The reason behind these sharp fronts is that each time flowrate changes, short transient periods are experienced before BDF can be established. At higher k_f (Example B and C), the discrepancies cannot be observed because transient periods are too short to be observed.

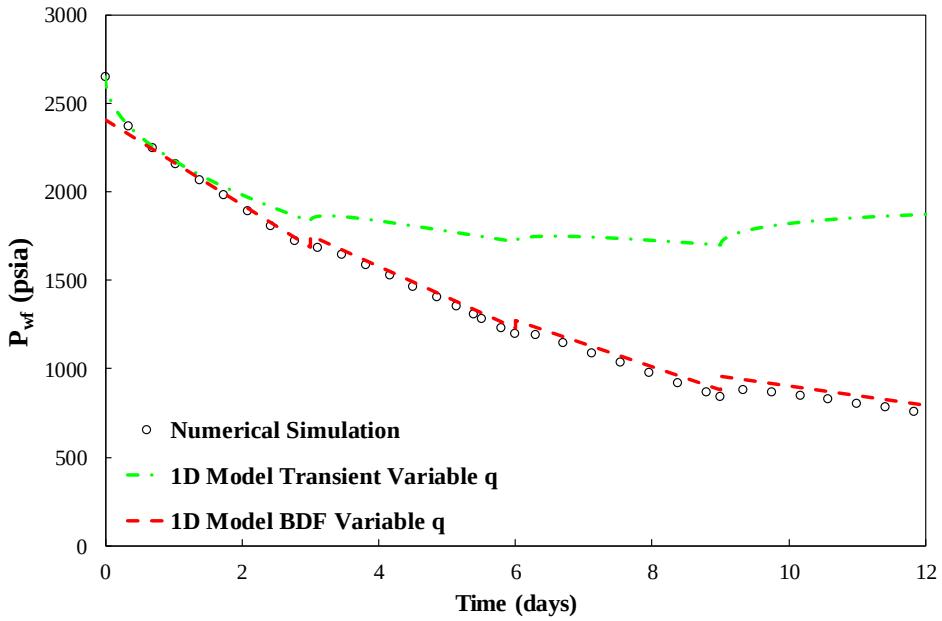

Figure 4.17: Predicted P_{wf} with time using 1D Transient Model and 1D BDF Model for Example A (k_f = 15 mD).

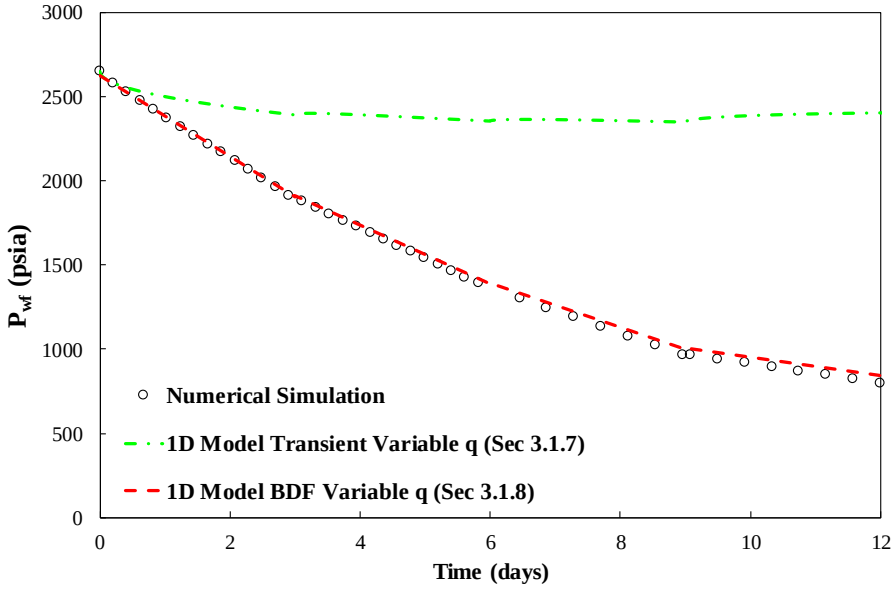

Figure 4.18: Predicted P_{wf} with time using 1D Transient Model and 1D BDF Model for Example B (k_f = 150 mD).

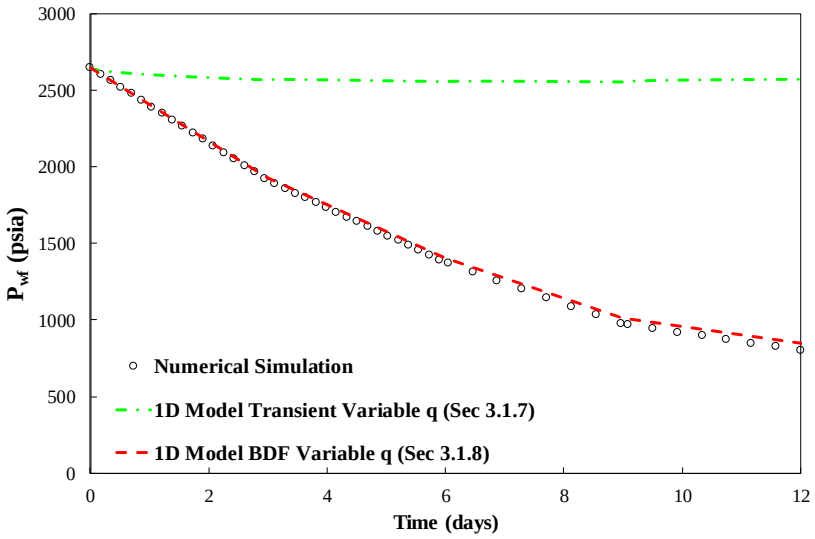

Figure 4.19: Predicted P_{wf} with time using 1D Transient Model and 1D BDF Model for Example C (k_f = 150 mD).

As discussed in **Chapter 3**, linear correlation can be found between pressure drawdown and superposition time and fracture properties can be estimated from the slope of the fitted linear line. In 1D Model Transient Variable q (Sec 3.1.7), fracture permeability can be determined by

$$k_f = 6344 \frac{B_w^2 \mu_w}{w_f^2 h^2 \phi_f c_t m^2}. \tag{4.10}$$

In 1D Model BDF Variable q (Sec 3.1.8), fracture half-length and permeability can be determined by

$$x_f = \frac{5.615 B_w}{w_f h m c_t \phi_f}, \tag{4.11}$$

$$k_f = 262.47 \frac{x_f \mu_w B_w}{b w_f h} \ (q_n), \tag{4.12}$$

where q_n is the current flowback rate.

The results of applying transient and BDF variable q models are plotted in Figures 4.20 and 4.21 for numerical Example C ($k_f = 1500$ mD).

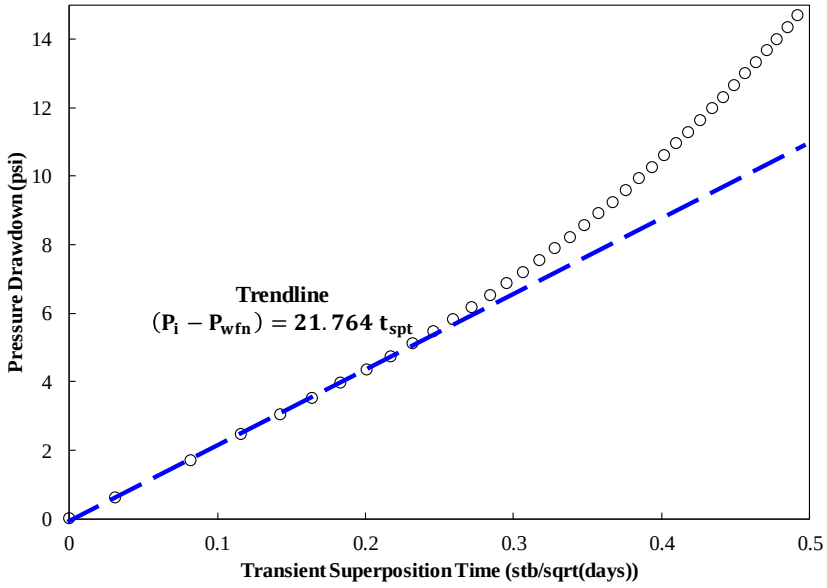

Figure 4.20: Pressure drawdown vs. t_{spt} using transient flowback data obtained from numerical simulation of Example C.

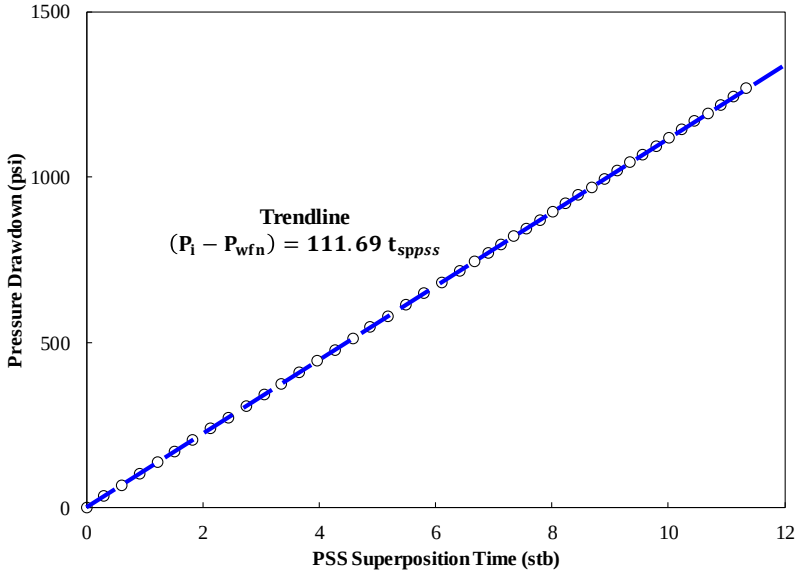

Figure 4.21: Pressure drawdown vs. t_{sppss} using BDF flowback data obtained from numerical simulation of Example C.

In Figure 4.20, linear relationship between $(P_i - P_{wfn})$ and t_{spt} can be expressed by

$$P_i - P_{wfn} = 21.764\, t_{spt}, \tag{4.13}$$

where the slope of fitted straight-line is found to be $21.764\ psi\ \sqrt{days}/stb$.

In Figure 4.21, linear relationship between $(P_i - P_{wfn})$ and t_{sppss} can be expressed by

$$P_i - P_{wfn} = 111.69\, t_{sppss} + 1.1301, \tag{4.14}$$

where the slope of fitted straight-line is $111.69\ psi\ /stb$ and the intercept is $1.1301\ psi$.

Using Equations (4.10) - (4.12), fracture permeability and fracture half-length can be estimated. Three numerical cases from very low fracture permeability $15\ mD$ to high fracture permeability $1500\ mD$ are applied to test the applicability of the transient and BDF flowback models with variable q. The results are summarized in Table 4.6.

The results show that the transient model provides a more accurate estimation of k_f than the BDF model. In the BDF model, k_f is determined from the intercept value of the trendline, which is extrapolated when production time is zero when fracture flow is still under transient period. Therefore, the BDF model may not give accurate result to estimate fracture permeability. As fracture permeability increases, percent error in estimate of k_f by the BDF model decreases as transient period is shortened.

Table 4.6: Summary of estimated values of fracture permeability (k_f) and fracture half-length (x_f) using 1D BDF and transient models.

Example	**k_f input**	**Transient**		**PSS**			
		k_f estimate	**error**	**k_f estimate**	**error**	**x_f estimate**	**error**
Example A	15.00	14.41	3.92 %	16.29	8.6 %	484.70	3.1 %
Example B	150.00	145.24	3.17 %	161.74	7.8 %	492.62	1.5 %
Example C	1500.00	1450.56	3.30 %	1425.03	5.0 %	488.60	2.3 %

4.2 Two-Phase Flowback Model

As mentioned in **Chapter 3**, two-phase flowback models are categorized, based on absence and presence of matrix influx. The EGP model works for two-phase flowback without matrix influx (Sec 3.2.1), while the LGP model works for two-phase flowback with matrix influx (Sec 3.2.2). In this chapter, EGP and LGP models are validated against numerical models shown in Figures 4.22 and 4.23, respectively.

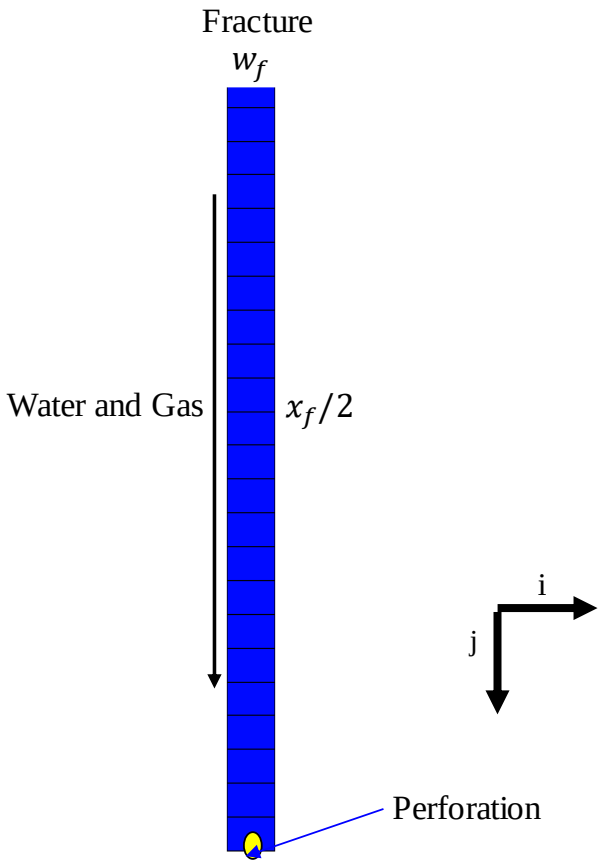

Figure 4.22: Numerical model for two-phase flowback without matrix influx (EGP).

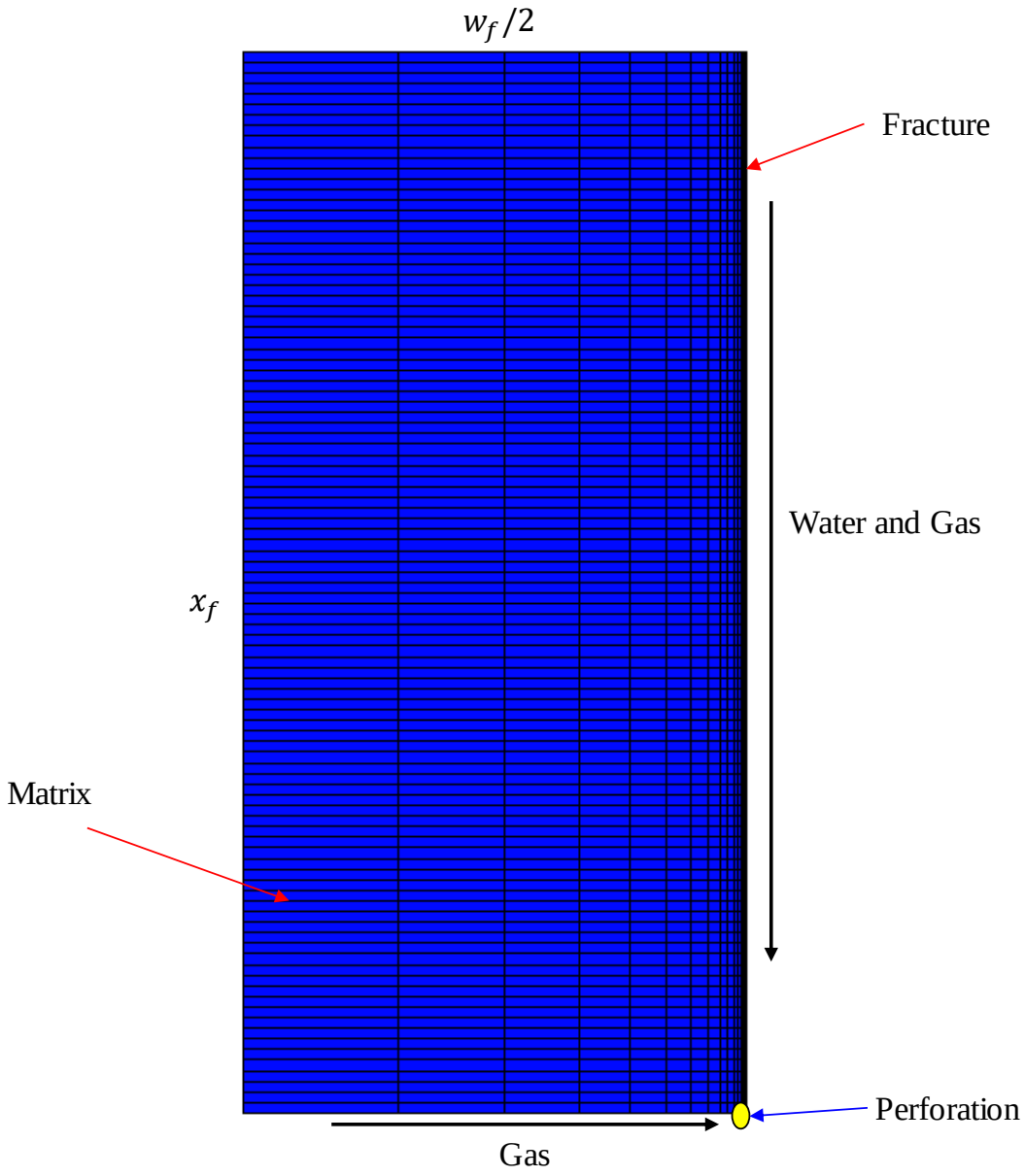

Figure 4.23 Numerical model for two-phase flowback with matrix influx (LGP). Only a quarter of fracture is considered.

4.2.1 HF Flow without Matrix Influx (EGP) Model

In this section, the proposed two-phase flowback model without matrix influx, described in Sec. 3.2.2, is used to estimate fracture attributes. For EGP, fracture depletion is the drive mechanism and fracture can be treated as a closed system with negligible matrix influx of gas and water. The fluid flow is a 1D flow in fracture with gas and water initially stored in fracture flowing from fracture tip to the perforation. Then the numerical model applied to validate the EGP model can be simplified as a 1D model, where only fracture grids have been modeled and no matrix blocks is considered.

The applied numerical model (see Figure 4.22) is same as the one applied for single-phase flowback (see Figure 4.1), but the fracture is partially saturated with gas, where initial gas saturation in fracture is set to simulate two-phase water and gas flow in fracture. Then relative permeability curve of gas and water in fracture needs to be carefully chosen. As a guideline, previous works (Clarkson, 2012; Alkouh, 2014) suggested gravity segregated relative permeability curve (see Figure 4.24 (a)) for two-phase gas and water flowback in fracture. In this work, pseudo time is properly defined in Equation (3.66) to be applicable for any type of relative permeability curve. Figure 4.24 (b) is an example of relative permeability curve that can typically found in shale sample if no relative permeability jail effect is considered (Alkouh, 2014). Table 4.7 lists the input reservoir parameters in the simulator.

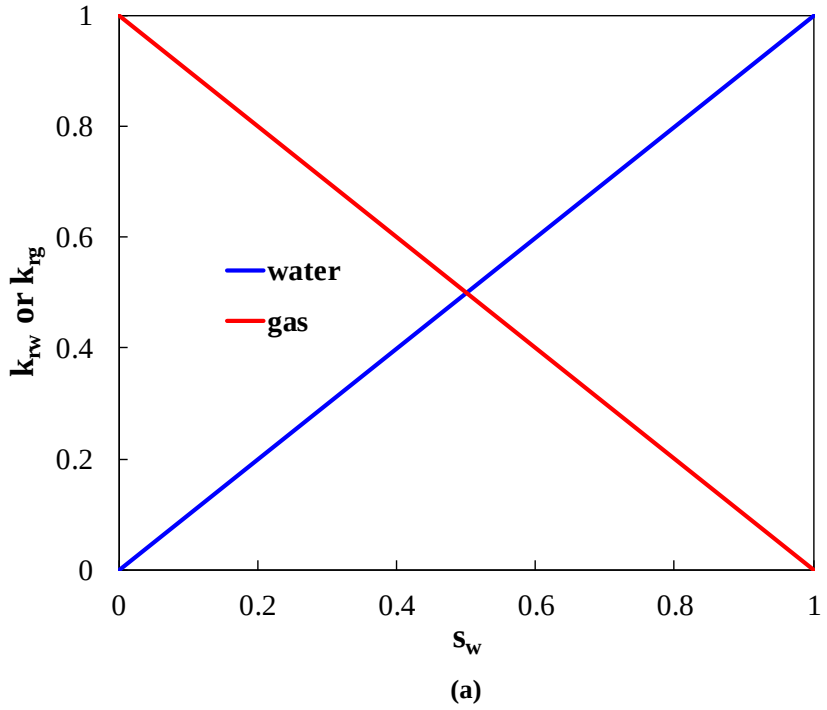

(a)

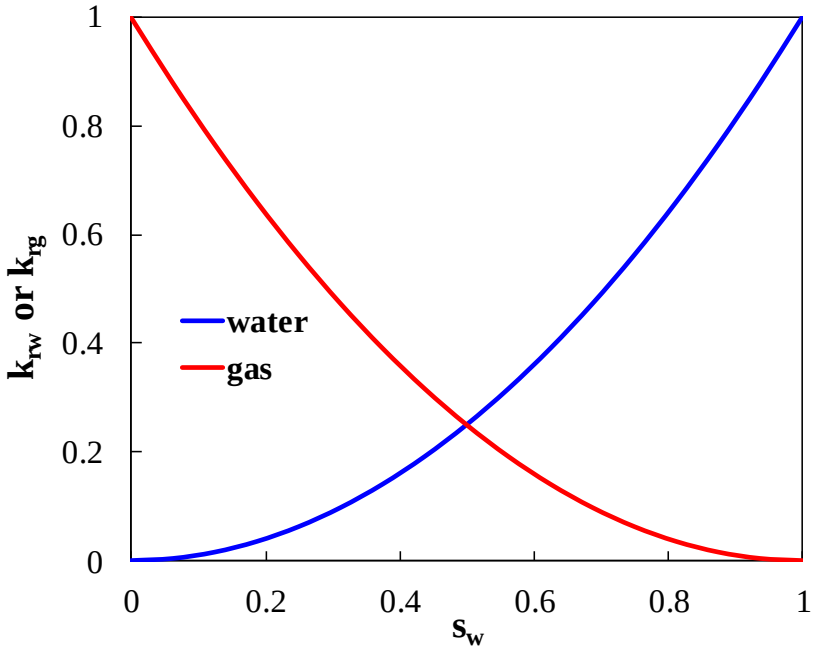

Figure 4.24: Relative permeability curve for fracture: (a) gravity segregated, (b) typical example from shale sample.

Table 4.7: Fracture and fluid properties used in numerical simulation for the EGP model.

Initial pressure, P_i(psi)	2650
Reservoir temperature, T (°F)	160
Specific gravity, SG_g	0.65
Water compressibility, c_w(psi^{-1})	3.33×10^{-6}
Fracture porosity, ϕ_f(fraction)	0.8
Proppant compressibility, c_p(psi^{-1})	1×10^{-6}
Reservoir thickness, h(ft)	300
Well constraint Flowing BH pressure, P_{wf}(psi)	500
Fracture width, w_f (ft)	0.1
Water formation volume factor, B_w(bbl/stb)	1.029
Water viscosity @P_i, μ_w(cp)	0.331
Water density @P_i, ρ_w(lb/ft^3)	61.9615
Fracture half length, x_f(ft)	500
Fracture permeability, k_f(mD)	1500
Initial water saturation in fracture, s_{wi} (fraction)	0.7

The two-phase flowback model of EGP are given by Equations (3.83b) and (3.81a). For flowback without matrix influx, the proposed MB (Equation (3.61)) is applied to determine average fracture pressure (P_f), where initial fracture volume (V_{fi}) can be estimated from the total injected volume (TIV) and the corresponding leak-off percentage. Leak-off percentage represents the extent of fracturing fluid loss into inactive natural fractures or into the matrix during the fracturing operation and the shut-in period, which can be obtained from the field experiment (Xu et al., 2016). In this example, the leak-off percentage is assumed to be 0.3, which is a typical value found in flowback on shale gas formation. The injection fluid volume is 9067 stb and thus, the initial fracture volume should be 56000 cf. Secant method is applied to obtain P_f profile iteratively using Equation

(3.61). The estimated average fracture pressure from material balance is then compared with the numerical simulation, which is shown in Figure 4.25.

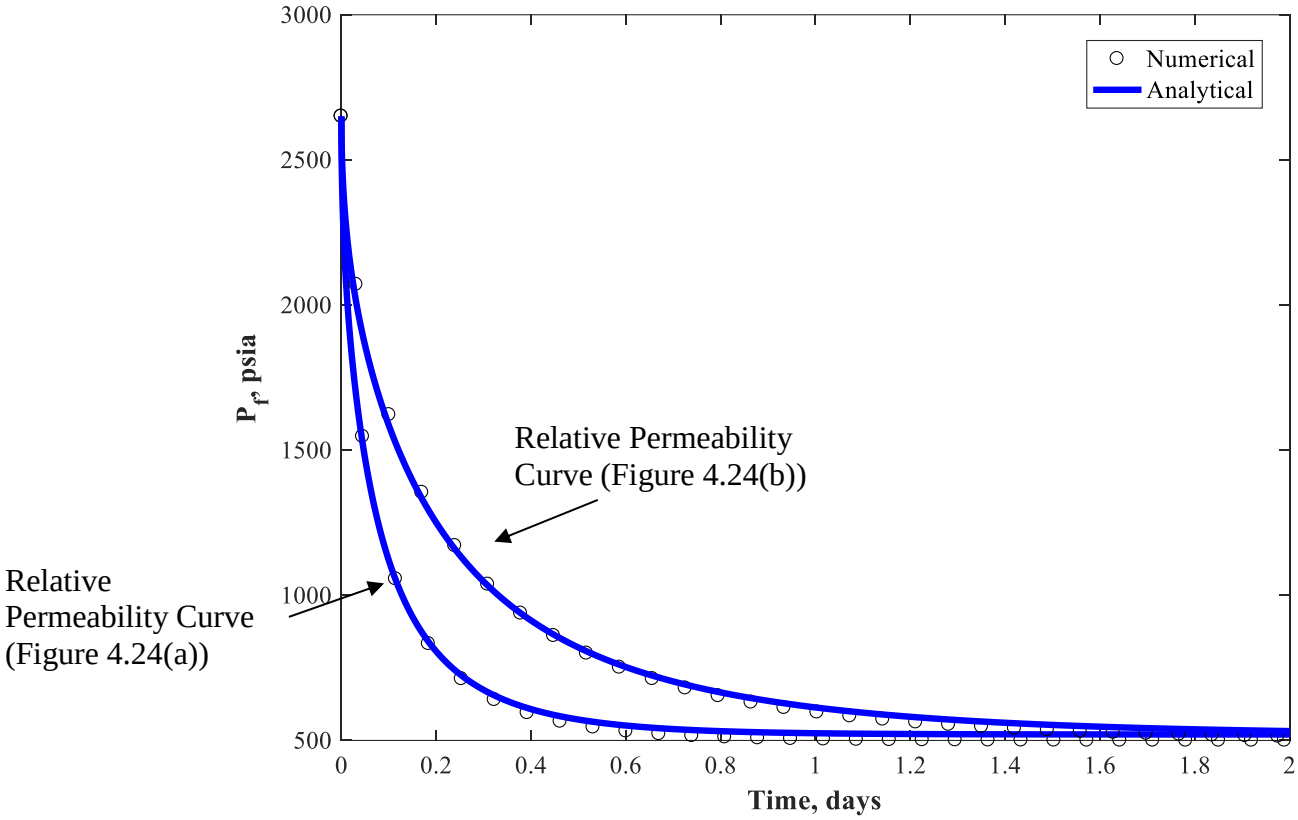

Figure 4.25: Average fracture pressure obtained analytically with Equation (3.61) are compared with the numerical simulation with relative permeability curve (see Figure 4.24) set in fracture.

In the plot of $ln(RNP)$ vs. t_e (see Figure 4.26), linear relationship can be found in BDF window as indicated by the late time approximation. If one of the fracture properties (k_f or x_f) is available, the other parameter can be determined from slope (m) of the straight line.

Fracture half-length can be determined by

$$x_f = 0.1249\sqrt{\frac{k_f}{m\,\phi_f \mu_w c_{ti}}}. \tag{4.15}$$

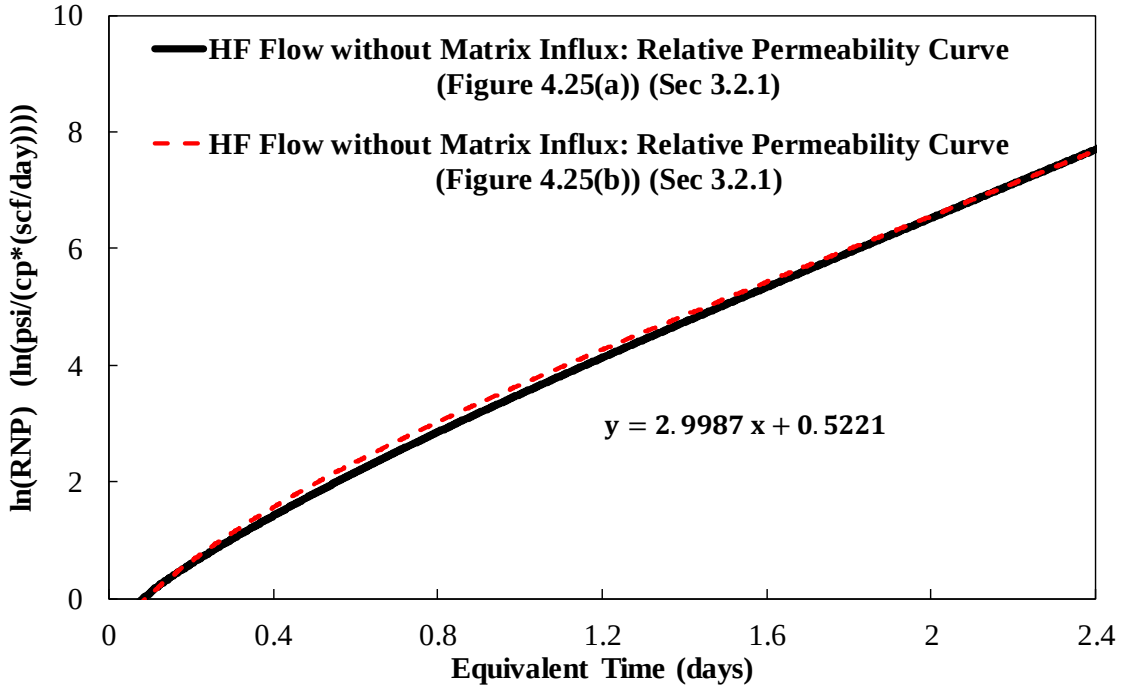

Figure 4.26: *ln(RNP)* vs. equivalent time (t_e) for EGP using relative permeability curve in fracture shown in Figure 4.25.

In Figure 4.26, lines with different types of input relative permeability curves overlap each other because RNP and t_e are pressure normalized parameter. For the same fracture properties, the plot of $ln(RNP)$ vs. t_e keep invariant. As analyzed, linear correlation can be established in the plot of $ln(RNP)$ against t_e for BDF window. With $k_f = 1500\ psi$, time to reach BDF window (t_{BDF}) is less than an hour and thus may be neglected in conventional flowback data. In this example, the corresponding equation for linear fitted line is given by

$$ln(RNP) = 2.9987\ t_e + 0.5221. \quad (4.16)$$

From the slope, fracture half-length (x_f) can be determined using Equation (4.15) as 513.78 ft. Compared with the input value with x_f to be $500\ ft$, the percent error is 2.76 %, which is within a satisfactory range of accuracy.

Adefidipe et al. (2014b) also proposed a two-phase flowback model without matrix influx. I validated their model with two-phase flowback data output from the same built numerical simulation (see Figure 4.22). The formula of their proposed material balance is given by

$$\frac{\partial P_f}{\partial t} = -\frac{q_t}{\widetilde{c_t} \mathrm{V_{fi}}}, \quad (4.15a)$$

$$q_t = q_g B_g + q_w B_w, \quad (4.15b)$$

$$\widetilde{c_t} = \left(1 - \frac{G_p}{G_{fi}}\right)\frac{B_g}{B_{gi}} s_{gi} c_g + \left(1 - \frac{W_p}{W_{fi}}\right) s_{wi} c_w + \frac{1}{V_{fi}}\frac{\partial V_f}{\partial P_f}, \quad (4.15c)$$

Where q_t is the total production rate of water and gas at reservoir condition, $\widetilde{c_t}$ is the total effective compressibility responsible for water and gas production derived from the proposed MB in their work.

Integrate Equation (4.15a), the final formula they proposed to solve for average fracture pressure (P_f) is given by

$$P_f = P_i - \int_0^t \frac{q_t}{\widetilde{c_t} \mathrm{V_{fi}}} \partial t. \quad (4.16)$$

Combine with two-phase diffusivity equation of gas phase, linear relationship can be established between defined *RNP* and t_a and is given by

$$RNP = \frac{2}{V_{fi}}\frac{P_i}{Z_i}B_{gi}t_a + \frac{\phi_f}{k_f}\left[\frac{2}{V_{fi}}\frac{P_i}{Z_i}B_{gi}\right]\frac{x_f^2}{3}, \quad (4.17a)$$

$$RNP = \frac{m(P_i)-m(P_{wf})}{q_g^*}, \quad (4.17b)$$

$$\mathrm{t_a} = \int_0^t \frac{k_{rg}}{\mu_g \widetilde{c_t}}dt, \quad (4.17c)$$

$$q_g^* = \frac{1}{B_g}\frac{(q_g B_g + q_w B_w)}{k_{rg}}. \quad (4.17d)$$

where $m(P_i)$ is the pseudo pressure at P_i, $m(P_{wf})$ is the pseudo pressure at P_{wf}, t_a is pseudo time, and q_g^* is the equivalent gas rate. The definition of pseudo pressure can be found in Dake (1983).

As defined in Equations (4.15b) and (4.15c), $\widetilde{c_t}$ and q_t are related to gas properties and pressure dependent. At this stage, without P_f profile is available, no correlation is established between $\widetilde{c_t}$ or q_t and time. Referred to routine RTA for dry gas reservoirs, pressure needs to be determined from cumulative production history without boundary conditions applied and then reservoir properties can be explicitly solved with diffusivity equation. However, P_f cannot be explicitly solved with Equation (4.16). Instead, the proposed MB in this work for EGP Equation (3.61) is applied to solve for average fracture pressure, which only cumulative production history of water and gas are required. Then their mathematical model Equation (4.17) is applied to solve for fracture attributes explicitly.

The model can be converted to field unit by

$$RNP = \frac{2}{V_{fi}}\frac{P_i}{Z_i}B_{gi}t_a + 158.37\frac{\phi_f}{k_f}\left[\frac{2}{V_{fi}}\frac{P_i}{Z_i}B_{gi}\right]\frac{x_f^2}{3}. \quad (4.18)$$

Assuming gravity segregated relative permeability curve in fracture, same average pressure profile should be obtained, as shown in Figure 4.25. However, when plotting RNP against t_a, no clear linear relationship could be found, as shown in Figure 4.27.

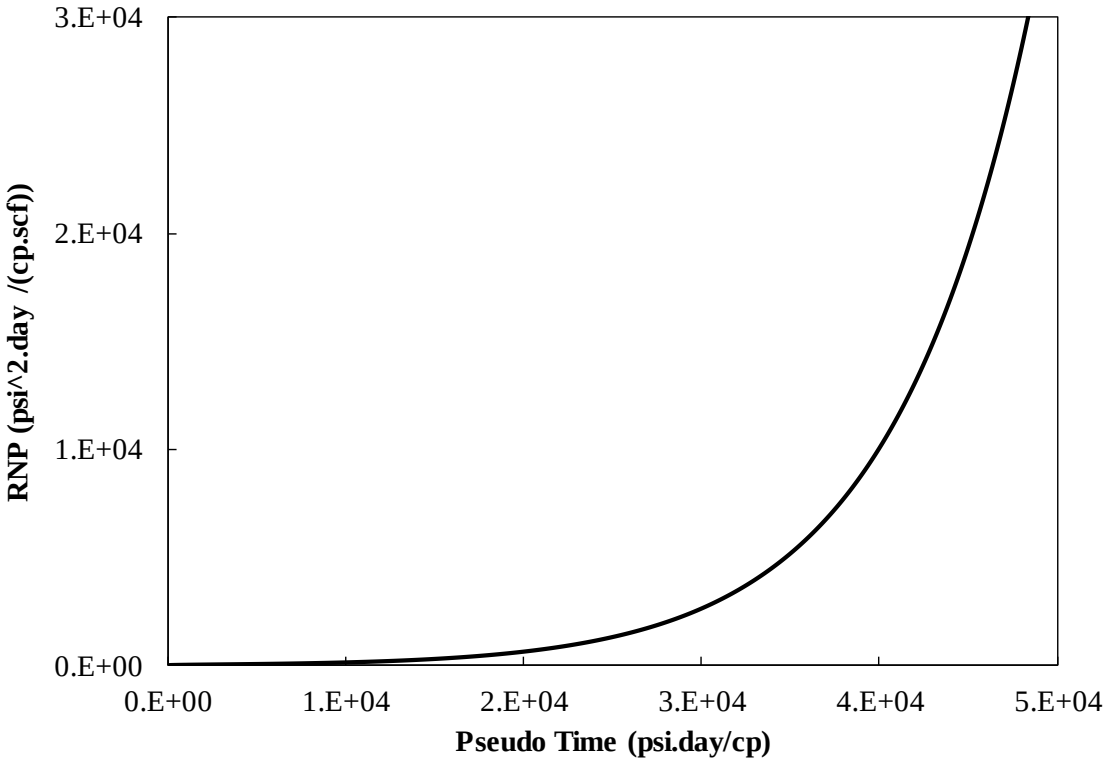

Figure 4.27: *RNP* vs. t_a using two-phase flowback model proposed in Adefidipe et al. (2014a); Xu et al. (2016).

The same problem found in the application of this model is shown in Xu et al. (2016). They applied the field data collected from Muskwa shale, and realized that the data points tend to follow a curve with an inflexion point rather than a linear relationship. They claimed that the assumption in their model neglected the difference between B_g and B_{gi} giving rise

to the non-linear behavior. After I carefully reviewed their derivation, I found that the defined equivalent gas rate (q_g^*) is assumed to be constant with space in fracture, which neglects the non-linear behavior of gas property. These assumptions cannot be properly applied, especially for fracture with high conductivity, since pressure drops in fracture cannot be neglected, even for early flowback period, and gas properties should be updated with change in fracture pressure. Since their model is based on two-phase diffusivity equation of gas phase, these assumptions cannot be properly applied due to the non-linear behavior of gas properties.

Compared with their methodology, the proposed two-phase flowback model (Sec 3.2.1) in this work is based on two-phase diffusivity equation of water phase, where water properties show linear behavior and can be properly assumed to be constant with pressure. As indicated in the validation, the proposed model (Sec 3.2.1) can be generally applied for fractures with high or low conductivity.

4.2.2 HF Flow with Matrix Influx

In this section, the proposed two-phase flowback model with matrix influx described in Sec. 4.2.2 is used to estimate fracture attribute with two-phase flowback data output from the 2D numerical model (see Figure 4.23). The conceptual model for flowback is depicted in Figure 3.1.

In the numerical model, only a quarter of matrix-fracture system is simulated by assuming symmetry with respect around perforation point. By downsizing the system, the number of grids can be reduced, and then less computational time is required in numerical simulator. Logarithmic grid size is assigned to accurately model flow in matrix. In literature (Shanley

et al., 2004), permeability jail (see Figure 4.28) is commonly found in the relative permeability curve of shale sample, which explains the poor well performance in tight formation. As Figure 4.28 illustrates, traditional and low-permeability reservoir rocks show different behaviors in critical water saturation (s_{wc}), critical gas saturation (s_{gc}), and irreducible water saturation (s_{wirr}). In traditional reservoirs, similar values of irreducible water saturation and critical water saturation can be found. There is a wide range of water saturations at which both water and gas can flow. In low-permeability reservoirs, however, dramatically different values of irreducible water saturation and critical water saturation are found. There is a broad range of water saturations in which neither gas nor water can flow. In some very low-permeability reservoirs, there is virtually no mobile water phase even at very high water saturations. Considering permeability jail in relative permeability curves of matrix, there should be a range of water saturations where no water or gas can flow. Figure 4.29 shows the relative permeability curve adopted in the numerical simulation.

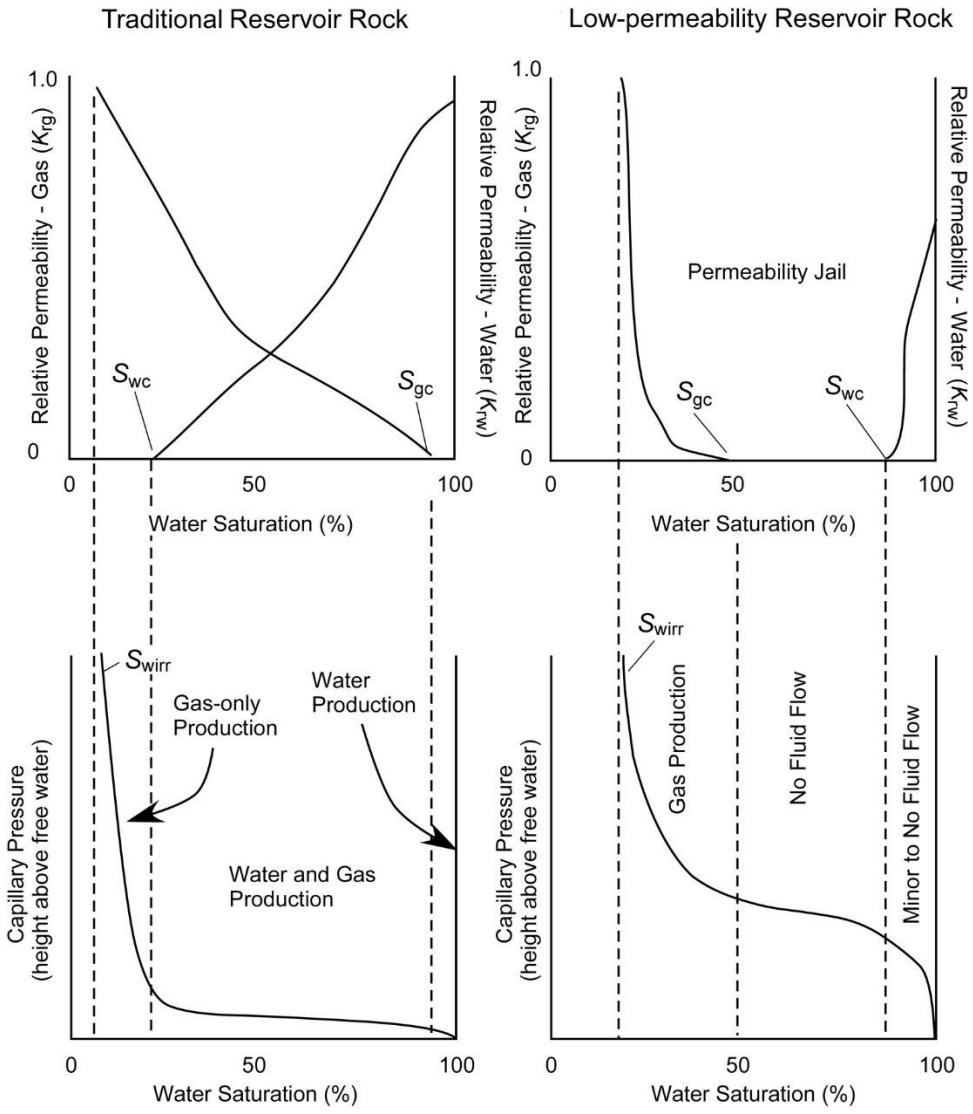

Figure 4.28: Relative permeability curve for conventional and unconventional reservoir, where irreducible water saturation differs from critical water saturation in tight formation (Shanley et al., 2004).

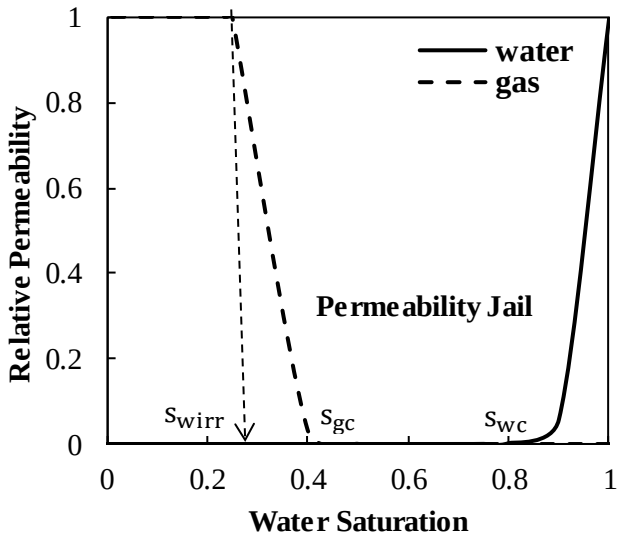

Figure 4.29: Application of permeability jail in the relative permeability curve of matrix in the numerical simulation

Applying the permeability jail in the relative permeability curve, gas is the dominant phase flowing in matrix. Water flow can be treated as 1D flow along the fracture, and gas flow is a combined 2D flow along the fracture and from matrix to fracture.

Several works on the well completion of hydraulically fractured wells are reviewed in order to assign the reasonable values to matrix and fracture properties in the numerical simulation. In Maxwell et al. (2013), they collected the well completion data for the hydraulically fractured wells completed in Anadarko Basin, where the average fracture spacing was about 165 ft. The typical fracture conductivity value was presented in Zhang et al. (2013). They conducted measurements on several core samples from Barnett Shale and reported that, for propped, induced fractures at instantaneous shut in pressure ($2000 - 3000\ psi$), the typical fracture conductivity was about 250 $mD.ft$. For the shale matrix, typical Barnett shale formation properties are provided in Alkouh (2014). Xu et al. (2016)

explained that during the shut-in period, water imbibition and gravity segregation are two important mechanisms responsible for gas movement from matrix surface to fracture, which causes initial free gas storage in fracture network. By analyzing field data collected from the fractured wells completed in Horn river basin, the initial gas saturation in fracture varies between 14.7% and 25.5%. In this work, the average value 20% is chosen to be the initial gas saturation in fracture in the numerical simulation. In reference to these well completion and core sample data on shale formation, the input values are set in the numerical simulation to simulate the flowback process under conditions that are as realistic as possible. Table 4.8 lists the parameters in the numerical simulation.

Table 4.8: Flowback Simulation Properties for Single Fracture and Two-Phase Model (LGP).

Initial pressure, P_i(psi)	2650
Reservoir temperature, T (°F) Specific gravity, SG_g	160 0.65
Water compressibility, c_w(psi^{-1})	3.33e-6
Fracture porosity, ϕ_f(fraction)	0.8
Proppant compressibility, c_p(psi^{-1})	1e-6
Reservoir thickness, h(ft)	300
Matrix porosity, ϕ_m (fraction)	0.08
Well constraint Flowing BH pressure, P_{wf}(psi)	 500
Fracture spacing, L_f(ft)	165
Fracture width, w_f (ft)	0.1
Water formation volume factor, B_w(bbl/stb)	1.029
Water viscosity @P_i, μ_w(cp)	0.331
Water density @P_i, ρ_w(lb/ft^3)	61.9615
Fracture half length, x_f(ft)	500
Fracture permeability, k_f(mD)	2500
Initial water saturation in fracture, s_{wi} (fraction)	0.8
Matrix permeability, k_m (mD)	1.5e-4

The dimensionless fracture conductivity (F_{CD}) defined in Palisch et al. (2007) is given by

$$F_{CD} = \frac{w_f k_f}{x_f k_m}, \tag{4.19}$$

where k_m is matrix permeability.

The dimensional fracture conductivity (F_{CD}) can be determined by (Aguilera, 1995)

$$F_{CD} = w_f k_f. \tag{4.20}$$

Using Equations (4.19) and (4.20), F_{CD} is determined as 3333 in dimensionless form and $250\ md.ft$ in dimensional form with the input values listed in Table 4.8.

The average pressure for the matrix-fracture system ($\bar{P}$) can be determined using the developed MB including free gas storage in matrix is given Equation (3.89). Using this equation, the average pressure of matrix-fracture system can be determined analytically with secant method as the iteration scheme. As discussed, only a single value ($\bar{P}$) is used as reservoir pressure for both fracture and matrix. However, in reality, fracture pressure should be much lower than matrix pressure. To accurately determine fracture pressure, coupling flow of gas needs to be evaluated, which greatly increases the computational complexity. Instead, homogeneous pressure is assumed for matrix-fracture system and then the sensitivity analysis is conducted to see when the assumption can be properly applied. In the numerical simulation, accurate fracture pressure can be evaluated. Table 4.30 shows the comparison between fracture pressure solved analytically with Equation (3.89) and numerically. It can be observed that average pressure estimated analytically differs significantly from its numerical result in the first 100 days of production. By carefully examining the two-phase flowback model described in Sec 3.2.2, we could see only $\frac{1}{s_w}\frac{\partial s_w}{\partial P_f}$ evaluated at average water saturation in fracture, where fracture pressure is required to be

obtained from Equation (3.89) and later substituted into Equation (3.85) to determine fracture attributes. Therefore, the two-phase flowback model is valid if $\frac{1}{s_w}\frac{\partial s_w}{\partial P_f}$ can be estimated accurately bearing the fact that analytical solution does not provide an acceptable estimate of P_f.

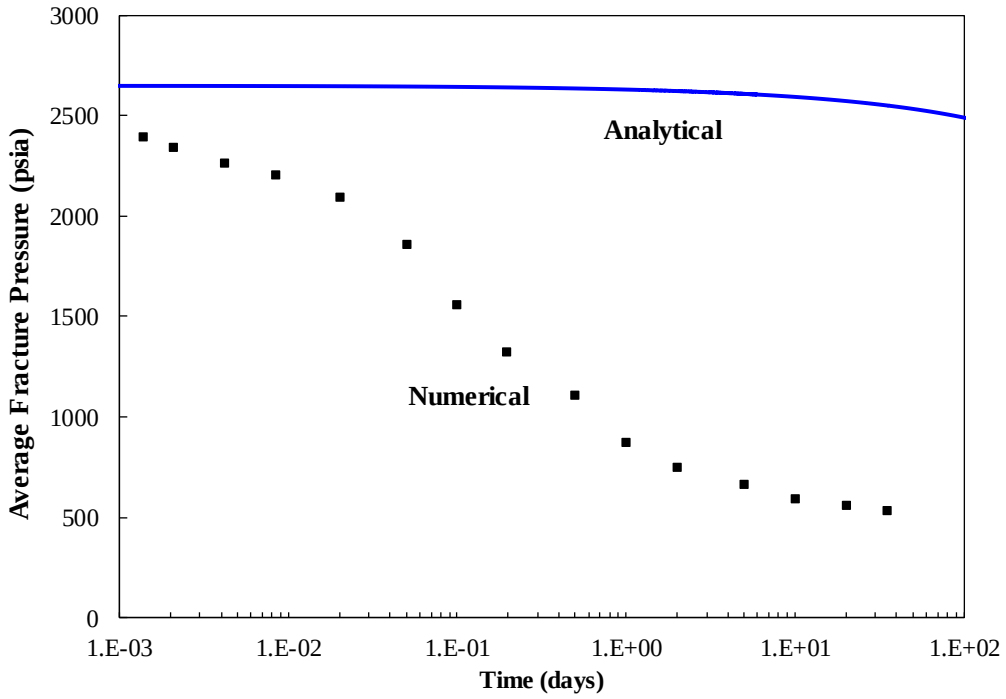

Figure 4.30: Average fracture pressure determined analytically with Equation (3.89) and numerically with 2D numerical model (see Figure 4.23).

Then test of accuracy in determination of $\frac{1}{s_w}\frac{\partial s_w}{\partial P_f}$ with Equation (3.89) is conducted. The term $\frac{1}{s_w}\frac{\partial s_w}{\partial P_f}$ can be decomposed using chain rule by

$$\frac{1}{s_w}\frac{\partial s_w}{\partial P_f} = \frac{\frac{1}{s_w}\frac{\partial s_w}{\partial t}}{\frac{\partial P_f}{\partial t}}, \tag{4.21}$$

The average water saturation in fracture (s_w) can be determined from cumulative water production using Equation (3.79b). Applying relative permeability jail, water is assumed to be immobile both in analytical and numerical modeling. Therefore, the change in s_w with time ($\frac{\partial s_w}{\partial t}$) should be the same for both numerical and analytical simulation, where s_w is only a function of cumulative water production data shown in Equation (3.79b). The discrepancy in estimating $\frac{1}{s_w}\frac{\partial s_w}{\partial P_f}$ should come from the determination of pressure decline rate in fracture. The analytical solution assumes pressure decline rate is the same for fracture and matrix where under realistic conditions, pressure depletes faster in fracture than in matrix. To prove the validity of the analytical model, the difference in pressure decline rate obtained analytically and numerically needs to be checked to see whether it is within an allowable range. If the difference is small enough, then the assumption on pressure decline rate is applicable, and the analytical model should yield satisfactory estimation of fracture properties.

Once the average fracture pressure is determined using Equation (3.89), the pressure decline rate is determined numerically with finite difference approximation. The estimated pressure decline rate is compared against the numerical simulation, where accurate pressure decline rate in fracture is obtained, and the compared results are shown in Figure 4.31.

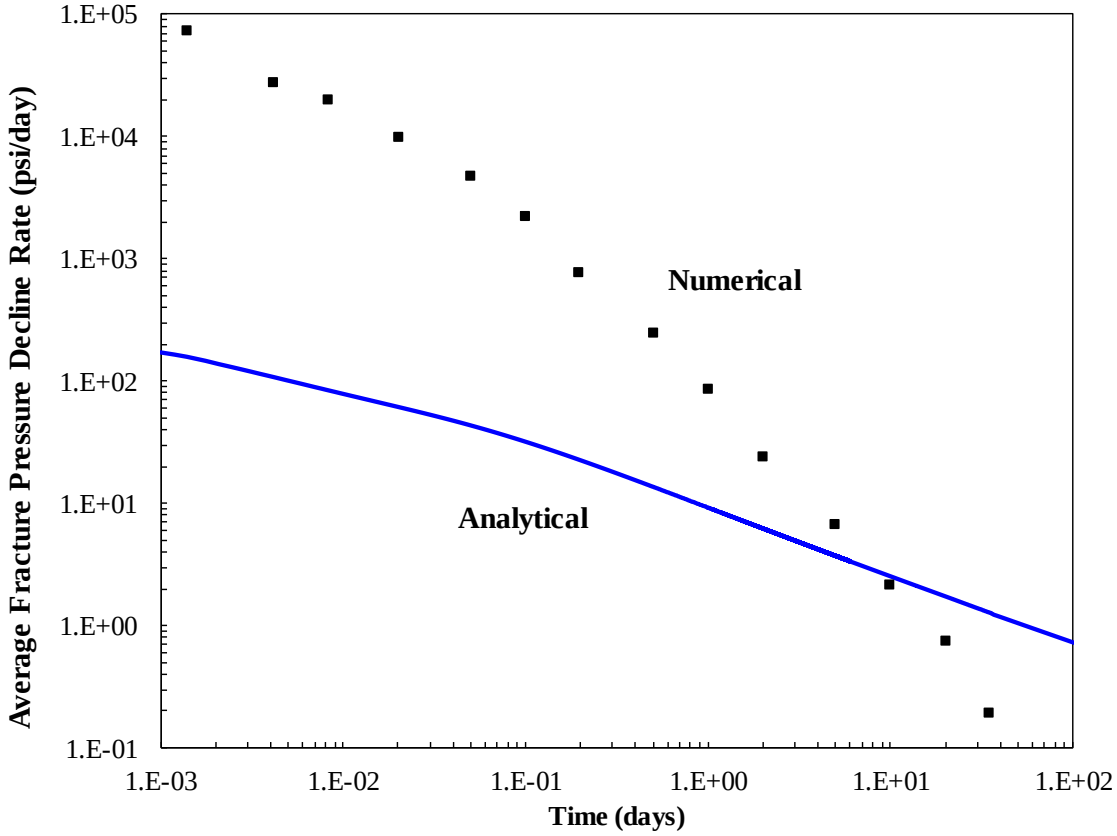

Figure 4.31: Pressure decline rate estimated analytically and numerically corresponding to average fracture pressure shown in Figure 4.30.

From Figure 4.31, it can be seen that initially, pressure drop in fracture is significantly faster than in matrix, then the difference is gradually minimized and equivalent rate is achieved between analytical solution and numerical result at around 10 days, as seen at the intersection of numerical and analytical curves. Beyond the flowback time corresponding to the equivalent rate, pressure decline rate in matrix is greater than fracture, since for later time, fracture pressure is stabilized at P_{wf} and $\frac{\partial P_f}{\partial t}$ of fracture approaches to a very small value. Therefore, the analytical model of LGP should be applied with flowback data, for

flowback time is greater than 10 days with diminished error in estimating pressure decline rate. On the other hand, our analytical solution, based on fracture depletion mechanism, should be applied before fracture pressure drops to stabilized pressure at around $500\ psi$, which is the well shut-in pressure set in the numerical simulation. In this case, the corresponding flowback time is around 30 days, as seen in Figure 4.30. Therefore, the appropriate flowback interval to apply analytical solution is between 10 to 30 days. From the plot of $ln(RNP)$ and $t_e$in log-log scale (see Figure 4.32), unit-slope can be found for t_e between 0.004 and 0.014 days. With Figure 4.33, the corresponding flowback time is determined to be between 12 and 38 days, which agrees with our earlier interpretation from the discrepancy in estimation of pressure decline rate in fracture. Thus, linear correlation can be established between $ln(RNP)$ and t_e from 12 to 38 days, and the two-phase flowback model is valid. By extrapolating and linear-fitting this interval of flowback data, fracture properties can be determined from the estimated slope of the linear trend line, as shown in Figure 4.34.

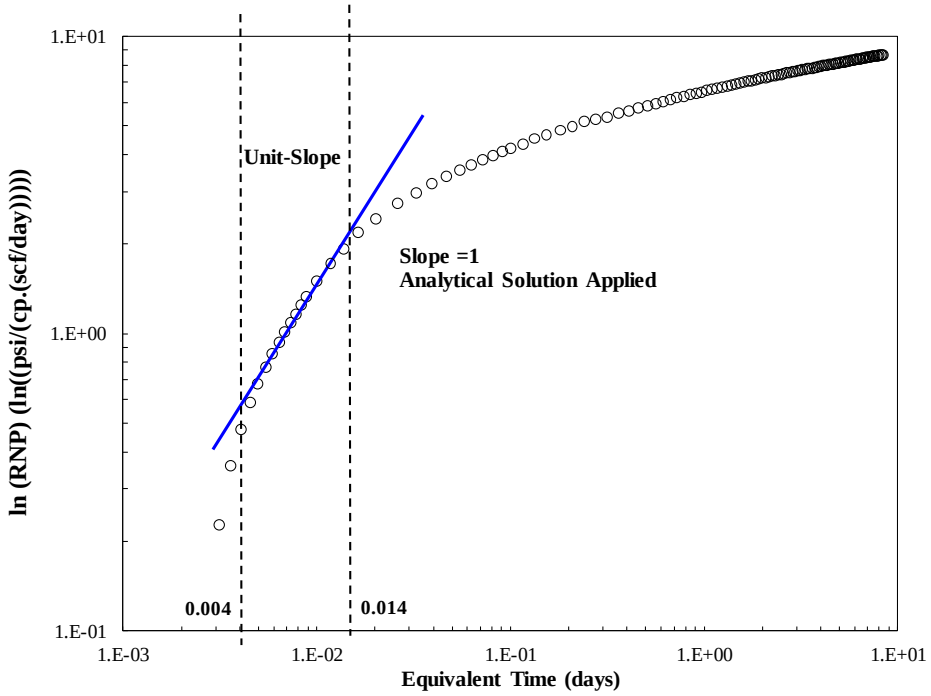

Figure 4.32: *ln (RNP)* vs. t_e in log-log scale. analytical solution is applicable for interval with unit-slope.

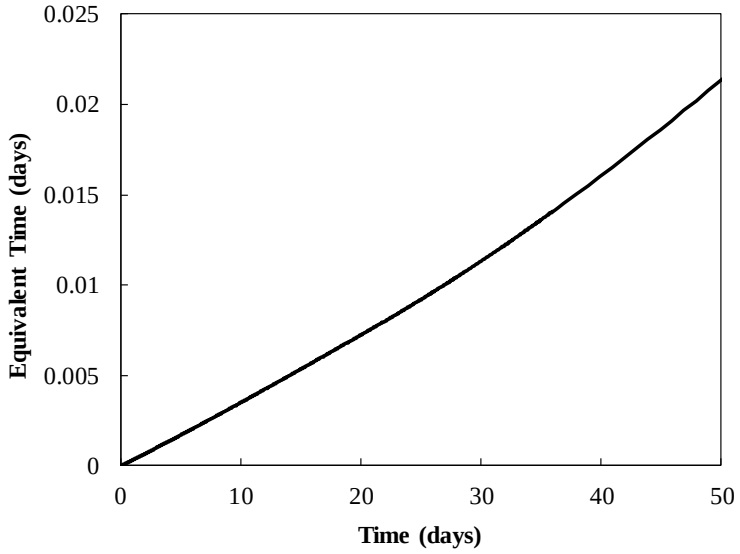

Figure 4.33: t_e vs. t, where equivalent time can be found as a function of production time as shown in Equation (3.54).

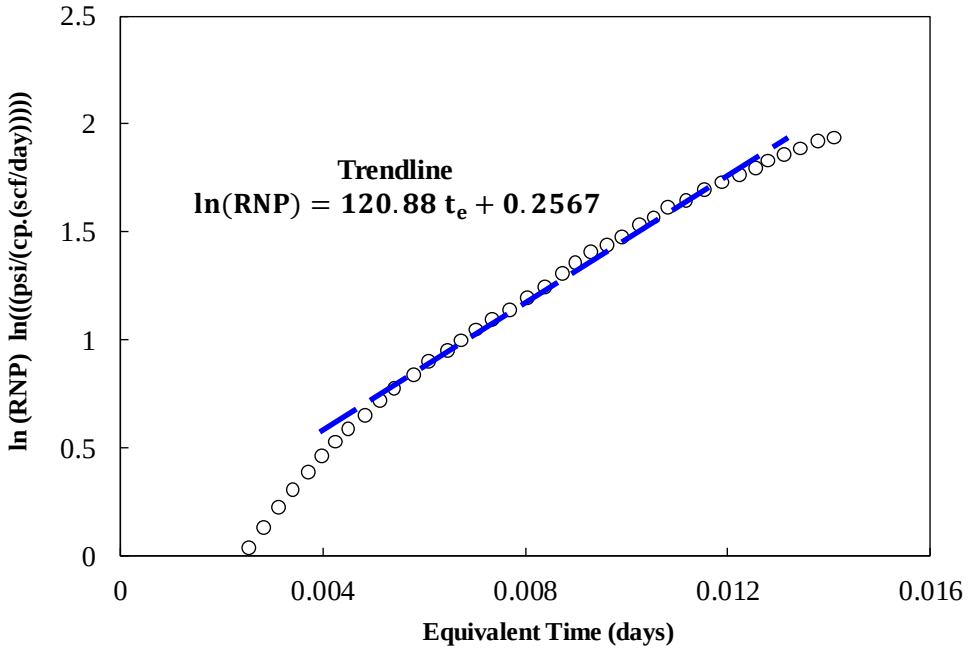

Figure 4.34: *ln(RNP)* vs. t_e between 0.004 and 0.014 days, which corresponds to the unit-slope shown in the log-log plot.

The fitted straight-line equation reads

$$ln(RNP) = 120.88\ t_e + 0.2567. \tag{4.22}$$

From the slope (m), fracture half-length (x_f) is evaluated by

$$x_f = \sqrt{\frac{0.0156\ k_f}{\phi_f \mu_w m}}. \tag{4.15}$$

With k_f to be 2500 mD set in the numerical simulation, $x_f$is calculated to be 455.67 ft, which is within 10 % error as the setup value of x_f in numerical simulator to be 500 ft. Since our model is developed based on two-phase diffusivity equation of water phase, s_{wi} is one of the key factors that may affect the accuracy of the method. Another important

factor that is considered in the analysis is the F_{CD} since homogeneous pressure decline rate is assumed for fracture and matrix behind the analytical model.

The first parameter that I conduct sensitivity analysis is dimensionless F_{cd} as defined in Equation (4.19). For the shale or tight sandstone formation, if lower value is found for F_{cd}, then smaller contrast should exist between matrix and fracture, where the assumption of homogeneous pressure decline rate is more applicable and the analytical model of LGP becomes more accurate. From the field data collected in Xu et al. (2016) on Horn River Basin, initial water saturation in fracture (s_{wi}) is usually around 0.7 to 0.8, due to water imbibition and gravity segregation during shut-in period before flowback operation. So I chose 0.8 as the value of s_{wi} to conduct sensitivity analysis of F_{cd} while F_{cd} varies as 10, 100, 1000 and 3333.3 (field case). Figure 4.35 shows the result of average fracture pressure estimated numerically and analytically.

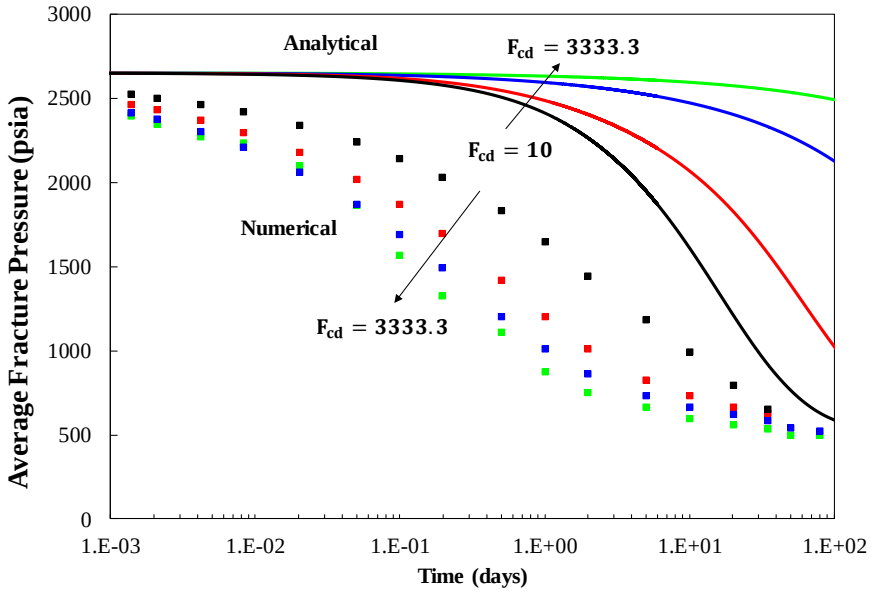

Figure 4.35: Estimation of average fracture pressure (P_f) numerically with 2D numerical model (see Figure 4.23) and analytically with Equation (3.61).

As Figure 4.35 shows, the discrepancy between numerical solution (exact P_f) and analytical result (approximate P_f) is gradually reduced as F_{cd} decreases. Although observable discrepancy can be found between analytical and numerical solution in estimating P_f, the analytical solution assumes fracture and matrix are under same pressure decline rate and comparison of average fracture pressure decline rate ($\frac{\partial P_f}{\partial t}$) estimated from numerical and analytical solution is plotted in Figure 4.36.

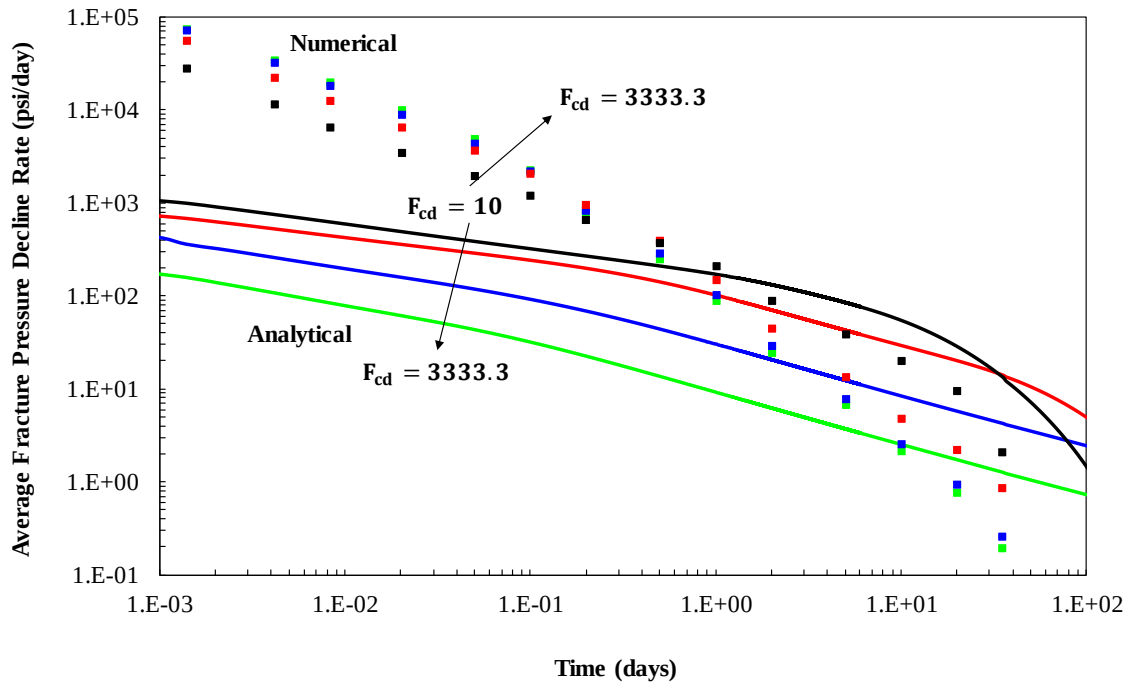

Figure 4.36: Estimation of average fracture decline rate numerically and analytically corresponding to Figure 4.35.

Initially, pressure decline rate in fracture is much faster than matrix and the equivalent rate is achieved as seen at the intersection of numerical and analytical curves. Beyond the flowback time corresponding to the equivalent rate, pressure decline rate in matrix is

greater than fracture since for late time, fracture pressure is stabilized at P_{wf} and $\frac{\partial P_f}{\partial t}$ of fracture approaches to a very small value or zero. As F_{cd} increases, greater contrast exists between fracture and matrix and, thus, a longer time is needed before analytical solution agrees with the numerical result. The time to achieve equivalent rate is around 0.8, 2, 5, and 10 days for F_{cd} as 10, 100, 1000 and 3333.3 respectively. For smaller F_{cd}, accuracy of estimation of fracture properties is improved as shown in Table 4.9, where the input value of x_f is $500\ ft$.

Table 4.9: Estimation of fracture half-length (x_f) under different F_{cd}.

F_{cd}	$x_f\ (ft)$	x_f error
10	499.63	0.07 %
100	501.65	0.33 %
1000	520.87	4.17 %
3333.3	455.67	8.87 %

Then the LGP model is tested under different s_{wif}. From the sensitivity analysis of F_{cd}, it can be determined that the analytical model of LGP bias toward fracture-matrix system with low F_{cd}. Therefore, I chose fracture-matrix system with low F_{cd} to conduct the sensitivity analysis of s_{wif}. Three synthetic numerical cases are set in the numerical simulation with s_{wif} to be 0.1, 0.5 and 0.9 with $k_m = 0.01\ md$, $L_f = 200\ ft$ and $k_f = 5000\ md$, which yields a round number of F_{cd} to be 100. The rest rock and fluid parameters are kept same as Table 4.9. I also compared the analytical model of LGP with EGP to see the effect of gas matrix influx on pressure decline in fracture. Figure 4.37 shows

the results of estimating P_f from the numerical solution and comparison of the analytical model of EGP and LGP.

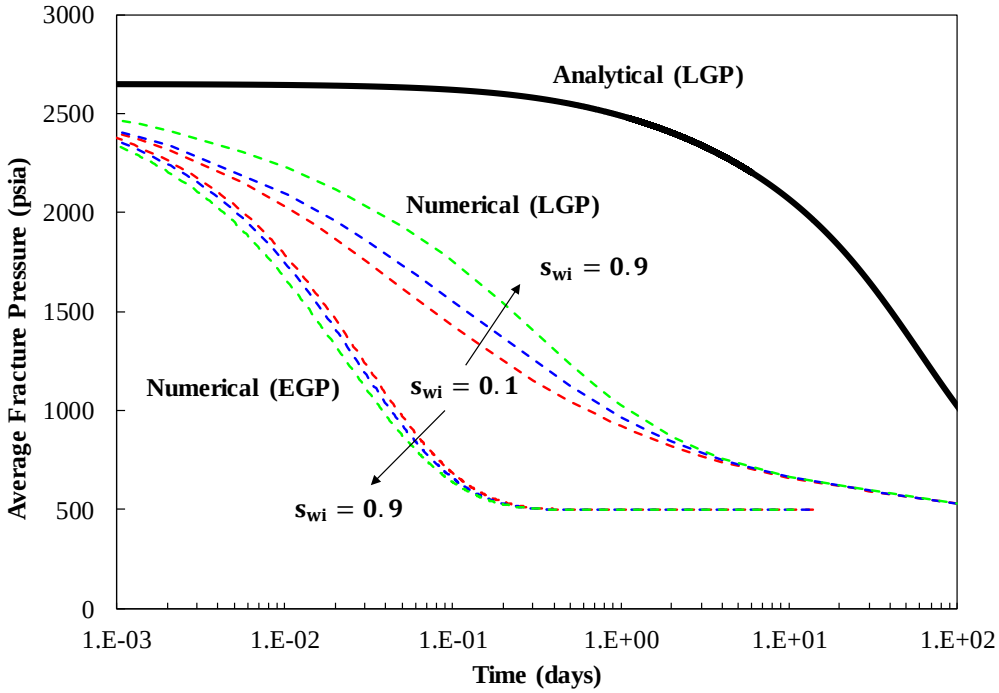

Figure 4.37: Estimation of P_f numerically and analytically with different s_{wi} for EGP and LGP periods (F_{cd} =100).

As discussed, for EGP period, the fracture can be treated as a closed tank with no matrix influx, where the analytical model can accurately estimate P_f and the numerical simulation agrees with the analytical model. As s_{wi} increases, more water presents in the fracture initially and less compressibility is expected, since less gas is available to expand and, thus, pressure drawdown increases. For LGP period, the reverse trend is observed, as depletion of pressure decreases as s_{wi} increases due to gas flow in matrix. As less gas is initially stored in the fracture (high s_{wi}), more gas in matrix would supply the pore volume vacated by water production. As a result, pressure drawdown is diminished as s_{wi} increases and

more gas presents in the fracture. The discrepancy in estimation of P_f between analytical solution and numerical result is reduced for high s_{wi}, which should be preferred in field practice, since the typical s_{wi} for shale is 0.8 and for tight sandstone is fully water-saturated. The analytical result of estimation of P_f in EGP period does not show in the comparison, because the material balance described in Equation (3.61) accurately predict pressure declined for EGP period with negligible matrix influx.

Table 4.10: Estimation of fracture half-length (x_f) under different s_{wi}.

s_{wi}	x_f (ft)	x_f error
0.1	587.6036	17.52 %
0.5	538.5263	7.71 %
0.9	497.5631	0.49 %

The error in determination of x_f is gradually reduced as s_{wi} increases, which is expected since the discrepancy in prediction of P_f decreases if more water initially presents in fracture as shown in Figure 4.37.

Another numerical case of higher F_{cd} is added to conduct the sensitivity analysis of s_{wi} to ensure the same trend found in Figure 4.37 is a general observation. Higher F_{cd} is set in the numerical simulaiton, where a lower matrix permeability is assigned to limit matrix flow of gas in LGP period. The input parameters source from field data of Barnett Shale described in Table 4.9, and the calculated F_{cd} is 3333.3. The k_m for typical shale sample is of $10^{-4}\ md$ magnitude, which is 100 times smaller than the previous numerical case with k_m to be $0.01\ md$. Thus, the gas flow in matrix should be significantly reduced.

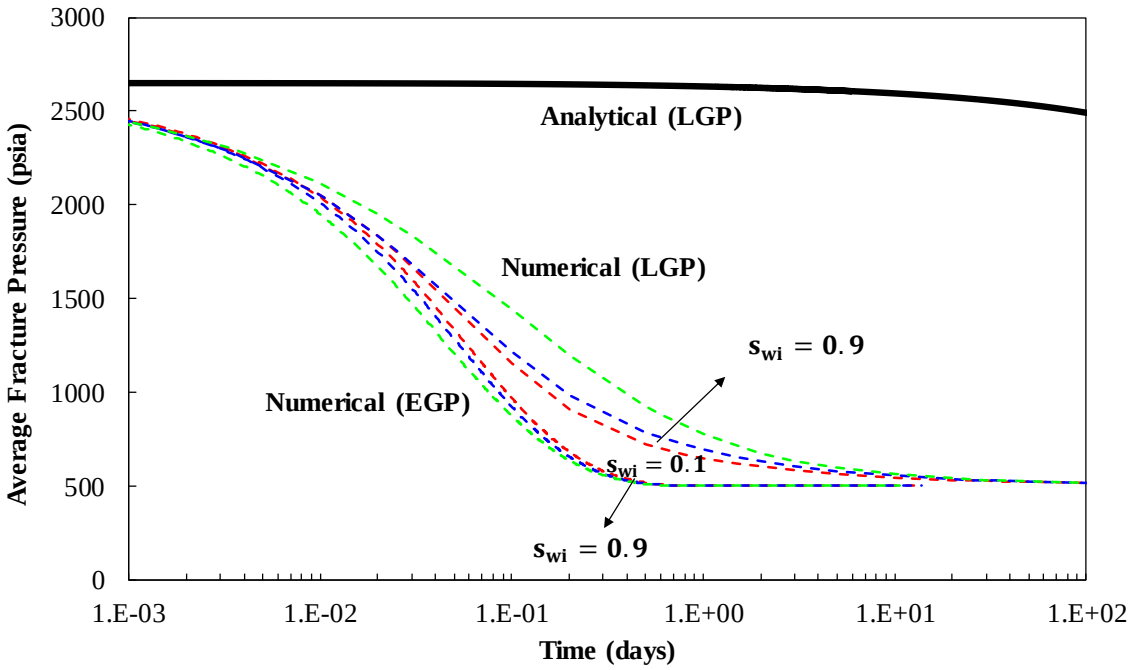

Figure 4.38: Estimation of P_f numerically and analytically with different s_{wi} for EGP and LGP periods (F_{cd} = 3333.3).

The same trend that pressure drawdown is gradually lowered as s_{wi} increases in LGP period due to the gas matrix influx into fracture was observed. Although the matrix flow is significantly limited by the lowered matrix permeability about two order of magnitude, gas matrix influx still help water production by supplying void space in fracture. Comparing Figure 4.37 and Figure 4.38, a larger gap occurs between analytical and numerical result for higher F_{cd}. As analyzed in the sensitivity analysis of F_{cd}, the accuracy of the analytical model of LGP is improved for lower F_{cd} because less discrepancy lies in estimation of pressure decline rate in fracture.

Although the mathematical model in Ezulike and Dehghanpour (2014) is applicable for flowback of LGP, their methodology is based on two-phase diffusivity equation of gas phase; unfortunately, coupling problem was encountered and this complicates the analysis, where the solution needs to be solved in Laplace domain, but is computationally expensive to do so. The other concept raised to develop their mathematical model is the dynamic-relative-permeability, where relative permeability can be expressed as an explicit function of time, and can cause the later derivation to become mathematically complex. However, this relationship (k_{rg} vs. t) is usually absent in conventional data gathering and usually varies among different geological locations. A typical plot of k_{rg} vs. t found from their field data may not applicable in other formations. Also the development of this correlation is not necessary since k_{rg} can be found as a function of s_g and it can be estimated with cumulative production history. Thus, direct relationship between k_{rg} and t is not required for development of mathematical model of flowback. The application of Laplace

transformation and dynamic relative permeability curve make their model not practical in application as the solution requires strong mathematical solving techniques.

Bearing the fact that analyzing coupling flow of gas in the development of mathematical model would obtain exact estimation of P_f, our analytical model of LGP takes advantage of 1D flow of water, avoiding the complexity brought about by coupling problem, and still yields estimation of fracture attributes within satisfactory accuracy. From the sensitivity analysis, the accuracy of application of analytical model of LGP for fracture with low F_{cd} and high s_{wi}. When the input values in numerical simulation are set, referring to field data of Barnett Shale with s_{wi} to be 0.8 and F_{cd} to be 3333.33, the analytical model of LGP can accurately determine x_f compared with the numerical input value. The analytical model of EGP can accurately determine P_f for flowback without matrix influx.

CHAPTER 5 : SUMMARY AND CONCLUSIONS

This work reviews the available literatures on flowback along with various mathematical models developed for flowback analysis. After re-deriving the available analytical models, the applicability of the previous models were examined and their limitation were discussed. It has been realized that analytical models for interpretation of flowback data are still at an early stage of development. Motivated by this, two sets of analytical models for flowback data analysis were developed: single-phase (i.e., fracturing fluid only) and two-phase (i.e., fracturing fluid and gas). In this work, water is considered as the fracturing fluid, and fracture as the porous medium. According to reported field data, single-phase flowback can be observed in tight sands, but two-phase flowback is expected in the case of shale gas. Thus, the flowback flow system can be single- or two-phase, depending on reservoir type. For single-phase systems, I propose a set of one-dimensional (1D) models developed under different boundary conditions. In contrast with previous single-phase models valid under pseudo steady-state (PSS) conditions, our simple 1D models are valid for transient and boundary-dominated flow regimes under constant bottomhole pressure (BHP), constant flowrate, and variable flowrate inner boundary conditions. For two-phase systems, I propose a 1D model to analyze water flow in fracture before gas influx from matrix to HF occurs; and a two-dimensional (2D) model to analyze water flow in fracture after gas flows into fracture.

5.1 Single-Phase Flowback

The mathematical developments for the single-phase flowback can be categorized into BDF and transient models. The work starts by re-deriving Abbasi et al.'s and Alkouh et al.'s models developed for analyzing single-phase flow of water in HF. Limitations in application are found in these two models, as they can only be accurately applied in PSS flow regime. However, transient period may be important, especially for fracture with poor treatment or low conductivity. 1D analytical models are therefore developed, valid for both BDF and transient periods under constant q and BHP production. A 1D numerical model (see Figure 3.1(b)) is developed in CMG (IMEX) to validate the previously developed models in literature and the proposed 1D analytical models in this thesis. The purpose of the validation is to reveal and compare the limitations behind different models. The validation can be subdivided into two steps: first analytical models are applied in forward prediction of flowback response (i.e., pressure drawdown or flowback rate) and compared against numerical simulation; then the analytical models are applied in inverse estimation of fracture attributes. (i.e., fracture half-length and fracture permeability). Abbasi et al.'s and Alkouh et al.'s models need to be further developed to predict flowback response, as some parameters (i.e., C_{st} and J_w) in their models are difficult to evaluate using the current mathematical expressions. It should be noted that after fully deriving the expression of J_w, two important fracture attributes (i.e. x_f and k_f) can be obtained using Alkouh et al.'s model, whereas the original work only focused on obtaining effective fracture volume. From forward prediction, 1D analytical model (Case 1) can accurately predict wellbore pressure for entire flowback period, whereas the other two models fail to history-match

transient flowback data. From inverse estimation, Abbasi et al.'s model can be applied to obtain the lump of x_f and k_f, and the other two models are used to evaluate k_f and x_f independently. The three models can accurately estimate fracture attributes as compared against numerical inputs, the errors are within 1%. The same validations are conducted for the other cases of 1D analytical models. Overall, by comparing against numerical simulations, the proposed transient models (1D analytical model (Case 3 and Case 4)) can accurately predict flowback response in transient period and estimate flowback properties with transient flowback data within 5% error. Overall, by comparing against numerical simulations, the proposed BDF models (1D analytical model (Case 1 and Case 2)) can be accurately applied in forward prediction of flowback response for entire flowback period and inverse estimation of flowback attributes with BDF flowback data within 5% error.

Another important point achieved in this thesis is to develop analytical solution of single-phase flowback under variable rate condition. In field operation, usually flowback rate cannot be maintained constant; thus, flowback models developed under constant q flowback may not be practical. Superposition principle is applied to superimpose 1D analytical model (Case 1 and Case 3) to account for change in flowback rate. Two sets of solution are obtained valid for flowback in BDF and transient periods under variable q. With the corresponding flowback time interval (i.e. BDF or transient) , the solutions can accurately predict fracture response and estimate fracture properties within 10% error.

5.2 Two-Phase Flowback

The mathematical developments for the two-phase flowback can be categorized into EGP and LGP models. A V-shape is commonly found in gas to water ratio (GWR) plot in flowback on shale gas formation, where flowback can be separated into two regions: EGP without matrix influx and LGP with matrix influx. The proposed two-phase flowback models are developed by combing material-balance equation (MB) and two-phase diffusivity equation of water phase, where fracture attributes can be determined.

For EGP, fracture can be treated as closed system and the 1D conceptual model (see Figure 3.1(b)) is applied to simulate flow of gas and water in the fracture. Two-phase diffusivity equation of water phase is developed by incorporating water saturation and relative permeability of water on top of the single-phase diffusivity equation of water in single-phase flowback. To solve for the diffusivity equation, no flow boundary as outer boundary and constant BHP as inner boundary are assumed and thus the model is applicable in flowback under constant BHP after BDF is reached. Water pseudo pressure (P_p) and equivalent time (t_e) are properly defined and used to linearize the diffusivity equation. Linear relationship can be found between natural log of rate normalized water pseudo pressure ($\ln(RNP)$) and equivalent time (t_e), where t_e is dependent on pressure decline rate in fracture and slope of the fitted line is used to evaluate fracture attributes. Then MB is developed to correlate average fracture pressure to flowback time, where fracture pressure decline rate can be estimated with algorithm of finite-difference approximation. A 1D numerical model is constructed to simulate two-phase fracture flow of water and gas and validate the analytical model. Two types of relative permeability curves are adopted in

the numerical simulation. I started with gravity segregation type of relative permeability curve, as it is the most common one found in fracture flow, where the numerical value of water saturation always equals to relative permeability of water. Later, a typical relative permeability curve obtained from shale sample is adopted to test applicability of the analytical model. With the developed MB, average fracture pressure (P_f) can be accurately predicted compared against numerical simulation and the time related parameter (t_e) can be determined from flowback time. Applying the two-phase diffusivity equation of water phase, linear correlations can always be found in the plot of $\ln(RNP)$ vs. t_e in BDF period and fracture half-length is accurately determined within 5% error, for both gravity segregated and typical shale type of relative permeability curves. It should be noted the plot of $\ln(RNP)$ vs. t_e is invariant with different types of relative permeability curves provided that fracture properties keep the same, which illustrates that the plotted parameters (i.e. RNP and t_e) are normalized with P_f.

For LGP, the 2D conceptual model (See Figure 3.1(c)) is applied to model two-phase flow of water and gas in fracture and single-phase flow of gas in matrix. As indicated in the literatures, water production in flowback period is usually assumed to be sourced from primary fracture network only, which indicates that water is immobile in matrix as initial water saturation is always lower than critical water saturation in matrix. In the two-phase flowback of LGP, water flow is assumed to be 1D flow in fracture whereas gas flow is 2D combined flow in fracture and matrix. As linear flow is still applicable for water flowback in LGP, the two-phase diffusivity equation of water phase developed for EGP is valid for LGP. But MB needs to be modified to account for the effect of gas matrix influx on pressure

decline in fracture, where free gas storage in matrix needs to be included. The challenging part is to determine the exact average fracture pressure, which requires the analysis of coupling problem encountered in gas flow. A common assumption that primary fracture network and stimulated matrix volume are under a homogeneous pressure is made in the development of MB to avoid the complexity brought about by coupling flow. Bearing the fact that significant discrepancy may be introduced by applying the assumption, the MB, however, is applied to obtain pressure decline rate in fracture and substitute into the two-phase diffusivity equation of water phase to estimate fracture attributes. To validate the analytical model, a 2D numerical model is set to simulate two-phase flowback of LGP, where the input parameters are referred to well completion information and typical rock and fluid properties collected from Barnett shale. Applying the MB, significant errors can be observed in the estimation of average fracture pressure compared against numerical simulation; nevertheless, errors are greatly diminished in the determination of average pressure decline in fracture. The plot of $\ln(RNP)$ and t_e is then constructed in log-log scale to accurately determine the flowback time interval where a linear correlation presents and the assumption is valid. The result shows that the determined flowback interval with unit-slope presenting in log-log plot also has the lowest error in estimation of pressure decline rate, which is within the expectation as the discrepancy is brought by the assumption on P_f. The estimated fracture half-length from the analytical model is within ten percent error. Sensitivity analysis of F_{CD} and s_{wi} are conducted to investigate limitations of the two-phase flowback model of LGP. F_{cd} is a key factor that would affect validity of the assumption on estimation of pressure drawdown in fracture. s_{wi} is treated as another important factor that may impact accuracy of the model as water-phase is the dominant

phase in the mathematical development. The results indicate that the model can be applied more accurately for fracture with smaller $F_{cd}$and higher s_{wi}. Within the physical range of F_{cd} and s_{wi}, the two-phase flowback model can accurately evaluate fracture attributes for LGP period.

Also, several two-phase flowback models were carefully re-derived in my work. Clarkson et al.'s model included free and adsorbed gas storage in matrix in the development of MB, where matrix-fracture system is assumed under unified pressure and average fracture pressure can be evaluated with Langmuir isotherm applied. Improvement is made to this model as matrix and fracture storage of water are evaluated separately in the development of MB. Their model is particularly useful if desorption of gas is significant in flowback period, but field observations or experimental works need to be conducted to justify whether the effect of desorption should be included in flowback analysis. The potential problem that may be encountered in applying this model is the non-uniqueness in the history-matching process as multiple combinations of k_f and x_f may match the production history. Also, justification of their assumption of unified pressure needs to be supplemented to their model, which is provided in my work, as indicated in the sensitivity analysis of F_{cd}. The two-phase flowback model proposed in Adefidipe et al. (2014b) was based on two-phase diffusivity equation of gas phase for EGP. Their mathematical development lay the foundation of two-phase flowback, excluding effect of desorption. I apply their model in the numerical simulation, but instead of a linear correlation, a polynomial relationship is obtained with the plotted parameters (i.e. RNP and t_a), and fracture properties cannot be evaluated. The same observation was found by the authors with the field data from Muskwa shale. I realized that they assumed B_g remains constant in EGP period in the mathematical

development. So their model fails to be applied for fracture with high conductivity where significant pressure drawdown should be found. The two-phase flowback model in Ezulike and Dehghanpour (2014) based on two phase diffusivity equation of gas phase is applicable in LGP, where Laplace transformation is applied extensively to analyze coupling flow of gas, which complicates the analysis. Compared with the previously developed models, the proposed two-phase flowback model in this work regards treated water as the dominant phase to analyze, which takes advantage of linear behavior of water properties and 1D flow of water. Although the assumption made in LGP period brings in significant discrepancy in estimation of average fracture pressure, the model can still estimate fracture attributes within satisfactory accuracy and avoids the complexity in solving the coupling problem, which should be a practical model in field application.

5.3 Recommendations

Three future researches are recommended. Desorption effect may be necessary to be included in flowback analysis. My recommendation for future researchers interested in further investigation of production mechanism in flowback are to collect experimental data to determine if desorption is significant in flowback period. If desorption needs to be considered, then I would recommend a new set of analytical solutions developed from Fick's law instead of Darcy's law.

The assumption on homogenous pressure in matrix-fracture system may be relaxed in future research to determine pressure decline rate in fracture with improved accuracy. I

also recommend that future researchers devise a practical and simplified solution to analyze the coupling flow of gas.

The validations of flowback models are dependent on numerical simulation, and CMG (IMEX) is extensively applied. But the numerical models adopted may not replicate the real case of flowback in the field. For future researchers, it would be helpful to conduct case studies in field to help complete and validate this study. Also, I recommend collecting micro-seismic information to know the distribution of hydraulic fracture and construct the numerical models of flowback in a more realistic manner.

REFERENCES

1. Abbasi, M., Dehghanpour, H., & Hawkes, R. V. (2012, Oct 30-Nov 1). *Flowback analysis for fracture characterization.* Paper presented at SPE Canadian Unconventional Resources Conference in Calgary, Albert, Canada.
2. Abassi, M. A., Ezulike, D. O., Dehghanpour, H., & Hawkes, R. V. (2014). "A comparative study of flowback rate and pressure transient behavior in multifractured horizontal wells completed in tight gas and oil reservoirs." *Journal of Natural Gas Science & Engineering, 17*, 82-93.
3. Adefidipe, O. A., Dehghanpour, H., & Virues, C. J. J. (2014a, Apr 1-3). *Immediate gas production from shale gas wells: a two-phase flowback model.* Paper presented at SPE Unconventional Resources Conference in The Woodlands, Texas.
4. Adefidipe, O. A., Xu, Y., Dehghanpour, H., & Virues, C. J. J. (2014b, Sept 30-Oct 2). *Estimating effective fracture volume from early-time production data: a material balance approach.* Paper presented at SPE/CSUR Unconventional Resources Conference–Canada in Calgary, Alberta, Canada.
5. Aguilera, R. (1995). *Naturally fractured reservoirs (*2nd ed.). Tulsa, OK: PennWell Books.
6. Alkouh, A. (2014). *New advances in shale gas reservoir analysis using water flowback data.* (Doctoral dissertation). Texas A & M University. Retrieved from
7. Alkouh, A., McKetta, S. F., & Wattenbarger, R. A. (2014). *Estimation of effective-fracture volume using water-flowback and production data for shale-gas wells. Journal of Canadian Petroleum Technology, 53*(5), 290-303.
8. Alkouh, A. B., Mcketta, S. F., & Wattenbarger, R. A. (2013). *Estimation of fracture volume using water flowback and production data for shale gas wells*. Paper presented at SPE Annual Technical Conference and Exhibition in New Orleans, Louisiana.
9. Andrews, A., Folger, P., Humphries, M., Copeland, C., Tiemann, M., Meltz, R., & Brougher, C. (2010). *Unconventional gas shales: development, technology, and policy issues*. Washington, DC: Congressional Research Service.
10. API — American Petroleum Institute Water Management Associated with Hydraulic Fracturing: API Guidance Document HF2 1st ed. 2010.
11. Behmanesh, H., Tabatabaie, S., Heidari Sureshjani, M., & Clarkson, C (2014). *Modification of the transient linear flow distance of investigation calculation for use in hydraulic fracture property determination*. Paper presented at SPE Unconventional Resources Conference in The Woodlands, Texas.
12. Cheng, Y. (2012). *Impacts of the number of perforation clusters and cluster spacing on production performance of horizontal shale-gas wells. SPE Reservoir Evaluation & Engineering, 15*(1), 31-40.
13. Churchill, R. V. (1972). *Operational mathematics* (3rd ed.). New York, NY: McGraw-Hill.

14. Clarkson, C. (2012). *Modeling two-phase flowback of multi-fractured horizontal wells completed in shale. SPE Journal, 18*(4).
15. Clarkson, C., Jordan, C., Ilk, D., & Blasingame, T. (2012). *Rate-transient analysis of 2-phase (gas + water) CBM wells. Journal of Natural Gas Science and Engineering, 8,* 106-120.
16. Clarkson, C., & McGovern, J. (2001). *Study of the potential impact of matrix free gas storage upon coalbed gas reserves and production using a new material balance equation*. Proceedings of the 2001 International Coalbed Methane Symposium at The University of Alabama in Tuscaloosa, Alabama.
17. Clarkson, C., & Williams-Kovacs, J. (2013a). *A new method for modeling multi-phase flowback of multi-fractured horizontal tight oil wells to determine hydraulic fracture properties*. Paper presented at SPE Annual Technical Conference and Exhibition in New Orleans, Louisiana.
18. Clarkson, C. R. (2013). *Production data analysis of unconventional gas wells: Review of theory and best practices. International Journal of Coal Geology, 109,* 101-146.
19. Clarkson, C. R., Ghaderi, S. M., Kanfar, M. S., Iwuoha, C. S., Pedersen, P. K., Nightingale, M., Shevalier, M., & Mayer, B. (2016). *Estimation of fracture height growth in layered tight/shale gas reservoirs using flowback gas rates and compositions - Part II: Field application in a liquid-rich tight reservoir. Journal of Natural Gas Science and Engineering, 36,* 1031-1049.
20. Clarkson, C. R., & McGovern, J. M. (2005). *Optimization of CBM reservoir exploration and development strategies through integration of simulation and economics. SPE Reservoir Evaluation & Engineering, 8*(6), 502-519.
21. Clarkson, C. R., & Williams-Kovacs, J. (2013b). *Modeling two-phase flowback of multifractured horizontal wells completed in shale. SPE Journal, 18*(4), 795-812.
22. Constanda, C. (2016). *Solution techniques for elementary partial differential equations* (3rd ed.). Boca Raton, FL: CRC Press.
23. Crafton, J. W. (1998, Sept 27-30). *Well evaluation using early time post-stimulation flowback data*. Paper presented at SPE Annual Technical Conference and Exhibition in New Orleans, Louisiana.
24. Crafton, J. W. (2008, Nov 16-18). *Modeling flowback behavior or flowback equals 'slowback.*' Paper presented at SPE Shale Gas Production Conference in Fort Worth, Texas.
25. Crafton, J. W. (2010, Feb 23-25). *Flowback performance in intensely naturally fractured shale gas reservoirs*. Paper presented at SPE Unconventional Gas Conference in Pittsburgh, Pennsylvania.
26. Crafton, J. W., & Gunderson, D. W. (2006, Sept 24-27). *Use of extremely high time-resolution production data to characterize hydraulic fracture properties*. Paper presented at SPE Annual Technical Conference and Exhibition in San Antonio, Texas.

27. Crafton, J. W., & Gunderson, D. W. (2007, Nov 11-14). *Stimulation flowback management—keeping a good completion good.* Paper presented at SPE Annual Technical Conference and Exhibition in Anaheim, California.
28. Craig, D. P., & Blasingame, T. A. (2006, May 15-17). *Application of a new fracture-injection/falloff model accounting for propagating, dilated, and closing hydraulic fractures.* Paper presented at SPE Gas Technology Symposium in Calgary, Alberta, Canada.
29. Dake, L. P. (1983). *Fundamentals of reservoir engineering*. Burlington, MA: Elsevier Science & Technology.
30. Economides, M. J., Hill, A. D., Ehlig-Economides, C., & Zhu, D. (2012). *Petroleum Production Systems* (2nd ed.). Austin, TX: Prentice-Hall.
31. Ezulike, O. D., & Dehghanpour, H. (2014). *Modelling flowback as a transient two-phase depletion process. Journal of Natural Gas Science and Engineering, 19,* 258-278.
32. Ezulike, O. D., & Dehghanpour, H. (2015). *A complementary approach for uncertainty reduction in post-flowback production data analysis. Journal of Natural Gas Science and Engineering, 27,* 1074-1091.
33. Ghanbari, E., Abbasi, M. A., Dehghanpour, H., & Bearinger, D. (2013). *Flowback volumetric and chemical analysis for evaluating load recovery and its impact on early-time production*. Paper presented at SPE Unconventional Resources Conference Canada in Calgary, Alberta, Canada.
34. Ilk, D., Anderson, D. M., Stotts, G. W., Mattar, L., & Blasingame, T. (2010a). *Production data analysis—Challenges, pitfalls, diagnostics. SPE Reservoir Evaluation & Engineering, 13*(3), 538-552.
35. Ilk, D., Currie, S. M., Symmons, D., Rushing, J. A., Broussard, N. J., & Blasingame, T. A. (2010b, Sept 19-22*). A comprehensive workflow for early analysis and interpretation of flowback data from wells in tight gas/shale reservoir systems*. Paper presented at SPE Annual Technical Conference and Exhibition in Florence, Italy.
36. King, G. (1990). *Material balance techniques for coal seam and devonian shale gas reservoirs*. Paper presented at SPE Annual Technical Conference and Exhibition in New Orleans, Louisiana.
37. Maxwell, S., Pirogov, A., Bass, C., & Castro, L. (2013, Feb 4-6). *A comparison of proppant placement, well performance, and estimated ultimate recovery between horizontal wells completed with multi-cluster plug & perf and hydraulically activated frac ports in a tight gas reservoir*. Paper presented at SPE Hydraulic Fracturing Technology Conference in The Woodlands, Texas.
38. Palisch, T. T., Duenckel, R. J., Bazan, L. W., Heidt, J. H., & Turk, G. A. (2007, Jan 29-31). *Determining realistic fracture conductivity and understanding its impact on well performance-theory and field examples.* Paper presented at SPE Hydraulic Fracturing Technology Conference in College Station, Texas.
39. Seidle, J. P. (1999, May 15-18). *A modified p/Z method for coal wells.* Paper presented SPE Rocky Mountain Regional Meeting in Gilette, Wyoming.

40. Shanley, K. W., Cluff, R. M., & Robinson, J. W. (2004). *Factors controlling prolific gas production from low-permeability sandstone reservoirs: Implications for resource assessment, prospect development, and risk analysis*. *AAPG bulletin 88*(8), 1083-1121.
41. Wattenbarger, R. A., & Alkouh, A. B. (2013, Aug 20-22). *New advances in shale reservoir analysis using flowback data*. Paper presented at SPE Eastern Regional Meeting in Pittsburgh, Pennsylvania.
42. Wattenbarger, R. A., El-Banbi, A. H., Villegas, M. E., & Maggard, J. B. (1998, Apr 5-8). *Production analysis of linear flow into fractured tight gas wells*. Paper presented at SPE Rocky Mountain Regional/Low-Permeability Reservoirs Symposium in Denver, Colorado.
43. Williams-Kovacs, J., & Clarkson, C. (2013a, Nov 5-7). *Stochastic modeling of multi-phase flowback from multi-fractured horizontal tight oil wells*. Paper presented at SPE Unconventional Resources Conference Canada in Calgary, Alberta, Canada.
44. Williams-Kovacs, J., & Clarkson, C. (2013b, Jul 20-22). *Stochastic modeling of two-phase flowback of multi-fractured horizontal wells to estimate hydraulic fracture properties and forecast production.* Paper presented at SPE Unconventional Resources Conference-USA in San Antonio, Texas.
45. Williams-Kovacs, J., & Clarkson, C. (2014a, Nov 5-7). *Analysis of stage-by-stage and multi-well flowback from multi-fractured horizontal wells.* Paper presented at SPE Unconventional Reservoir Conference-Canada in Calgary, Alberta. Canada.
46. Williams-Kovacs, J., & Clarkson, C. (2014b). *A new tool for prospect evaluation in shale gas reservoirs. Journal of Natural Gas Science & Engineering, 18*: 90-103.
47. Williams-Kovacs, J., & Clarkson, C. (2015, Jul 20-22). *A modified approach for modeling 2-phase flowback from multi-fractured horizontal shale gas wells*. Paper presented at Unconventional Resources Technology Conference in San Antonio, Texas.
48. U.S. Energy Information Administration. (2016, May 5). *Independent statistics and analysis: Hydraulically fractured wells provide two-thirds of U.S. natural gas production.*
49. U.S. Energy Information Administration. (2011, Jul 8). *Review of emerging resources: U.S. shale gas and shale oil plays.*
50. Xu, Y., Adefidipe, O., & Dehghanpour, H. (2015a). *Estimating fracture volume using flowback data from the Horn River Basin: A material balance approach. Journal of Natural Gas Science & Engineering, 25,* 253-270.
51. Xu, Y., Adefidipe, O., & Dehghanpour, H. (2016). *A flowing material balance equation for two-phase flowback analysis. Journal of Petroleum Science & Engineering, 142,* 170-185.
52. Xu, Y., Adefidipe, O., Dehghanpour, H., & Virues. C. (2015b, Apr 27-30). *Volumetric analysis of two-phase flowback data for fracture characterization*. Paper presented at SPE Western Regional Meeting in Garden Grove, California.

53. Xu, Y., O. A. Adefidipe and H. Dehghanpour (2015c). *Estimating fracture volume using flowback data from the Horn River Basin: A material balance approach. Journal of Natural Gas Science & Engineering, 25,* 253-270.
54. Zhang, J., Kamenov, A., Zhu, D., & Hill, A. (2013, Mar 26-28). *Laboratory measurement of hydraulic fracture conductivities in the Barnett shale*. Paper presented at International Petroleum Technology Conference in Beijing, China.
55. Zhang, Y., & Ehlig-Economides, C. (2014, May 25-27). *Accounting for remaining injected fracturing fluid in shale gas wells.* Paper presented at Unconventional Resources Technology Conference in Denver, Colorado.

APPENDIX A : ABBASI ET AL.'S MODEL

Abbasi et al.'s model is designed to analyze single-phase flowback of water. Linear relationship can be found between RNP and MBT and the lump of x_f and k_f can be estimated from the slope and intercept of the fitted linear line.

In the original work, the authors adopted a dimension that was based on a combination of field and SI units, which creates confusion when applying their model. In this work, I carefully reviewed their model and determined the coefficient of field unit. Their model can be expressed in field unit as,

$$RNP = \frac{B_w}{C_{st}} t + 52.7 \frac{\phi_f c_t \mu_w B_w}{k_f C_{st}} x_f^2. \tag{A.1}$$

By combing slope (m) and intercept (b), fracture properties can be estimated by

$$x_f = \sqrt{\frac{b k_f}{52.7 \phi_f c_t \mu_w m}}, \tag{A.2}$$

$$k_f = \frac{52.7 \phi_f c_t \mu_w x_f^2 m}{b}. \tag{A.3}$$

In this thesis, C_{st} should be properly defined to apply to this model to predict flowback behavior. In the original publication, C_{st} is defined as,

$$C_{st} = \frac{\partial V_f}{\partial P_f} + V_f c_f + V_{wb} c_{wb}, \tag{A.4}$$

where c_f is defined as fracture fluid compressibility, c_{wb} is defined as wellbore fluid compressibility, V_f is fracture volume, and V_{wb} is wellbore volume .

In Equation (A.4), C_{st} is not clearly derived, and causes problem in evaluation. To be clear, the definition of fracture compressibility is given by,

$$c_r = -\frac{1}{V_f}\frac{\partial V_f}{\partial P_f}\bigg|_T. \tag{A.5}$$

Also, if c_f and c_{wb} turn out to be water compressibility in fracture and wellbore, then C_{st} can be developed as,

$$C_{st} = c_r V_f + c_w V_f + c_w V_{wb}. \tag{A.6}$$

If fracture properties are available, then RNP can be evaluated as a function of time with Equation (A.1). This model can be applied to estimate fracture properties for single-phase flowback under PSS and to predict flowback rate and pressure when fracture properties are provided.

APPENDIX B : ALKOUH ET AL.'S MODEL

Alkouh et al. (2014) proposed an analytical model on flowback to estimate fracture volume, where linear relationship can be established between RNP and MBT. The model is given by

$$RNP = \frac{V_w C_t}{B_w} MBT, \tag{B.1}$$

Theirs is a significant work that lays the foundation to construct a numerical model of flowback. Unfortunately, they did not fully develop their mathematical model, which leads to discrepancies during validation. In this thesis, my work extends Alkouh et al's mathematical model to evaluate k_f and x_f simultaneously, where in their model, only effective fracture volume or x_f could be determined.

For fracture depletion, pressure drawdown can be estimated by

$$P_i - P_f = \frac{W_P B_w}{W_i B_{wi} c_t}, \tag{B.2}$$

where W_p is cumulative water production, W_i is initial water storage in fracture, B_w is water compressibility, and B_{wi} is water compressibility at initial fracture pressure.

The well inflow equation developed for linear flow is combined with Equation (B.2) to provide full development of this model.

Figure B.1 depicts the 1D linear flow along the fracture under fracture depletion mechanism.

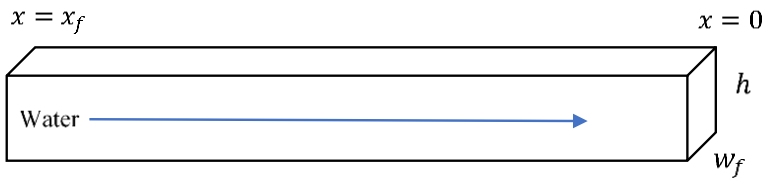

Figure B.1: Linear flow of water along fracture during single-phase flowback period

For small element of dx along the fracture, the material balance equation can be stated as,

$$q_w\rho_w|_{x+d_x} - q_w\rho_w|_x = \frac{\partial}{\partial t}\left(dx\phi_f w_f h\rho_w\right), \tag{B.3}$$

where q_w is water flow rate at reservoir condition, ρ_w is *in situ* water density, *w* is fracture width, *h* is fracture height, and ϕ_f is fracture porosity.

Assuming fracture is homogeneous and anisotropic, and water is incompressible fluid, then Equation (B.3) can be simplified as,

$$\rho_w \frac{\partial q}{\partial x} = w_f h \frac{\partial}{\partial t}\left(\phi_f \rho_w\right). \tag{B.4}$$

For linear flow, Darcy's law can be expressed as,

$$q_w = \frac{k_f w_f h}{\mu_w}\frac{\partial P}{\partial x}. \tag{B.5}$$

Combining Equations (B.4) and (B.5), diffusivity equation for linear flow of water along the fracture is determined as,

$$\frac{\partial^2 P}{\partial x^2} = \frac{\phi_f \mu_w c_t}{k_f}\frac{\partial P}{\partial t}, \tag{B.6}$$

where $c_t = c_w + c_r$.

The boundary conditions for PSS are given by

$$\frac{\partial P}{\partial x}|_{x=x_f} = 0, \tag{B.7}$$

$$\frac{\partial P}{\partial x}|_{x=0} = \frac{q_w \mu_w}{k_f w_f h}, \tag{B.8}$$

where q_w is both the specified water production rate, as well as constraint.

Applying Equation (B.7), the PDE Equation (B.6) can be solved as,

$$\frac{\partial P}{\partial x} = \frac{\phi_f \mu_w c_t}{k_f} x \frac{\partial P}{\partial t} + \frac{q_w \mu_w}{w_f h k_f}. \tag{B.9}$$

Total compressibility (c_t) can be estimated from water production as,

$$c_t = -\frac{1}{W_p} \frac{\partial W_p}{\partial P}. \tag{B.10}$$

When chain rule is applied,

$$c_t W_p \frac{\partial P}{\partial t} = -\frac{\partial W_p}{\partial t}. \tag{B.11}$$

Since there is no flow boundary at fracture tip Equation (B.7), pseudo steady state flow can be established under constant rate production. The rate of increase in cumulative water production should be constant, and expressed as

$$\frac{\partial W_p}{\partial t} = q_{\mathrm{w}}. \tag{B.12}$$

When this is substituted into (B.11), pressure decline rate in fracture can be evaluated by

$$\frac{\partial P}{\partial t} = -\frac{q_w}{c_t w_f h x_f \phi_f}. \tag{B.13}$$

Under constant rate production, pressure decline rate ($\frac{\partial P}{\partial t}$) holds constant in fracture. Substitute into Equation (B.9),

$$\frac{\partial P}{\partial x} = -\frac{q_w \mu_w}{w_f h x_f k_f} x + \frac{q_w \mu_w}{w_f h k_f}. \tag{B.14}$$

Integration is then applied as,

$$\int_{x=0}^{x=x^*} \partial P = \int_{x=0}^{x=x^*} (-\frac{q_w \mu_w}{w_f h x_f k_f} x + \frac{q_w \mu_w}{w_f h k_f}) \partial x, \tag{B.15}$$

where x^* is any space in the fracture.

After integration, fracture pressure is determined as,

$$P - P_{wf} = -\frac{q_w \mu_w}{2 w_f h x_f k_f} x^2 + \frac{q_w \mu_w}{w_f h k_f} x. \tag{B.16}$$

Pressure is a function of space and bottom hole pressure (P_{wf}), which varies with time.

At x=x_f, the pressure drawdown ($P_e - P_{wf}$) across the fracture can be determined as,

$$P_e - P_{wf} = \frac{q_w \mu_w x_f}{2 w_f h k_f}, \tag{B.17}$$

where P_e is fracture pressure at fracture boundary.

The average pressure in fracture (P_f) can be determined based on volumetric average as,

$$P_f = \frac{\int_0^{x_f} P dV_f}{\int_0^{x_f} dV_f}, \tag{B.18}$$

$$dV_f = w_f h \phi_f dx, \tag{B.19}$$

$$P_f - P_{wf} = \frac{x_f \mu_w}{3 w_f h k_f} q_o, \tag{B.20}$$

where V_f is *in situ* fracture volume.

This equation expresses well inflow for linear flow, and the general formula of well inflow equation is stated as

$$\bar{P} - P_{wf} = Jq, \tag{B.21}$$

where $\bar{P}$ is average pressure in the system, and q is flow rate of the fluid in the system.

From Equation (B.21), the productivity index of water in fracture (J_w) can be determined as,

$$J_w = \frac{x_f \mu_w}{3 w_f h k_f}. \tag{B.22}$$

Expressed in field unit, Equation (B.22) is converted thus:

$$J_w = 296.408 \frac{x_f \mu_w}{w_f h k_f}. \tag{B.23}$$

When Equation (B.2) is combined with Equation (B.22),

$$RNP = J_w + \frac{5.615 B_w}{c_t V_f \phi_f} MBT. \tag{B.24}$$

Expressed in field unit, Equation (B.23) is converted by

$$RNP = 5.615 \frac{B_w}{c_t w_f h x_f \phi_f} MBT + 296.41 \frac{x_f \mu_w B_w}{w_f h k_f}. \tag{B.25}$$

In Alkouh et al. (2014), the authors neglected any consideration of J_w which, at a later stage, the mathematical model can be simplified as,

$$RNP = \frac{B_w}{V_w c_t} MBT. \tag{B.26}$$

In their solution, only V_w or x_f if cross-sectional area of fracture is available, can be estimated from the slope. By developing and applying well inflow equation of linear flow,

both x_f and k_f can be evaluated from the flowback data as shown in Equation (B.26). From the linear relationship that can be established after BDF is stabilized, slope (m) and intercept (b) can be determined by linear curve fitting. k_f and x_f can be determined by

$$x_f = \frac{5.615 B_w}{w_f h m c_t \phi_f}, \tag{B.27}$$

$$k_f = 295.77 \frac{x_f \mu_w B_w}{b w_f h}. \tag{B.28}$$

APPENDIX C : 1D ANALYTICAL MODEL ON SINGLE-PHASE FLOWBCAK

The 1D model is developed to analyze flowback behavior for single-phase water flow under fracture depletion mechanism.

Flow of fracturing fluid (water) along fracture is depicted similar to Figure B.1.

The diffusivity equation for single-phase water flow in fracture is given by

$$\frac{\partial(\rho_w v)}{\partial x} = \frac{\partial(\rho_w \phi_f)}{\partial t}, \tag{C.1}$$

where v_w is velocity of water flow in fracture.

Assuming fracture is homogeneous and isotropic and water is incompressible fluid, Equation (C.1) can be simplified as,

$$\rho_w \frac{\partial(v_w)}{\partial x} = \rho_w \phi_f (c_r + c_w) \frac{\partial P}{\partial t}. \tag{C.2}$$

In terms of field units, Darcy's law for linear flow can be expressed as,

$$v_w = 0.006328 \frac{k_f}{\mu_w} \frac{\partial P}{\partial x} \quad . \tag{C.3}$$

When this is substituted into Equation (C.2),

$$\frac{\partial^2 P}{\partial x^2} = \frac{1}{\eta} \frac{\partial P}{\partial t}, \tag{C.4}$$

where $\eta = 0.006328 \frac{k_f}{\phi_f c_t \mu_w}$.

Equation (C.4) is the governing partial differential equation to analyze single-phase flowback of water. Under different well constraints, different solutions can be obtained,

which makes the mathematical model of single-phase flowback versatile in field application.

C.1 1D Analytical Model (Case 1)

The first case of 1D analytical model of single-phase flowback is developed under PSS, where the boundary conditions are given by

$$\frac{\partial P(t,x_f)}{\partial x} = 0, \tag{C.5}$$

$$\frac{\partial P(t,0)}{\partial x} = \frac{q_w B_w \mu_w}{k_f w_f h}. \tag{C.6}$$

The initial condition at the start of flowback period can be expressed as,

$$P(0,x) = P_i. \tag{C.7}$$

Boundary conditions have to be homogenized before applying the solution technique of PDE: separation of variables. Dimensionless parameters are defined as,

$$x_D = \frac{x}{x_f}, \tag{C.8}$$

$$t_D = \frac{t\eta}{x_f^2}, \tag{C.9}$$

$$q_{Dw} = \frac{q_w x_f \mu_w B_w}{k_f w_f h P_i}, \tag{C.10}$$

$$P_D = 1 - P/P_i. \tag{C.11}$$

When the dimensionless group is applied, the initial condition and boundary conditions can be converted into,

$$\frac{\partial P_D(0,t_D)}{\partial x_D} = q_{Dw}, \tag{C.12}$$

$$\frac{\partial P_D(1,t_D)}{\partial x_D} = 0, \tag{C.13}$$

$$P_D(0, x_D) = 0. \tag{C.14}$$

The diffusivity equation Equation (C.4) in dimensionless form is given by

$$\frac{\partial^2 P_D}{\partial x_D^2} = \frac{\partial P_D}{\partial t_D}. \tag{C.15}$$

To homogenize the boundary condition, P_D is decomposed as,

$$P_D = P(t_D, x_D) + S(t_D, x_D), \tag{C.16}$$

where $S(t_D, x_D)$ is an intermediate parameter used to homogenize boundary condition.

When this is substituted into Equation (C.15),

$$\frac{\partial P}{\partial t_D} + \frac{\partial S}{\partial t_D} = \frac{\partial^2 P}{\partial x_D^2} + \frac{\partial^2 S}{\partial x_D^2}. \tag{C.17}$$

When we rearrange the equation,

$$\frac{\partial P}{\partial t_D} = \frac{\partial^2 P}{\partial x_D^2} + A, \tag{C.18}$$

where $A = -\frac{\partial S}{\partial t_D} + \frac{\partial^2 S}{\partial x_D^2}$.

Assuming S is a polynomial function expressed in this form,

$$S = a + bx_D + ct_D + dx_D^2, \tag{C.19}$$

where a, b, c, d are the coefficients that need to be determined for S.

Substituting Equation (C.19) into Equation (C.18),

$$\frac{\partial P}{\partial t_D} = \frac{\partial^2 P}{\partial x_D^2} - c + 2d. \tag{C.20}$$

Substituting Equation (C.16) into boundary and initial conditions Equations (C.12) – (C.14), then

$$\frac{\partial P(0,t_D)}{\partial x_D} + \frac{\partial S(0,t_D)}{\partial x_D} = q_{Dw}, \tag{C.21}$$

$$\frac{\partial P(1,t_D)}{\partial x_D} + \frac{\partial S(1,t_D)}{\partial x_D} = 0, \tag{C.22}$$

$$P(t_D = 0) + S(t_D = 0) = 0. \tag{C.23}$$

Thus, we should have

$$\frac{\partial P(0,t_D)}{\partial x_D} = 0, \tag{C.24}$$

$$\frac{\partial S(0,t_D)}{\partial x_D} = q_{Dw}, \tag{C.25}$$

$$\frac{\partial P(1,t_D)}{\partial x_D} = 0, \tag{C.26}$$

$$\frac{\partial S(1,t_D)}{\partial x_D} = 0. \tag{C.27}$$

The solution of S is determined as,

$$S(x_D, t_D) = q_{Dw}\left(\frac{x_D^2}{2} - x_D + t_D\right). \tag{C.28}$$

The solution of P at initial condition is determined as,

$$P(t_D = 0) = q_{Dw}(x_D - \frac{x_D^2}{2}). \tag{C.29}$$

Applying separation of variables, solution of fracture pressure is given by

$$P = X(x_D)T(t_D), \tag{C.30}$$

where $X(x_D)$ is some function of x_D and $T(t_D)$ is some function of t_D.

The fundamental solution of pressure is given by

$$P_n(x_D, t_D) = X_n(X_D)T_n(t_D). \tag{C.31}$$

Substituting Equation (C.30) into Equation (C.15), then

$$\frac{1}{X}\frac{\partial^2 X}{\partial x_D^2} = \frac{1}{T}\frac{\partial T}{\partial t_D} = -\lambda^2. \tag{C.32}$$

where λ is the separation constant and can be either a negative or positive number.

Then, function of $X(x_D)$ and $T(t_D)$ can be determined as,

$$X''(x_D) + \lambda^2 X(x_D) = 0, \tag{C.33}$$

$$T'(t_D) + \lambda^2 T(t_D) = 0. \tag{C.34}$$

The boundary conditions for function $X(x_D)$ are given by

$$\frac{\partial X}{\partial x_D}(0, t_D) = 0, \tag{C.35}$$

$$\frac{\partial X}{\partial x_D}(1, t_D) = 0. \tag{C.36}$$

The nonzero solutions of X are the eigenfunctions of the Sturm-Liouville problem and are given by

$$X_n(x_D) = cos(\lambda_n x_D). \tag{C.37}$$

where eigenvalue $\lambda_n = n\pi$ $(n = 0,1,2 \dots \dots)$.

Integrating the equation satisfied by T with $\lambda = \lambda_n, n = 0,1,2 \ldots\ldots$, we obtain the associated time components as,

$$T_n(t_D) = \exp(-\lambda_n^2 t_D). \tag{C.38}$$

The expected series representation of dimensionless pressure is given by

$$P_D(x_D, t_D) = \sum_{n=1}^{\infty} b_n \cos(\lambda_n x_D)\, e^{-\lambda_n^2 t_D}. \tag{C.39}$$

where b_n are arbitrary numbers.

To solve for expression of b_n, substitute initial condition Equation (C.29) into Equation (C.39), then

$$\sum_{n=1}^{\infty} b_n \cos(\lambda_n x_D) = q_{Dw}\left(x_D - \frac{x_D^2}{2}\right). \tag{C.40}$$

For $n = 0$,

$$b_0 = \frac{\int_0^1 q_{Dw}\left(x_D - \frac{x_D^2}{2}\right)dx}{\int_0^1 1\,dx} \tag{C.41}$$

$$b_0 = \frac{q_{D0}}{3}. \tag{C.42}$$

For $n > 0$,

$$b_n = \frac{\int_0^1 q_{Dw}\left(x_D - \frac{x_D^2}{2}\right)\cos(\lambda_n x_D)dx}{\int_0^1 \cos^2(\lambda_n x_D)\,dx}, \tag{C.43}$$

$$b_n = -2\frac{q_{D0}}{\lambda_n^2}. \tag{C.44}$$

So the solution of $P_D(x_D, t_D)$ is given by

$$\frac{P_D(x_D,t_D)}{q_{Do}} = \frac{1}{3} + t_D - x_D + \frac{x_D^2}{2} - 2q_{Dw}\sum_{n=1}^{\infty}\frac{1}{(n\pi)^2}\cos(n\pi x_D)\, e^{-(n\pi)^2 t_D}. \tag{C.45}$$

In dimensional form,

$$\frac{(P_i - P_{wf})}{q_w} = \frac{x_f \mu_w B_w}{0.001127 k_f w_f h}\left(\frac{1}{3} + t_D - 2\sum_{n=1}^{\infty}\frac{e^{-(n\pi)^2 t_D}}{(n\pi)^2}\right). \quad \text{(C.46)}$$

At a later time, the sum of infinite series is negligible. The solution of (C.46) can be simplified as,

$$RNP = \frac{5.615 B_w}{w_f h x_f c_t \phi_f} t + 296\frac{x_f \mu_w B_w}{k_f w_f h}, \quad \text{(C.47)}$$

where $RNP = \frac{(P_i - P_{wf})}{q_w}$ and the coefficients are applied for field units.

The late-time approximation of 1D model (Case 1) uses the same formula as Alkouh et al.'s model, where k_f and x_f can be estimated from the slope and intercept of the fitted straight line. By involving the infinite series, this model can also be used to predict flowback behavior for transient period.

C.2 1D Analytical Model (Case 2)

The 1D analytical model (Case 2) is developed to analyze single-phase flowback for BDF under constant BHP production. The same governing diffusivity equation Equation (C.4) is also applied here. For constant BHP flowback, only boundary condition differs from Case 1 and is given by

$$P(0, t) = P_{wf}, \quad \text{(C.48)}$$

$$\frac{\partial P(x_f, t)}{\partial x} = 0. \quad \text{(C.49)}$$

To homogenize the boundary condition, the dimensionless group is given by

$$P_D = \frac{P-P_{wf}}{P_i-P_{wf}}, \tag{C.50}$$

$$x_D = \frac{x}{x_f}, \tag{C.51}$$

$$t_D = t\frac{\eta}{x_f^2}. \tag{C.52}$$

Then the initial and boundary conditions are converted as,

$$P_D(x_D, 0) = 1, \tag{C.53}$$

$$P_D(0, t_D) = 0, \tag{C.54}$$

$$\frac{\partial P_D(1,t_D)}{\partial x_D} = 0. \tag{C.55}$$

The governing diffusivity equation in dimensionless form is the same as Case 1 and expressed as Equation (C.15).

Separation of variables is applied to solve for fracture pressure as a function of time and distance. This diffusivity equation is analogous to heat equation and the solution can be referred to on page 97 of Constanda (2016).

The corresponding eigenvalue and eigenfunctions are given by

$$\lambda_n = \frac{(2n-1)^2\pi^2}{4}, \tag{C.56}$$

$$X_n(x_D) = \sin\frac{(2n-1)\pi x_D}{2}, \tag{C.57}$$

$$T_n(t) = e^{-\frac{(2n-1)^2\pi^2 t_D}{4}}. \tag{C.58}$$

where $n = 1,2, \ldots$

The series representation of dimensionless pressure is given by

$$P_{D_n}(x_D, t_D) = X_n(x_D)T_n(t_D), \quad \text{(C.59)}$$

$$P_D(x_D, t_D) = \sum_{n=1}^{\infty} c_n P_{D_n}(x_D, t_D) \quad \text{(C.60)}$$

where c_n are arbitrary numbers.

Applying initial condition, coefficient c_n can be determined as,

$$c_n = \frac{4}{(2n-1)\pi}. \quad \text{(C.61)}$$

Substituting Equations (C.56) – (C.59) and (C.61) into Equation (C.60),

$$P_D(x_D, t_D) = \sum_{n=1}^{\infty} \frac{4}{(2n-1)\pi} \sin\frac{(2n-1)\pi x_D}{2} e^{-\frac{(2n-1)^2\pi^2 t_D}{4}}. \quad \text{(C.62)}$$

In dimensional form,

$$P(x,t) = \left(P_i - P_{wf}\right) \sum_{n=1}^{\infty} \frac{4}{(2n-1)\pi} \sin\frac{(2n-1)\pi x}{2x_f} e^{-\frac{0.001582(2n-1)^2\pi^2 t k_f}{\phi_f c_t \mu_w x_f^2}} + P_{wf}. \quad \text{(C.63)}$$

Applying Darcy's law for linear flow, RNP can be determined as,

$$RNP = \frac{887.31\, B_w \mu_w}{k_f w_f h \sum_{n=1}^{\infty} \frac{2}{x_f} e^{-\frac{0.001582(2n-1)^2\pi^2 t k_f}{\phi_f c_t \mu_w x_f^2}}}. \quad \text{(C.64)}$$

If fracture properties (x_f and k_f) are available, RNP can be predicted as a function of flowback time.

C.3 1D Analytical Model (Case 3)

The 1D model (Case 3) is developed to analyze flowback for transient period under constant BHP production. The same governing diffusivity equation of water Equation (C.4) is also applied here. The boundary conditions are given by

$$P(0,t) = P_{wf}, \tag{C.65}$$

$$P(\infty,t) = P_i. \tag{C.66}$$

Equation (C.66) is put in to the semi-infinite domain to represent that pressure propagation has not reached fracture boundary for transient period. The dimensionless group is defined same as Case 2 as Equations (C.50) – (C.52).

Then the initial and boundary conditions are converted as,

$$P_D(x_D,0) = 1, \tag{C.67}$$

$$P_D(0,t_D) = 0, \tag{C.68}$$

$$P_D(\infty,t_D) = 1. \tag{C.69}$$

The governing diffusivity equation of water flow along the fracture in dimensionless form is shown in Equation (C.14).

Laplace transformation is applied to find the solution of fracture pressure, dependent on flowback time and space of fracture. Laplace transformation is applied as,

$$L\big(P_D(x_D,t_D)\big) = U(x_D,s), \tag{C.70}$$

where s is the transformation parameter related to time, U is the function of P_D in Laplace domain.

The diffusivity equation can be placed in Laplace domain as,

$$U''(x_D, s) - sU(x_D, s) + 1 = 0. \quad \text{(C.71)}$$

The corresponding boundary conditions in Laplace domain are described as,

$$U(0, s) = 0, \quad \text{(C.72)}$$

$$U(\infty, s) = \frac{1}{s}. \quad \text{(C.73)}$$

The general solution of U can be found as,

$$U(x_D, s) = C_1(s)e^{\sqrt{s}x_D} + C_2(s)e^{-\sqrt{s}x_D} + \frac{1}{s}, \quad \text{(C.74)}$$

where C_1 is some function of s and C_2 is some function of s.

Applying boundary conditions, C_1 and C_2 can be determined as,

$$C_1(s) = 0, \quad \text{(C.75)}$$

$$C_2(s) = -\frac{1}{s}. \quad \text{(C.76)}$$

The general solution of U as a function of x_D and S is obtained as,

$$U(x_D, s) = -\frac{1}{s}e^{-\sqrt{s}x_D} + \frac{1}{s}. \quad \text{(C.77)}$$

Inversion of Laplace solution is applied to transfer U in Laplace domain to P in normal domain. Referring to Appendix A in Churchill (1972) and the inverted solution of U ($P_D(x_D, t_D)$) can be derived as,

$$P_D(x_D, t_D) = L^{-1}(U(x_D, s)), \quad \text{(C.78)}$$

$$P_D(x_D, t_D) = \text{erf}(\frac{x_D}{2\sqrt{t_D}}), \quad \text{(C.79)}$$

$$P(x,t) = \left(P_i - P_{wf}\right) \text{erf}\left(\frac{x}{2\sqrt{t\eta}}\right) + P_{wf}, \quad \text{(C.80)}$$

where erf()is the error function.

Applying Darcy's law for linear flow, RNP is determined as,

$$RNP = 125 \frac{B_w}{w_f h} \sqrt{\frac{\mu_w t}{k_f \phi_f c_t}}, \quad \text{(C.81)}$$

where 125 is the coefficient for unit conversion for application in field unit.

In Equation (C.80), linear relationship can be obtained between RNP and $\sqrt{t}$ as,

$$RNP = m\sqrt{t}, \quad \text{(C.82)}$$

where $m = 125 \frac{B_w}{w_f h} \sqrt{\frac{\mu_w}{k_f \phi_f c_t}}$.

In the plot of RNP vs. $\sqrt{t}$, fracture permeability (k_f) can be estimated from the slope (m) as,

$$k_f = 15625 \frac{B_w^2 \mu_w}{w_f^2 h^2 \phi_f c_t m^2}. \quad \text{(C.83)}$$

C.4 1D Analytical Model (Case 4)

The 1D model (Case 4) is developed to analyze flowback for transient period under constant q production. The same governing diffusivity equation Equation (C.4) is also applied here. The boundary conditions are given by

$$\frac{\partial P(t,0)}{\partial x} = \frac{q_w B_w \mu_w}{k_f w_f h}, \quad \text{(C.84)}$$

$$P(\infty, t) = P_i. \quad \text{(C.85)}$$

Equation (C.85) is put in the semi-infinite domain to represent that pressure propagation has not reached fracture boundary for transient period.

The dimensionless group is defined as,

$$\mathrm{x_D} = \frac{x}{x_f}, \tag{C.86}$$

$$\mathrm{t_D} = \frac{t\eta}{x_f^2}, \tag{C.87}$$

$$\mathrm{P_D} = 1 - \frac{P}{P_i}. \tag{C.88}$$

Then the initial and boundary conditions can be converted as,

$$\mathrm{P_D}(x_D, 0) = 0, \tag{C.89}$$

$$\frac{\partial \mathrm{P_D}(0, t_\mathrm{D})}{\partial \mathrm{x_D}} = \mathrm{q_{Dw}}, \tag{C.90}$$

$$\mathrm{P_D}(\infty, t_D) = 0. \tag{C.91}$$

The governing diffusivity equation in dimensionless form is described in Equation (C.15). Laplace transformation is applied to solve for fracture pressure as a function of flowback time and space in the fracture as Case 3.

Laplace transformation is applied to find the solution of fracture pressure dependent on flowback time and space of fracture. In Laplace domain, the diffusivity equation can be written as,

$$U''(x_D, s) - sU(x_D, s) = 0. \tag{C.92}$$

The corresponding boundary conditions in Laplace domain are described as,

$$U'(0, s) = -\frac{q_{Dw}}{s}, \tag{C.93}$$

$$U(\infty, s) = \frac{1}{s}. \tag{C.94}$$

The general solution of U as a function of x_D and S is obtained as,

$$U(x_D, s) = C_1(s)e^{\sqrt{s}x_D} + C_2(s)e^{-\sqrt{s}x_D}. \tag{C.95}$$

where C_1 is some function of s and C_2 is some function of s.

Applying boundary conditions, C_1 and C_2 are determined as,

$$C_1(s) = 0, \tag{C.96}$$

$$C_2(s) = \frac{q_{Dw}}{s\sqrt{s}}. \tag{C.97}$$

The general solution of U as a function of x_D and S is obtained as,

$$U(x_D, s) = \frac{q_{Dw}}{s\sqrt{s}} e^{-\sqrt{s}x_D}. \tag{C.98}$$

Inversion of Laplace solution is applied to transfer *U* in Laplace domain to *P* in normal domain. Referring to appendix A of Churchill (1972) and the invert solution of U ($P_D(x_D, t_D)$) can be derived as,

$$P_D(x_D, t_D) = q_{Dw}(2\sqrt{\frac{t_D}{\pi}}\exp\left(-\frac{x_D^2}{4t_D}\right) - x_D erfc\left(\frac{x_D}{2\sqrt{t_D}}\right)). \tag{C.99}$$

where $\text{erfc}() = 1 - \text{erf}()$,and is complete error function.

Applying definition of dimensionless parameters as described in Equations (C.89) –(C.91), the solution of *P* in dimensional form can be determined as,

$$P(x, t) = \left(1 - q_{Dw}\left(2\sqrt{\frac{t_D}{\pi}}\exp\left(-\frac{x_D^2}{4t_D}\right) - x_D erfc\left(\frac{x_D}{2\sqrt{t_D}}\right)\right)\right)P_i. \tag{C.100}$$

Well flowing pressure (P_{wf}) can be found at $x = 0$ and is given by

$$P_{wf} = P_i - \frac{2q_w x_f \mu_w B_w}{0.001127 k_f w_f h P_i} P_i 2\sqrt{\frac{t\eta}{x_f^2 \pi}}. \quad \text{(C.101)}$$

Then RNP can be determined as,

$$RNP = 79.65 \frac{B_w}{w_f h}\sqrt{\frac{\mu_w t}{k_f \phi_f c_t}}. \quad \text{(C.102)}$$

where 79.65 is the coefficient for unit conversion in application of field unit.

In Equation (C.102), linear relationship can be obtained between RNP and $\sqrt{t}$ as,

$$RNP = m\sqrt{t}$$

where $m = 79.65 \frac{B_w}{w_f h}\sqrt{\frac{\mu_w}{k_f \phi_f c_t}}$.

In the plot of RNP vs. $\sqrt{t}$, fracture permeability (k_f) can be estimated from the slope (m) as,

$$k_f = 6344 \frac{B_w^2 \mu_w}{w_f^2 h^2 \phi_f c_t m^2}. \quad \text{(C.103)}$$

C.5 1D Analytical Model (Variable *q*)

To obtain solution forvariable flow rate production, superposition principle explained in (Dake, 1983) is applied to superimpose analytical solution for flowback under constant production rate. The general formula of superposition principle is given by

$$\frac{2\pi kh}{\mu}\left(P_i - P_{wfn}\right) = \sum_{j=1}^{n} \Delta q_j (t_{Dn} - t_{Dj-1}), \quad \text{(C.104)}$$

where P_{wfn} is wellbore pressure at the end of period t_n, Δq_j is the change in flow rate, P can be substituted with any general expression of pressure and k, h, q and μ can be substituted with fracture and water properties for flowback analysis.

The 1D analytical solution under PSS (Case 1) is given by

$$\frac{P_i - P_{wf}}{q_o} = \frac{5.615 B_w}{\phi_f c_t w_f h x_f} t + \frac{x_f \mu_w B_w}{0.003381 k_f w_f h}. \quad \text{(C.47)}$$

Applying Superposition Principle, the pressure drawdown at $\mathrm{t} = \mathrm{t_n}$ can be determined as,

$$\mathrm{P_i} - P_{wfn} = \frac{5.615 B_w}{\phi_f c_t w_f h x_f} \sum_{j=1}^{n} (q_j - q_{j-1})(t_n - t_{j-1}) + \frac{x_f \mu_w B_w}{0.003381 k_f w_f h} (q_n), \text{(C.105)}$$

where q_n is the flow rate at $t = t_n$.

Then the linear relationship can be established between RNP and BDF superposition time (t_{sppss}) and the definition of t_{sppss} is given by

$$t_{sppss} = \sum_{j=1}^{n} (q_j - q_{j-1})(t_n - t_{j-1}). \quad \text{(C.106)}$$

In Equation (C.105), linear relationship can be obtained between RNP and t_{sppss} as,

$$\mathrm{P_i} - P_{wfn} = B t_{sppss} + C, \quad \text{(C.107)}$$

where $B = \frac{5.615 B_w}{\phi_f c_t w_f h x_f}$ and $C = \frac{x_f \mu_w B_w}{0.003381 k_f w_f h} q_n$.

In the plot of RNP vs. t_{sppss}, a straight line should be found and fracture properties can be estimated from the slope. On the other hand, pressure drop at the end of t_n can be predicted if k_f and x_f are available.

The same methodology can be applied to superimpose 1D solution (Case 4) that works for flowback under transient period for variable flowrate case.

The 1D analytical solution under transient and constant q (Case 4) is given by

$$P_{wf} = P_i - 79.65\frac{q_w B_w}{w_f h}\sqrt{\frac{\mu_w t}{k_f \phi_f c_t}}. \quad \text{(C.108)}$$

Applying superposition principle, the pressure drawdown at $\mathrm{t} = \mathrm{t_n}$ is found as,

$$P_i - P_{wfn} = 79.65\frac{B_w}{w_f h}\sqrt{\frac{\mu_w}{k_f}\phi_f c_t}\sum_{j=1}^{n}\Delta q_j\sqrt{(t_n - t_{j-1})}. \quad \text{(C.109)}$$

Then the linear relationship can be established between RNP and transient superposition time (t_{spt}) and the definition of $t_{spt}$is given by

$$t_{spt} = \sum_{j=1}^{n}\Delta q_j\sqrt{(t_n - t_{j-1})}. \quad \text{(C.110)}$$

In Equation (C.109), linear relationship can be obtained between RNP and t_{spt} as,

$$P_i - P_{wfn} = At_{spt}, \quad \text{(C.111)}$$

where $A = 79.65\frac{B_w}{w_f h}\sqrt{\frac{\mu_w}{k_f}\phi_f c_t}$.

In the plot of RNP vs. t_{spt}, a straight line should be found and fracture properties can be estimated from the slope. On the other hand, pressure drop at the end of t_n can be predicted if k_f and x_f are available.

APPENDIX D : CLARKSON ET AL.'S MODEL

Clarkson (2012) proposed an analytical model for two-phase flowback in shale gas formation based on their previous work (Clarkson & McGovern, 2005) on production data analysis of CBM. In this model, both free and adsorbed gas storage are considered and the material balance is used to determine average pressure for the matrix-fracture system, where they assume fracture and matrix are under homogenous pressure; similar assumptions were made in this work on two-phase flowback model with justification. The material balance in his work is given by

$$\frac{\bar{P}}{\bar{P}+P_L}+\frac{32037[\phi_f(1-s_{wf})+\phi_m(1-s_{wm})]}{V_L B_g \rho_b}=-\frac{0.7355}{V_L A L_f \rho_b}G_P+[\frac{P_i}{P_i+P_L}+$$

$$\frac{32037[\phi_f(1-s_{wif})+\phi_m(1-s_{wim})]}{V_L B_{gi} \rho_b}]. \qquad \text{(D.1)}$$

where $\bar{P}$ is average pressure of matrix-fracture system, ρ_b is bulk density, in g/cc, P_L is the critical desorption pressure in Langmuir isotherm, V_L is maximum adsorption volume in scf/ton, s_{wi} is initial water saturation in fracture, s_{wim} is initial water saturation in matrix, A is cross sectional area of fracture, in acre, B_{gi} is gas formation factor at initial fracture pressure, in cf/Mscf, and G_p is in cumulative gas production, in $Mscf$.

Langmuir isotherm were used to model the adsorption\desorption process and $\bar{P}$ can be determined from the isotherm equation if desorption volume is known. The Langmuir isotherm is described as,

$$V=\frac{P}{P+P_L}V_L, \qquad \text{(D.2)}$$

where $V$is adsorption volume at P.

However, one potential problem in their development is that they did not distinguish matrix from fracture volume, and thus treating both as a common term AL_f. This assumption may be valid for CBM, since natural fracture volume is comparable to matrix volume. For shale gas formation with induced fracture, fracture volume is usually much smaller than matrix volume. To accurately determine $\bar{P}$ during the two-phase flowback period, we modify (D.1) to separate fracture volume from matrix volume. The original gas in place ($OGIP$) in Mscf can be determined as,

$$OGIP = \frac{43560A\left(w_f\phi_f(1-s_{wif})+L_f\phi_m(1-s_{wim})\right)}{B_{gi}} + 1.3597\frac{P_i}{P_i+P_L}V_L AL_f(1-\phi_m)\rho_b. \quad \text{(D.3)}$$

The current gas in place ($CGIP$) in Mscf is found as,

$$CGIP = \frac{43560A\left(w_f\phi_f(1-s_{wif})+L_f\phi_m(1-s_{wim})\right)}{B_g} + 1.3597\frac{P}{P+P_L}V_L AL_f(1-\phi_m)\rho_b. \quad \text{(D.4)}$$

The cumulative gas production (G_p) in Mscf is the difference between $OGIP$ and $CGIP$ and is given by

$$G_p = OGIP - CGIP. \quad \text{(D.5)}$$

The average pressure for matrix and fracture system is determined as,

$$\frac{\bar{P}}{\bar{P}+P_L} + \frac{32037\left[w_f\phi_f(1-s_{wf})+L_f\phi_m(1-s_{wm})\right]}{V_L B_g\rho_b L_f(1-\phi_m)} = -\frac{0.7355}{V_L A\rho_b L_f(1-\phi_m)}G_P + \left[\frac{P_i}{P_i+P_L} + \frac{32037\left[w_f\phi_f(1-s_{wif})+L_f\phi_m(1-s_{wim})\right]}{V_L B_{gi}\rho_b L_f(1-\phi_m)}\right]. \quad \text{(D.6)}$$

Iteration schemes is required to determine $\bar{P}$ at each time step. If $\bar{P}$ is specified, then flowback rate of gas and water can be determined as,

$$q_g = \frac{k_{rg}k_f w_f(m(\bar{P})-m(P_{wf}))}{1422T(\ln(\frac{r_e}{r_w})-0.75+S)}, \quad \text{(D.7)}$$

$$q_w = \frac{k_{rw}k_f L_f(\bar{P}-P_{wf})}{141.2\mu_w B_w(\ln(\frac{r_e}{r_w})-0.75+S)}, \quad \text{(D.8)}$$

where m is pseudo pressure, r_e is drainage radius equivalent to fracture half-length in the conceptual model, S is skin factor, and T is reservoir temperature in Rankine.

From their conceptual model, they assumed cylindrical shape of fracture and thus, $r_e = x_f$. At each time step, they calculated the corresponding flowback rate of gas and water and update G_p and s_{wf} and a new P_{ave} was determined for the next step. Flowback rate of gas and water can be determined if r_e and k_f are available. To determine the fracture properties, history match process is required to adjust r_e and k_f simultaneously until the predicted q_g and q_w can match the field production data. This semi-analytical method may have a non-uniqueness problem and is, therefore, not very practical. Also, reservoir pressure may not deplete to critical desorption pressure during the short flowback period and, therefore, Langmuir isotherm is not applicable, and the proposed material balance is not valid. A more practical analytical model for two-phase flowback is needed and developed in Appendix E.

APPENDIX E: TWO-PHASE FLOWBACK MODEL

Single-phase flowback can only be found in tight gas formation and instead, immediate gas breakthrough is commonly found in flowback on shale gas formation. Clarkson's model assumes that water saturation in matrix is typically less then critical water saturation and, thus, water is immobile in matrix and water production in flowback are the only sources from fracture. Then flowback of water is still a 1D flow along the fracture, whereas gas flow may be a 1D flow along fracture, or a 2D flow along the fracture, followed by matrix to fracture, depending on whether gas matrix influx significantly affects the flowback.

The two-phase diffusivity equation of water phase is given by

$$q_w\rho_w|_{x+dx} - q_w\rho_w|_x = \frac{\partial}{\partial t}(dxw_f h\phi_f \rho_w s_w), \tag{E.1}$$

where dx is a small element along fracture, and s_w is water saturation in fracture. For single-phase flowback, s_w is always assumed to be 1.

Applying Taylor expansion and chain rule, Equation (E.1) can be developed as,

$$\frac{\partial q_w}{\partial x} = w_f h\phi_f \left(s_w c_w + s_w c_r + \frac{\partial s_w}{\partial P}\right)\frac{\partial P}{\partial t}. \tag{E.2}$$

where water is assumed to be an incompressible fluid, and water properties hold constant with pressure.

In field unit, flowrate of water can be determined using Darcy's law as

$$q_w = 0.006328\frac{k_{rw}w_f h k_f}{\mu_w}\frac{\partial P}{\partial x}, \tag{E.3}$$

where k_{rw} is relative permeability of water to include the effect of gas phase flow on water phase flow.

Substituting Equation (E.3) into Equation (E.2), then

$$\frac{\partial}{\partial x}(0.006328\frac{k_{rw}k_f}{\mu_w}\frac{\partial P}{\partial x}) = \phi_f(s_w c_w + s_w c_r + \frac{\partial s_w}{\partial P})\frac{\partial P}{\partial t}. \quad \text{(E.4)}$$

Known, k_{rw} is function of s_w and thus pressure dependent. To reduce the non-linearity brought about by k_{rw}, pseudo pressure of water (P_p) is defined as,

$$P_p = \int_{P_b}^{P} \frac{k_{rw}}{\mu_w} dP. \quad \text{(E.5)}$$

Applying pseudo pressure Equation (E.5) in Equation (E.4), then

$$\frac{\partial^2 P_p}{\partial x^2} = \frac{\phi_f}{0.006328\, k_f}\mu_w \frac{s_w}{k_{rw}}(c_w + c_r + \frac{1}{s_w}\frac{\partial s_w}{\partial P})\frac{\partial P_p}{\partial t}. \quad \text{(E.6)}$$

Pseudo time (t_a) is applied to further reduce the non-linearity on the left side of Equation (E.6) and is defined as,

$$t_a = \frac{k_{rw}}{s_w} t. \quad \text{(E.7)}$$

Substitute Equation (E.7) into Equation (E.6), then

$$\frac{\partial^2 P_p}{\partial x^2} = \frac{\phi_f}{0.006328\, k_f}\mu_w (c_w + c_r + \frac{1}{s_w}\frac{\partial s_w}{\partial P})\frac{\partial P_p}{\partial t_a}. \quad \text{(E.8)}$$

The only non-linear term left is $\frac{1}{s_w}\frac{\partial s_w}{\partial P}$ and can only be evaluated numerically. If the flowback is operating at constant BHP under BDF, the initial and boundary conditions are given by

$$P_p(x, 0) = P_{pi}, \quad \text{(E.9)}$$

$$P_p(0,t) = P_{pwf}, \tag{E.10}$$

$$\frac{\partial P_p(x_f,t_a)}{\partial x} = 0, \tag{E.11}$$

where P_{pi} is pseudo pressure at initial fracture pressure, and P_{pwf} is pseudo pressure at P_{wf}.

Dimensionless group are applied to homogenize the boundary condition and given by

$$P_{pD} = \frac{P_p - P_{pwf}}{P_{pi} - P_{pwf}}, \tag{E.12}$$

$$x_D = \frac{x}{x_f}, \tag{E.13}$$

$$t_D = t_a \frac{0.006328\, k_f}{\phi_f \mu_w\, x_f^2}. \tag{E.14}$$

where P_{pD} is the dimensionless pseudo pressure.

Then Equation (E.8) can be put in dimensionless group as,

$$\frac{\partial^2 P_{pD}}{\partial x_D^2} = (c_w + c_r + \frac{1}{s_w}\frac{\partial s_w}{\partial P})\frac{\partial P_{pD}}{\partial t_D}. \tag{E.15}$$

The initial and boundary conditions are homogenized as,

$$P_{pD}(x_D,0) = 1, \tag{E.16}$$

$$P_{pD}(0,t_D) = 0, \tag{E.17}$$

$$\frac{\partial P_{pD}(1,t_D)}{\partial x} = 0. \tag{E.18}$$

In Equation (E.15), $\frac{1}{s_w}\frac{\partial s_w}{\partial P}$ is a function of time and space. In order to obtain the solution of pressure, we neglect the variation in $\frac{1}{s_w}\frac{\partial s_w}{\partial P}$ with space and evaluate it numerically at

average fracture pressure (P_f) and average water saturation ($\bar{s}_w$) in fracture. Applying separation of variables, the expression of fracture pressure in dimensionless form is obtained as,

$$P_{pD}(x_D, t_D) = \sum_{n=1}^{\infty} \frac{4}{(2n-1)\pi} \sin \frac{(2n-1)\pi x_D}{2} \exp\left(-\frac{(2n-1)^2\pi^2}{4} \int_0^{t_a} \frac{1}{c_w + c_r + \frac{1}{s_w}\frac{\partial s_w}{\partial P}} \partial t_D\right). \quad \text{(E.19)}$$

To linearize the formula, equivalent time is defined as,

$$t_e = c_{ti} \int_0^{t_a} \frac{1}{c_w + c_r + \frac{1}{s_w}\frac{\partial s_w}{\partial P}} \partial t_a. \quad \text{(E.21)}$$

where c_{ti} is total compressibility of fracture fluid and porous media at initial fracture pressure and $c_{ti} = c_r + s_{gi}c_{gi} + s_{wi}c_{wi}$.

$\frac{1}{s_w}\frac{\partial s_w}{\partial P}$ can be determined from the corresponding material balance equation (MB) numerically using finite-difference approach, where average fracture pressure correlates to cumulative production. Substituting Equation (E.21) into Equation (E.19),

$$P_p(x,t) = \left(P_{pi} - P_{pwf}\right) \sum_{n=1}^{\infty} \frac{4}{(2n-1)\pi} \sin \frac{(2n-1)\pi x}{2x_f} \exp\left(-(2n-1)^2\pi^2 \frac{0.001582\, k_f}{\phi_f \mu_w x_f^2} \frac{t_e}{c_{ti}}\right) + P_{pwf}. \quad \text{(E.22)}$$

The water flowback rate can be found by

$$q_w = \left.\frac{\partial P_p}{\partial x}\right|_{x=0}. \quad \text{(E.23)}$$

The linear relationship can be established between $\ln(RNP)$ and t_e as,

$$ln(RNP) = \frac{0.0156\, k_f}{\phi_f \mu_w x_f^2 c_{ti}} t_e + \ln\left(\frac{79.01\, x_f B_w}{w_f h k_f}\right). \quad \text{(E.24)}$$

where $RNP = \frac{P_{pi} - P_{pwf}}{q_w}$.

In Equation (E.24), the lump of fracture properties ($\frac{k_f}{x_f^2}$) can be estimated from the slope of the fitted linear line between $\ln(RNP)$ and t_e.

The development of MB is needed to develop to evaluate $\frac{1}{s_w}\frac{\partial s_w}{\partial P}$ numerically and obtain defined parameters RNP and t_e. MB is developed for both EGP and LGP. In EGP, fracture is treated as a closed tank. In LGP, gas matrix influx is included.

The general expression of material balance for gas production is,

$$G_p = G_i - G_r. \tag{E.25}$$

where G_p is cumulative gas production, G_i is initial gas storage in fracture, and G_r is remaining gas in fracture, all expressed at surface condition.

The remaining gas in fracture can be determined as,

$$G_r = \frac{V_f - V_w}{B_g}, \tag{E.26}$$

where V_f is pore volume of fracture, V_w is remaining water volume in fracture and B_g is gas formation factor at current fracture pressure.

Assuming rock and water compressibility are constant with pressure, pore volume of fracture (V_f) can be determined as,

$$V_f = V_{fi}(1 - c_r(P_i - P_f)), \tag{E.27}$$

where V_{fi} is initial pore volume in fracture and $V_{fi} = w_f h x_f \phi_f$.

Remaining water volume (V_{wr}) and initial gas storage (G_i) in fracture can be found by

$$V_{wr} = (V_{fi} s_{wif} - W_p) B_w, \tag{E.28}$$

$$G_i = \frac{V_{fi}(1-s_{wi})}{B_{gi}}. \quad \text{(E.29)}$$

Then average fracture pressure (P_f) can be found as,

$$P_f = P_i - \frac{V_{fi}-((G_{fi}-G_p)B_g+(W_{fi}-W_p)B_w)}{V_{fi}c_r}. \quad \text{(E.30)}$$

In Equation (E.30), since B_g is dependent on pressure. P_f needs to be evaluated with appropriate iteration scheme. Once P_f is specified, flowback rate and bottomhole pressure can be converted to RNP and t_e and plot of $\ln(RNP)$ and t_e can be constructed. With Equation (E.24), fracture attributes can be evaluated from slope of the linear fitted line.

For LGP, matrix storage should be included in the development of material balance. Several assumptions were made in the material balance.

- Water is immobile in matrix and water production sources only from induced fracture network.
- Pressure decline rate in matrix and fracture are equivalent in late flowback period.

Therefore, water storage in matrix remains constant, since initial water saturation in matrix is below immobile water saturation. Initial gas storage needs to be modified to include free gas storage in fracture and to consider the effect of matrix flow on flowback. Initial gas storage is found by

$$G_i = G_{fi} + G_{mi}, \quad \text{(E.31)}$$

where $G_{fi} = \frac{x_f w_f h \phi_f S_{gi}}{B_{gi}}$ and $G_{mi} = \frac{x_f L_f h \phi_m S_{gim}}{B_{gi}}$.

The expression of remaining gas storage in fracture (G_r) is same as development of EGP in Equation (E.26). Initial pore volume (V_{pi}) needs to be modified to include matrix storage as,

$$V_{pi} = x_f w_f h \phi_f + x_f L_f h \phi_m. \quad \text{(E.32)}$$

Applying Equation (E.31- E.32), average fracture pressure (P_f) is determined by

$$P_f = P_i - \frac{V_{pi} - ((G_i - G_p)B_g + (W_{fi} - W_p)B_w)}{V_{pi} c_r}. \quad \text{(E.33)}$$

In Equation (E.33), fracture pressure (P_f) can be determined iteratively.

The discrepancy is brought by assuming homogenous pressure decline rate in fracture and matrix and the validity of this assumption is addressed in the sensitivity analysis discussed in Chapter 4. Once the average fracture pressure (P_f)is specified, RNP and t_e can be determined, and fracture attributes can be evaluated from the slope of fitted linear line in the plot of $\ln(RNP)$ and t_e.In practical application, log-log plot of $\ln(RNP)$ and t_e should be constructed, and the interval with unit-slope is the proper flowback time region when the analytical model Equation (E.24) is valid to be applied.